IMPACTS OF SELF-ORGANIZING MECHANISM AND TOPOGRAPHY ON WETLAND ECOSYSEM DYNAMICS

A Dissertation
Presented to
The Academic Faculty

By

Yiwei Cheng

In Partial Fulfillment
of the Requirements for the Degree
Doctor of Philosophy in the
School of Civil and Environmental Engineering

Georgia Institute of Technology
May 2013

IMPACTS OF SELF-ORGANIZING MECHANISMS AND TOPOGRAPHY ON WETLAND ECOSYSEM DYNAMICS

Approved by:

Dr. Marc Stieglitz, Advisor
School of Civil and Environmental Engineering, and School of Earth and Atmospheric Science
Georgia Institute of Technology

Dr. Mustafa Aral
School of Civil and Environmental Engineering
Georgia Institute of Technology

Dr. Greg Turk
School of Interactive Computing
Georgia Institute of Technology

Dr. Philip Roberts
School of Civil and Environmental Engineering
Georgia Institute of Technology

Dr. Kevin Haas
School of Civil and Environmental Engineering
Georgia Institute of Technology

Date Approved: 04 April 2013

To my wife and daughter, Evy and Emma. The two most important women in my life.

ACKNOWLEDGEMENTS

First and foremost, I would like to express my sincere gratitude and appreciation to my PhD advisor and mentor Dr. Marc Stieglitz. Marc, I am extremely thankful for your guidance, financial support, and selfless sharing of ideas throughout my PhD research.

I would also like to thank my PhD committee members Dr. Greg Turk, Dr. Mustafa Aral, Dr. Philip Roberts, and Dr. Kevin Haas for their valuable guidance and suggestions.

I would like to express gratitude to my lab mates Alex Abdelnour and Sopan Patil for their support and collaboration. Thanks to both of you.

Finally, I am most grateful to my family: to my wife Evy. Your endless love has always been a beacon of support for me and has motivated me through all these years. This journey would have been impossible without your support and constant encouragement. To my daughter Emma, your recent presence in my life has brought about boundless joys that have uplifted my spirits during many tough times.

TABLE OF CONTENTS

LIST OF TABLES

LIST OF FIGURES

SUMMARY

Understanding the first order controls over resource cycling and limitation in ecosystems is critical for predicting ecosystem response to disturbances. Topography and vegetation self-organizing mechanisms are first order controls over resource fluxes across the landscape. Topography controls downslope flow of resources (i.e water and nutrients). Through spatial feedbacks, vegetation is able to actively modify its environment and maximize resource flows towards it. To date, the impacts of these controls on ecosystem dynamics have mostly been investigated separately. As such, there is a knowledge gap in the understanding of how these first order controls together dictate the dynamics of the ecosystem. This dissertation aims to gain a better understanding of how self-organizing mechanisms and topography operate together to affect wetland ecosystem dynamics.

A spatially explicit wetland vegetation patterning model that includes for both vegetation self-organizing control and topographic control is developed (Nutrient Depletion Model, NDM). The model describes a scale dependent feedback between vegetation, transpiration and nutrient accumulation that drives the formation of vegetation patterns. The model is applied to investigate the effects of topography and self-organizing mechanisms on the form and orientation of vegetation patterns and vegetation growth dynamics of wetland ecosystems. Results show that the two first order controls synergistically impact the formation of the various patterns as observed in wetland ecosystems. Results also show the following: (1) Self-organizing mechanisms result in a more efficient retention of resources, which result in higher biomass in the

model that include for both self-organizing mechanism and topographic control (SO+TC) than in the model that that includes only for topographic control (TC). (2) However, when resources or topographic gradients increase or when annual rainfall decreases, the vegetation growth dynamics of the SO+TC and TC models converge. The NDM is applied to arctic Alaska to investigate how the two first order controls impact present and future C-N dynamics of an arctic ecosystem. Simulation results show no significant difference in the dynamics between the SO+TC model and the TC model. The climate change simulation results suggest that changes in daily variability of temperature and precipitation can impact ecosystem dynamics as much as the changes in mean temperature and precipitation.

This dissertation provides a more complete picture on controls over ecosystem nutrient cycling and vegetative growth dynamics. Results from this study suggest that self-organizing processes can impact regional scale vegetation growth dynamics of a nutrient limited ecosystem where the terrain is flat or topographic gradient is gentle. However, incorporation of self-organizing processes (such as nutrient accumulation mechanism) may not be necessary when dealing with large scale climate model that operate at spatial resolutions that are orders of magnitude coarser than the spatial resolution at which vegetation self-organizing feedbacks operate.

1. INTRODUCTION

1.1 Vegetation Self-Organization and Resource Cycling

Vegetation patterns have been observed across a variety of terrestrial ecosystems. In the bogs in North America and Eurasia, maze patterns on flat ground have been observed [*Rietkerk et al,* 2004]. These patterns consist of interconnected vegetation ridges that are slightly elevated above waterlogged hollows. Another pattern characteristic of the northern bogs is the string pattern [*Sakaguchi,* 1980*; Foster et al.,* 1983] which consists of waterlogged hollows between bands of elevated vegetation that are orientated perpendicular to the water flow direction ("perpendicular strings"). Vegetation bands that are orientated parallel to the prevailing flow direction ("parallel strings") are characteristic of the ridge and slough ecosystem, such as the Florida Everglades [*Ogden, 2005*]. Stripes ("tiger bush") [*Valentin et al, 1999*], labyrinths [*Von Hardenberg et al, 2001*], spots ("leopard bush") [*Barbier et al. 2006*] and gaps [*Barbier et al., 2006*] are vegetation patterns that have commonly been observed in arid and semi-arid ecosystems.

A number of hypotheses have been proposed to explain the formation of vegetation patterns. *Boalger and Hodge* [1962] suggested that heterogeneity in soil texture as the mechanism responsible for stripe formation. Several authors attributed pattern formation to the development of non-vegetated regions within homogenous vegetation cover due to external disturbance events such as fire, termites and selective grazing [*Kellner and Bosch,* 1992*; Jeltsch et al,* 1997*; Bromley et al,* 1997]. In wetland ecosystems, *Hilbert et al.* [2000] invoked a peat accumulation mechanism to explain the

formation of maze patterns on flat ground. The Hilbert model describes the interaction between peat production and depth to water table. At sites where the peat surface is sufficiently high above the water table, vegetation growth is near optimal, the rate of organic matter input into the soil is higher than the rate of decomposition, and thus peat accumulates. On the other hand, at saturated sites, vegetation growth is limited, the rate of organic matter input into the soil is lower than the rate of decomposition, and thus peat depth decreases. With time, sites with moderate soil wetness connect and form maze-like structures that surround waterlogged hollows. A ponding mechanism has been invoked to explain the development of perpendicular strings [*Swanson and Grigal,* 1988] in bogs. Specifically, a vegetation patch impedes the downslope flow of water. This then leads to ponding of upslope water, which locally increases hydroperiod and water depth and which can inhibits the upslope expansion of emergent vegetation. At a distance further upslope the water surface is lower, which provides favorable conditions for patch growth. At the same time that the alternating conditions lead to growth or inhibition along the hydrologic gradient, individual patches may expand in the direction perpendicular to the hydrologic gradient. Together, these processes ultimately yield strings of vegetation perpendicular to the prevailing flow.

However, many of these proposed mechanisms are not necessarily self-organizing processes and do not relate vegetation patterning to resource scarcity. Growth of vegetation and the productivity of ecosystems are often limited by the availability of one or more types of resources [Vitousek and Howarth, 1991; Vitousek et al, 2010]. Vegetation growth in arid ecosystems is limited by the availability of soil water. On the other hand, vegetation growth in wetland ecosystems can be limited by the availability of

phosphorus [Vitousek et al, 2010]. Perhaps the most widespread resource limitation is that of nitrogen on ecosystem productivity [Vitousek and Howarth, 1991]. Fertilization experiments conducted in various ecosystem types such as arctic tundra, temperature forests, grasslands and boreal forests have shown that the addition of N increases vegetation productivity [*Shaver and Chapin*, 1980; *Bonan*, 1990. *Hunt et al*., 1988].

Recently, short distance facilitation and long distance competition between vegetation (a.k.a scale dependent feedback) has been proposed as a generic mechanism for vegetation pattern formation [*Rietkerk and van de Koppel,* 2008]. This mechanism was first proposed by Turing to explain regular pattern formation in chemical systems [*Turing,* 1953]. Also known as the activator-inhibitor principle, the mechanism describes the following: a chemical increases its concentration locally via autocatalytic reaction (short-range activation) and reduces its concentration at farther distances through the production of a chemical inhibitor that diffuses faster than itself (long-range inhibition). The activator-inhibitor principle has been applied in biology to explain the process of morphogenesis [*Meinhardt,* 1982*; Murray,* 1989]. Conceptually, in ecosystem studies, this mechanism explicitly relates vegetation patterning to spatial redistribution of growth limiting resources. Based on this principle, *Lefever and Lejeune* [1997] developed a propagation-inhibition model that generates stable periodic vegetation patterns that have dimensions similar to the *tiger bush* observed in arid and semi arid ecosystems. *Klausmeir* [1999] developed a mathematical model that incorporates diffusive plant dispersal and downhill surface water flow, which produce vegetation stripes that are consistent with the characteristic wavelength and biomass of the tiger stripes as observed in semi-arid and arid regions in Africa. Similarly, *Von Hardenberg et al* [2001]

developed a mathematical diffusion-reaction model that produces a wide range of vegetation patterns in water-limited regions.

In wetland ecosystems, *Rietkerk et al.* [2004b] developed a model that incorporates a positive feedback between the plant biomass, transpiration, and nutrient accumulation that describes the formation of the vegetation patterns in the northern bogs (a.k.a nutrient accumulation mechanism). Specifically, vegetation induces water and nutrient fluxes towards itself through transpiration, activating further growth, which increases transpiration and nutrient accumulation locally. Thus, plants deplete nutrients from their surrounding and inhibit plant growth at a farther distance. The scale dependent feedback concept highlighted by the *Rietkerk et al.* [2004b] model is that vegetation facilitates local growth by developing mechanisms to extract growth limiting resources at-distance. As such, at-distance, where resources are extracted and depleted, growth is inhibited. Simulation models developed using these concepts have reproduced vegetation patterns that are spatially consistent with the observed vegetation patterns and biomass amounts in nature [*Klausmeier,* 1999*; Von Hardenberg et al.,* 2001*; Rietkerk et al.,* 2002*; Lejeune et al.,* 2002*; Gilad et al.,* 2004*; Rietkerk et al.,* 2004b*; Eppinga et al.,* 2009*; von Hardenberg et al.,* 2010*; Meron et al.,* 2010]. More importantly, these simulation studies demonstrate the strong control that vegetation exerts over modifying the resource fluxes to their advantage.

1.2 Topography and Resource Cycling

Another pertinent control over resource flow is topography. Modeling studies over the last forty years have shaped our views of watershed form and function, especially as they pertain to the role that topography plays in transport of water and nutrients within a watershed. Early land surface models viewed the one-dimensional soil column as a fundamental hydrologic unit, and did not adequately represent topographic controls over water and nutrient fluxes. As a result, these models were effective in simulating vertical processes such as ground temperature evolution, but unable to simulate the impact of topography on surface hydrology. The development of TOPMODEL [*Beven*, 1986a; *Beven*, 1986b; *Beven et al.*, 1994; *Ambroise et al.* 1996], a conceptual rainfall-runoff model in which the impact of topography is accounted for using quasi-statistical techniques, permitted the spatio-temporal prediction of the development and dissipation of surface waters. TOPMODEL, in which the watershed is defined as the fundamental hydrologic unit, was a conceptual breakthrough in understanding watershed form and function. The success of the TOPMODEL approach in simulating watershed hydrologic characteristics highlighted the importance of incorporating topographic control for successful hydrologic prediction [*Stieglitz et al*, 1997, 1999, 2000, 2003; *Shaman et al*, 2002].

Consequently, the improvement in understanding watershed hydrologic characteristics through the incorporation of topographic control also contributes to the better understanding of nutrient cycling and limitation in terrestrial ecosystem; through the coupling of biogeochemical models and hydrologic models. Recently, distributed coupled hydrological-biogeochemical models have been developed for climate studies

and to study landscape responses to resource management and climate change. These models typically operate over relatively large grids, as such, they cannot, and do not, account for the vegetative control of water and nutrient flow paths. Instead, water and nutrient flow is strictly governed by the local topographic gradients, which result in homogenous vegetation covers. Spatially distributed and process oriented models such as DHSVM [*Wigmosta et al.,* 2002], VELMA [*Abdelnour et al.,* 2011] and RHESSys [*Tague and Band*, 2001] have been used to study how logging practices and climate change affect the hydrologic and carbon (C) and nitrogen (N) cycling of the old growth forests of the Pacific Northwest. The DHSVM has also been applied to a forested catchment in British Columbia to investigate the effects of clear cutting on peak flow sensitivity [*Whitaker et al*., 2002]. A distributed hydrological model, OHDIS-KWMSS [*Tachikawa et al.,* 2004] has been applied to investigate the interaction between sources and age of flow within forested catchments in the Pacific Northwest [*Sayama and McDonnell,* 2009]. Another distributed model, HillVi has been utilized to investigate the impact of porosity and soil depth variability on flow and transport processes [*Weiler and McDonnell*, 2004]. SWAT-N model [*Pohlert et al*., 2007] has been employed to study discharge and N loading of German forests. ELM [*Fitz and Trimble*, 2006] has been used to study the response of the ridge and slough habitat to water management and climate changes in the Florida Everglades. Another distributed model, the Soil and Water Integrated Model (SWIM), has been utilized to investigate different fertilization strategies and N leaching associated with each strategy [*Krysanova and Haberlandt,* 2002].

In wetland ecosystems, topography controls transport of water and hence the spatial distribution of water table depth and soil moisture across the landscape. Water table depth and soil moisture control net primary productivity, decomposition, and CO_2 and CH_4 sink-source strength [*Moore et al.,* 1998*; Oechel et al.,* 1993]. Modeling studies have demonstrated how eco-hydrological processes that control water and nutrient fluxes impact spatial distribution of water table depth and soil moisture within the peatland, and subsequently affect ecosystem productivity [*Sonnentag et al.,* 2008] and, CH_4 production [*Baird et al.,* 2009]. *Sonnentag et al.* [2008] employed a spatially distributed model, the Boreal Ecosystem Productivity Simulator (BEPS), to examine the effects of topography on wetness (water table depth and soil moisture content), evapotranspiration and gross ecosystem productivity in the Mer Bleue peatland, Canada. Their results showed that the model tended to underestimate daily evapotranspiration and gross ecosystem productivity by ~10 – 12% when topographically driven lateral fluxes were neglected from the model framework.

1.3 Research Objectives and Approach

As discussed above, to date, impacts of topography and self-organizing mechanism on wetland ecosystem dynamics have been explored separately. This dissertation aims to gain a better understanding of how self-organizing mechanism and topography operate together to affect wetland ecosystem dynamics. The following research questions are to be addressed in this study:

1. How do self-organizing mechanism and topography together affect form and orientation of wetland vegetation patterns?
2. How do self-organizing mechanism and topography together impact vegetation growth dynamics of a nutrient limited wetland ecosystem?
3. How does the incorporation of a vegetation self-organization mechanism into a topographically driven model impact present and future spatial vegetation patterning and carbon-nitrogen cycling of an arctic ecosystem?

To address the research questions raised, a model that incorporates both topographic control and self-organizing control over water and nutrient flows is developed, henceforth known as the Nutrient Depletion Model (NDM). In Chapter 2, the dynamics of the NDM is described in details.

The model is applied to two study sites: (1) the Great Vasyugan Bog, Siberia, and (2) a study site located on the North Slope of Alaska (69°35'48.74"N, 149°26'47.60"W). Both study sites are located in northern peatlands. Northern peatlands hold approximately one third of the world's soil organic carbon [*Gorham*, 1995] and play a critical role in the global carbon cycle [*Cox et al*., 2000; *Meehl et al*., 2005]. Distinct spatial vegetation patterns have been observed in both sites. In the Great Vasyugan Bog, vegetation stripes [*Sakaguchi,* 1980*; Foster et al.,* 1983] and maze patterns [*Rietkerk and van de Koppel*, 2008] have been observed. *Rietkerk et al*. [2004] developed a nutrient accumulation model to study the vegetation patterns observed in the Great Vasyugan Bog. *Eppinga et al*. [2008] conducted field measurements in this region to test the mechanisms of this nutrient accumulation mechanism. For the study site located on the North Slope of Alaska, distinct vegetation stripes oriented parallel to the hillslope

direction [*Hastings et al*. 1989; *Walker et al*. 1989] have been observed. The site is located approximately 100 km north of the Arctic Long Term Ecological Research Station (LTER) (68°38′N, 149°34′). Field experiments have been conducted and maintained at the LTER since 1981. Aboveground and belowground plant biomass measurements are conducted regularly during the growing seasons in both the experimental plots and control plots [*Bret-harte et al*., 2001; *Shaver et al*., 2001; *Mack et al*., 2004].

In Chapter 3, study sites and the data utilized in this thesis are discussed. In Chapter 4, the simulations that are conducted in this thesis are discussed in detail. In Chapter 5, the NDM is applied to address research question 1. In Chapter 6, the NDM is applied to address research question 2. In Chapter 7, the NDM is applied to address research question 3. In the concluding chapter, main findings from this thesis are first summarized, follow by discussions on future modifications to the NDM and the corresponding management and/or climate change scenarios that the model can be utilized to address in Arctic Alaska.

1.4 References

Abdelnour, A., M. Stieglitz, F. Pan, and R. McKane (2011), Catchment hydrological responses to forest harvest amount and spatial pattern, *Water Resour. Res.*, *47*.

Ambroise, B., Beven, K J., and Freer, J. (1996) Toward a~generalization of the TOPMODEL concepts: topographic indices of hydrological similarity, Water Resour. Res., 32, 2135–2145.

Baird, A.J., Belyea, L.R. and Morris, P.J. (2009) Upscaling peatland-atmosphere fluxes of carbon gases: small-scale heterogeneity in process rates and the pitfalls of 'bucket-and-slab' models. In Baird, A.J., Belyea, L.R., Comas, X., Reeve, A. and Slater, L., editors, Carbon Cycling in Northern Peatlands, Washington D.C.: American Geophysical Union.

Barbier, N., Couteron, P., Lejoly, J., Deblauwe, V. & Lejeune, O. (2006) Self-organized vegetation patterning as a fingerprint of climate and human impact on semi-arid ecosystems. *Journal of Ecology,* 94, 537-547.

Belyea, L. R., and R. S. Clymo (2001), Feedback control of the rate of peat formation., *Proceedings of the Royal Society B: Biological Sciences*, *268*, 1315-1321.

Beven, K J. (1986a) Hillslope Runoff Processes and Flood Frequency Characteristics. In A. D. Abrahams (ed.) Hillslope Processes, 187-202, Allen and Unwin, Boston.

Beven, K J. (1986b), Runoff production and flood frequency in catchments of order n: an alternative approach, in V K Gupta, I Rodriguez-Iturbe and E F Wood (Eds.), Scale Problems in Hydrology, Reidel, Dordrecht, 107-131.

Beven, K.J., and Kirkby, M.J. (1979). A physically based, variable contributing area model of basin hydrology. Hydrol. Sci. Bull. 24, 43-69.

Beven, K J, Lamb, R, Quinn, P F, Romanowicz, R and Freer, J, (1995) TOPMODEL, in V P Singh (Ed). Computer Models of Watershed Hydrology, Water Resources Publications, 627-668.

Bonan, G. B, (1990) Carbon and nitrogen cycling in North American boreal forests. II. Biogeographic patterns. *Can. J. Forest Res*. 20: 1077 – 1088.

Bret-Harte, M. S., G. R. Shaver, J. P. Zoerner, J. F. Johnstone, J. L. Wagner, A. S. Chavez, R. F. Gunkelman, S. C. Lippert, and J. A. Laundre (2001), Developmental plasticity allows Betula nana to dominate tundra subjected to an altered environment, *Ecology*, *82*(1), 18-32.

Bromley, J., Brouwer, J., Barker, A. P., Gaze, S. R. & Valentin, C. (1997) The role of surface water redistribution in an area of patterned vegetation in a semi-arid environment, south-west Niger. *Journal of Hydrology,* 198, 1-29.

Cheng, Y., M. Stieglitz, G. Turk, and V. Engel (2011), Effets of anisotropy on pattern formation in wetland ecosystems, *Geophysical Research Letter*.

Couwenberg, J. (2005), A simulation model of mire patterning - revisited, *Ecography*, *28*, 653-661.

Couwenberg, J., and H. Joosten (2005), Self-organization in raised bog patterning: the origin of microtope zonation and mesotope diversity, *Journal of Ecology*, *93*, 1238-1248.

Eppinga, M. B., M. Rietkerk, W. Borren, E. D. Lapshina, W. Bleuten and M. J. Wassen, (2008), Regular surface patterning of peatlands: Conforming theory with field data, *Ecosystems*, *11*(4), 520-536.

Eppinga, M. B., P. C. de Ruiter, M. J. Wassen, and M. Rietkerk (2009), Nutrients and hydrology indicate the driving mechanisms of peatland surface patterning, *The American naturalist*, *173*(6), 803-818.

Fitz, H. C., and B. Trimble (2006), Documentation of the Everglades Landscape Model: ELM v2.5*Rep.*, South Florida Water Management District, West Palm Beach, FL.

Foster, D. R., G. A. King, P. H. Glaser, and H. E. Wright (1983), Origin of string patterns in boreal peatlands, *Nature*, *306*, 256-258.

Gilad, E., J. von Hardenberg, A. Provenzale, M. Shachak, and E. Meron (2004), Ecosystem engineers: from pattern formation to habitat creation, *Physical review letters*, *93*(9), 098105.

Gorham, E. (1991), Northern Peatlands - Role in the Carbon-Cycle and Probable Responses to Climatic Warming, *Ecol Appl*, *1*(2), 182-195.

Hastings, S. J., S. A. Luchessa, W. C. Oechel, J. D. Tenhunen, (1989), Standing biomass and production in water drainages of the foothills of the Philip Smith Mountains. Holarctic Ecology 12(3), 304-311.

Hilbert, D. W., N. Roulet, and T. Moore (2000), Modelling and analysis of peatlands as dynamical systems, *Journal of Ecology*, *88*(2), 230-242.

Hunt, H. W., E. R. Ingham, D. C. Coleman, E. T. Elliott, C. P. P. Reid (1988), Nitrogen limitation of production and decomposition in prairie, mountain meadow, and pine forest, *Ecology*, 69: 1009 – 1016.

Govind, A., J. M. Chen, and W. Ju (2009), Spatially explicit simulation of hydrologically controlled carbon and nitrogen cycles and associated feedback mechanisms in a boreal ecosystem, *J. Georphys Res.*, *114*.

Jeltsch, F., Milton, S. J., Dean, W. R. J. & vanRooyen, N. (1997) Simulated pattern formation around artificial waterholes in the semi-arid Kalahari. *Journal of Vegetation Science,* 8, 177-188.

Kellner, K. & Bosch, O. J. H. (1992) Influence of Patch Formation in Determining the Stocking Rate for Southern African Grasslands. *Journal of Arid Environments,* 22, 99-105.

Klausmeier, C. A. (1999), Regular and irregular patterns in semiarid vegetation, *Science*, *284*(5421), 1826-1828.

Krysanova, V., and U. Haberlandt (2002), Assessment of nitrogen leaching from arable land in large river basins:: Part I. Simulation experiments using a process-based model, Ecological Modelling, 150(3), 255-275.

Lefever, R., and O. Lejeune (1997), On the origin of tiger bush, *Bull. Math. Biol*. 59(2), 263 – 294.

Lejeune, O., M. Tlidi, and P. Couteron (2002), Localized vegetation patches: a self-organized response to resource scarcity, *Physical review. E, Statistical, nonlinear, and soft matter physics*, *66*(1 Pt 1), 010901.

Lejeune, O., M. Tlidi, and R. Lefever (2004), Vegetation spots and stripes: Dissipative structures in arid landscapes, *International Jounal of Quantum Chemistry*, *98*, 10.

Meinhardt, H (1995) The algorithmic beauty of sea shells, Springer.

Moore, T. R., N. T. Roulet, and J. M. Waddington (1998), Uncertainty in predicting the effect of climatic change on the carbon cycling of Canadian peatlands, Clim. Change, 40, 229 – 245, doi:10.1023/A:1005408719297.

Murray, J. D. (1988) Mathematical Biology, Springer.

Oechel, W. C., S. J. Hastings, G. Vourlitis, M. Jenkins, G. Riechers, and N. Grulke (1993), Recent change of Arctic tundra ecosystems from a net carbon sink to a source, Nature, 361, 520–523, doi:10.1038/361520a0.

Ogden (2005) Everglades ridge and slough conceptual ecological model. *Wetlands,* 25, 810 - 820.

Pohlert, T., L. Breuer, J. A. Huisman, and H. G. Frede (2007), Assessing the model performance of an integrated hydrological and biogeochemical model for discharge and nitrate load predictions, *Hydrol. Earth Syst. Sci.*, *11*, 14.

Rietkerk, M., M. C. Boerlijst, F. van Langevelde, R. Hillerislambers, J. de Koppel, L. Kumar, H. H. Prins, and A. M. de Roos (2002), Self-organization of vegetation in arid ecosystems, *The American naturalist*, *160*(4), 524-530.

Rietkerk, M., S. C. Dekker, P. C. de Ruiter, and J. van de Koppel (2004a), Self-organized patchiness and catastrophic shifts in ecosystems, *Science*, *305*(5692), 1926-1929.

Rietkerk, M., S. C. Dekker, M. J. Wassen, A. W. Verkroost, and M. F. Bierkens (2004b), A putative mechanism for bog patterning, *The American naturalist*, *163*(5), 699-708.

Rietkerk, M., and J. van de Koppel (2008), Regular pattern formation in real ecosystems, *Trends in ecology & evolution*, *23*(3), 169-175.

Sakaguchi, Y. (1980), On the genesis of banks and hollows in peat bogs: an explanation by a thatch line theory., *Bulletin of the Department of Geography University of*

Tokyo, *12*, 35-58.

Shaman, J., Stieglitz, M., Engel, V., Koster, R., Stark, C. (2002) Representation of subsurface storm flow and a more responsive water table in a TOPMODEL-based hydrology model. *Water Resources Research,* 38, -.

Shaver, G. R., and Chapin F. S. III (1980), Responses to fertilization by various plant growth forms in an Alaska tundra: nutrient accumulation and growth, *Ecology*, 61: 662 – 675.

Sonnentag, O. J., J. M. Chen, N. T. Roulet, and W. Ju (2008), Spatially explicit simulation of peatland hydrology and carbon dioxide exchange: Influence of mesoscale topography, *J. Georphys Res.*, *113*.

Stieglitz, M., D. Rind, J. Famiglietti, and C. Rosenzweig (1997), An efficient approach to modeling the topographic control of surface hydrology for regional and global climate modeling, *J. of Climate*, *10*(1), 19.

Stieglitz, M., Hobbie, J., Giblin, A., Kling, G. (1999) Hydrologic modeling of an arctic tundra watershed: Toward Pan-Arctic predictions. *Journal of Geophysical Research-Atmospheres,* 104, 27507-27518.

Stieglitz, M., Giblin, A., Hobbie, J., Williams, M., Kling, G. (2000) Simulating the effects of climate change and climate variability on carbon dynamics in Arctic tundra. *Global Biogeochemical Cycles,* 14, 1123-1136.

Stieglitz, M., Ducharne, A., Koster, R., Suarez, M. (2001) The impact of detailed snow physics on the simulation of snow cover and subsurface thermodynamics at continental scales. *Journal of Hydrometeorology,* 2, 228-242.

Stieglitz, M., Déry, S. J., Romanovsky, V. E. and Osterkamp, T. E. (2003) The role of snow cover in the warming of arctic permafrost. *Geophysical Research Letters,* 30.

Swanson, D. K., and D. F. Grigal (1988), A simulation model of mire patterning, *Oikos*, *53*, 309-314.

Tachikawa, Y., G. Nagatani, and K. Takara (2004), Development of stage discharge relationship equation incorporating saturated-unsaturated flow mechanism,

Annual Journal of Hydraulic Engineering, Japan. Society of Civil Engineers, 48, 7-12.

Tague, C. L., and L. E. Band (2004), RHESSys: Regional Hydro-Ecologic Simulation System - An object-oriented approach to spatially distributed modeling of carbon, water and nutrient cycling, *Earth Interact*, *8*, 42.

Valentin, C., d'Herbes, J. M. & Poesen, J. (1999) Soil and water components of banded vegetation patterns. *Catena,* 37, 1-24.

van de Koppel, J., and M. Rietkerk (2004), Spatial interactions and resilience in arid ecosystems, *The American naturalist*, *163*(1), 113-121.

von Hardenberg, J., A. Y. Kletter, H. Yizhaq, J. Nathan, and E. Meron (2010), Periodic versus scale-free patterns in dryland vegetation, *Proceedings. Biological sciences / The Royal Society*, *277*(1688), 1771-1776.

von Hardenberg, J., E. Meron, M. Shachak, and Y. Zarmi (2001), Diversity of vegetation patterns and desertification, *Physical review letters*, *87*(19), 198101.

Vitousek, P. M., R. W. Howarth (1991), Nitrogen limitation on land and in the sea: How can it occur?, Biogeochemistry, 13: 87 – 115.

Vitousek, P. M., S. Porder, B. Z. Houlton and O. A. Chadwick (2010), Terrestrial phosphorus limitation: mechanisms, implications, and nitrogen-phosphorus interactions, Ecol Appl, 20(1): 5 – 15.

Walker, M. D., D. A. Walker, K. R. Everett, (1989) Wetland soils and vegetation, arctic foothills, AK. US Department of the Interior Biological Report 889 (7).

Wang, X., L. O. Sternberg, M. S. Ross and V. C. Engel (2011), Linking water use and nutrient accumulation in tree island upland hammock plant communities in the Everglades National Park, USA.

Weiler, M. and J.J. McDonnell 2004. Virtual experiments: A new approach for improving process conceptualization in hillslope hydrology. Journal of Hydrology, 285: 3-18, doi:10.1016/S0022 1694(03)00271-3

Whitaker, A., Y. Alila, J. Beckers, and D. Toews (2002), Evaluating peak flow sensitivity to clear-cutting in different elevation bands of a snowmelt-dominated mountainous catchment, Water Resources Research, 38(9), 1172, doi:1110.1029/2001WR000514.

Wigmosta, M. S., B. Nijssen, P. Stork, and D. P. Lettenmaier (2002), The Distributed Hydrology Soil Vegetation Model. , in *Mathematical models of small watershed hydrology and application*, edited by V. P. Singh and D. K. Frevert, Water Resource Publications, Littleton, CO.

2. THE NUTRIENT DEPLETION MODEL

2.1 Introduction

Among the spatial vegetation mechanisms proposed to explain wetland vegetation patterning, the nutrient accumulation mechanism as proposed by *Rietkerk et al.* [*2004b*] will be explored in this study. Originally developed for nutrient limited wetland ecosystems such as northern bogs, a scale dependent feedback between plant and resource flows describe the formation of the vegetation patterns. Specifically, vegetation induces water and nutrient fluxes towards itself through transpiration, activating further growth, which increases transpiration and nutrient accumulation locally. Thus plants deplete nutrients from their surrounding, which inhibit plant growth a distant away. The basic dynamics of the nutrient accumulation mechanism is illustrated in Figure 2.1. Starting from a random distribution, the plants self organize into coherent patterns with time. The relatively high evapotranspiration rates within vegetation patches alter the local hydraulic gradients and drive the convergence of water and dissolved nutrients towards the growing patch (Figure 2.1).

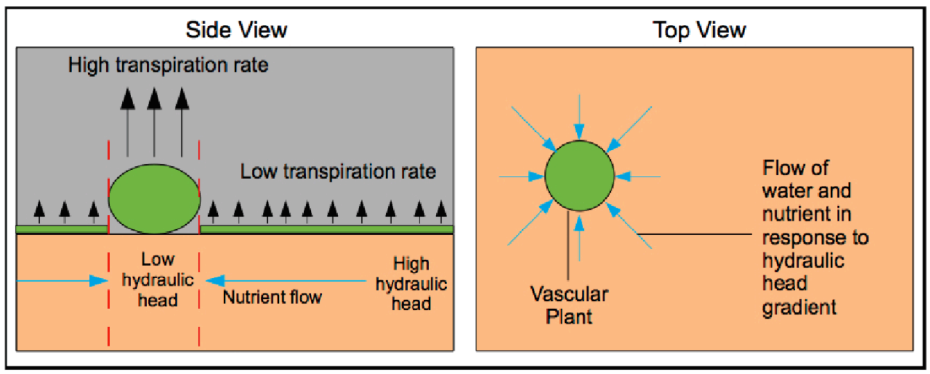

Figure 2.1: Schematic representation of the nutrient accumulation mechanism as proposed by Rietkerk et al (2004).

Field measurements conducted at wetland ecosystems such as the Great Vasyugan bog in Siberia [*Eppinga et al.,* 2008] and tree islands in the Everglades National Park, Florida [*Wang et al.,* 2011] have corroborated with this evapotranspiration-driven nutrient accumulation mechanism as postulated by *Rietkerk et al.* [2004b]. *Eppinga et al*. [2008] measured water table levels and water chemistry in the Great Vasyugan bog, Siberia, where extensive maze patterning occurs across the landscape. They found that nutrient concentrations are higher on the vegetated ridges than in the hollows. The authors also found that water table levels in the vegetated ridges are lower than the water table levels in the hollows.

The Rietkerk model [*Rietkerk et al*, 2004] is modified to include for a regional hydraulic gradient and effective anisotropy in hydraulic conductivity. The modified Rietkerk model, henceforth known as the Nutrient Depletion Model (NDM), includes for both topographic control and vegetation self-organizing control over water and nutrient fluxes and will be the model utilized that to address the questions posed in this thesis. In this chapter, a baseline NDM is first described in detail. This baseline NDM is utilized in Chapter 5 to investigate the impact of topography and self-organizing feedback on wetland vegetation patterning. Subsequently, modifications that are systematically made to the baseline NDM in order to address the research questions posed in Chapters 6 and 7 are also discussed in detail in this chapter. Finally, the implementation of the NDM on graphics processors is discussed. The implementation of NDM on graphics processors is necessary in order to overcome computational limitations and simulate dynamics over a wide range of spatial scales.

2.2 Model Description

2.2.1 Modification of the Rietkerk Model

The Rietkerk model describes the dynamics of three state variables in x and y direction: vascular plant biomass (B), hydraulic head (H) and nutrient concentration in groundwater (N).

$$\frac{\partial B}{\partial t} = \underbrace{g \cdot N \cdot B \cdot f[h(H)]}_{\textbf{(B1)}} - \underbrace{d \cdot B}_{\textbf{(B2)}} - \underbrace{b \cdot B}_{\textbf{(B3)}} + \underbrace{D_B \cdot \left[\frac{\partial^2 B}{\partial x^2} + \frac{\partial^2 B}{\partial y^2}\right]}_{\textbf{(B4)}} \tag{2.1}$$

$$\frac{\partial H}{\partial t} = \underbrace{\frac{p}{\theta}}_{\textbf{(W1)}} - \underbrace{\frac{t_v \cdot B \cdot f\left[h(H)\right]}{\theta}}_{\textbf{(W2)}} - \underbrace{\frac{e \cdot f \cdot \left[h(H)\right]}{\theta}}_{\textbf{(W3)}} + \underbrace{\frac{1}{\theta} \cdot \left[\frac{\partial}{\partial x} \cdot \left(H \cdot \frac{\partial (kH)}{\partial x}\right) + \frac{\partial}{\partial y} \cdot \left(H \cdot \frac{\partial (kH)}{\partial y}\right)\right]}_{\textbf{(W4)}} \tag{2.2}$$

$$\frac{\partial N}{\partial t} = \underbrace{\frac{N_{in} - \mu \cdot N \cdot B \cdot f[h(H)] + d \cdot (\frac{\mu}{g}) \cdot B - r \cdot N - N \cdot \theta \frac{\partial H}{\partial t}}{H \cdot \theta}}_{\textbf{(N1)}} + \underbrace{D_N \cdot \left[\frac{\partial^2 N}{\partial x^2} + \frac{\partial^2 N}{\partial y^2}\right]}_{\textbf{(N2)}} + \underbrace{\frac{1}{\theta} \cdot \left[\frac{\partial}{\partial x} \cdot \left(N \cdot \frac{\partial (kH)}{\partial x}\right) + \frac{\partial}{\partial y} \cdot \left(N \cdot \frac{\partial (kH)}{\partial y}\right)\right]}_{\textbf{(N3)}} \tag{2.3}$$

The term B1 describes plant growth, which is nutrient limited and increases linearly with increasing plant nutrient uptake. Plant growth is also affected by water stress. The soil water stress function $f[h(H)]$ ranges from zero to unity and is a function of the pressure head, h. Pressure head is calculated as the difference between hydraulic head, H, and elevation head, z. B2 represents the fraction of dead biomass that is returned to litter while B3 represents the fraction of dead biomass that is lost from the ecosystem. B4 describes the lateral spread of biomass by diffusion. W1 represents the increase in hydraulic head due to local precipitation, while W2 and W3 represent the decrease in hydraulic head due to plant transpiration and evaporation respectively. W4

describes the advection of hydraulic head according to Darcy's Law. N1 describes the rate of change of nutrient availability due to anthropogenic input, uptake by plants, recycling of dead plant material and nutrient losses. N2 is the rate of Fickian diffusion of the dissolved nutrients while N3 is the advection of dissolved nutrients by groundwater flow.

Equations 2.2 and 2.3 of the Rietkerk model are modified to allow for constant advection of water and nutrients in the *y*-direction due to a regional hydraulic gradient. After modification, terms W4 of equation 2.2 and N3 of equation 2.3 take the following forms:

W4: $$\frac{1}{\theta}\cdot\left[\frac{\partial}{\partial x}\left(H\cdot\frac{\partial(kH)}{\partial x}\right)+\frac{\partial}{\partial y}\left(H\cdot\frac{\partial(kH)}{\partial y}+H\cdot\frac{\partial(kc)}{\partial y}\right)\right]$$

N3: $$\frac{1}{\theta}\cdot\left[\frac{\partial}{\partial x}\cdot\left(N\cdot\frac{\partial(kH)}{\partial x}\right)+\frac{\partial}{\partial y}\cdot\left(N\cdot\frac{\partial(kH)}{\partial y}+N\cdot\frac{\partial(kc)}{\partial y}\right)\right]$$

Where $\partial c/\partial y$ is the regional hydraulic gradient in the *y*-direction. Therefore d*c*/d*y* indicates the change of hydraulic head (d*c*) between two adjacent grid cells of size, d*y*. In this scheme, the regional hydraulic gradient is identical to the land-surface slope. k_x and k_y (m day^{-1}) represent the hydraulic conductivity of peat in *x* and y directions, respectively. k_x/k_y represents the degree of anisotropy in the hydraulic conductivities and ranges from 0 – 1. When $k_x/k_y = 1$, the soil is isotropic.

The modified Rietkerk model, henceforth known as the baseline NDM, has the following form:

$$\frac{\partial B}{\partial t} = g \cdot N \cdot B \cdot f[h(H)] - d \cdot B - b \cdot B + D_B \cdot \left[\frac{\partial^2 B}{\partial x^2} + \frac{\partial^2 B}{\partial y^2}\right] \tag{2.4}$$

(B1) **(B2)** **(B3)** **(B4)**

$$\frac{\partial H}{\partial t} = \frac{p}{\theta} - \frac{t_v \cdot B \cdot f\left[h(H)\right]}{\theta} - \frac{e \cdot f \cdot \left[h(H)\right]}{\theta} + \frac{1}{\theta} \cdot \left\{\left[\frac{\partial}{\partial x} \cdot \left(H \cdot \frac{\partial (kH)}{\partial x} + H \cdot \frac{\partial (kc)}{\partial x}\right)\right] + \left[\frac{\partial}{\partial y} \cdot \left(H \cdot \frac{\partial (kH)}{\partial y} + H \cdot \frac{\partial (kc)}{\partial y}\right)\right]\right\} \tag{2.5}$$

(W1) **(W2)** **(W3)** **(W4)**

$$\frac{\partial N}{\partial t} = \frac{N_{in} - \mu \cdot N \cdot B \cdot f[h(H)] + d \cdot (\frac{\mu}{g}) \cdot B - r \cdot N - N \cdot \theta \frac{\partial H}{\partial t}}{H \cdot \theta}$$

(N1)

$$+ D_N \cdot \left[\frac{\partial^2 N}{\partial x^2} + \frac{\partial^2 N}{\partial y^2}\right] + \frac{1}{\theta} \cdot \left\{\left[\frac{\partial}{\partial x} \cdot \left(N \cdot \frac{\partial (kH)}{\partial x} + N \cdot \frac{\partial (kc)}{\partial x}\right)\right] + \left[\frac{\partial}{\partial y} \cdot \left(N \cdot \frac{\partial (kH)}{\partial y} + N \cdot \frac{\partial (kc)}{\partial y}\right)\right]\right\} \tag{2.6}$$

(N2) **(N3)**

The baseline NDM, as described by Equations 2.4, 2.5 and 2.6, is employed in Chapter 5 to investigate the impact of topography and self-organizing feedback on wetland vegetation patterning.

2.2.2 Incorporation of Peat Dynamics

In Chapter 6, the impacts of topography and self-organizing feedback on vegetation growth dynamics of a western Siberian peatland are examined using the NDM. For more realistic scenario studies, peat dynamics (equation 2.9) are incorporated into the NDM.

$$\frac{\partial B}{\partial t} = g \cdot N \cdot B \cdot f[h(H)] - b \cdot B + D_B \cdot \left[\frac{\partial^2 B}{\partial x^2} + \frac{\partial^2 B}{\partial y^2}\right] \tag{2.7}$$

(B1) (B2) (B3)

$$\frac{\partial H}{\partial t} = \frac{p}{\theta} - \frac{t_v \cdot B \cdot f\left[h(H)\right]}{\theta} - \frac{e \cdot f \cdot \left[h(H)\right]}{\theta} + \frac{1}{\theta} \cdot \left\{\left[\frac{\partial}{\partial x} \cdot \left(H \cdot \frac{\partial (kH)}{\partial x} + H \cdot \frac{\partial (kc)}{\partial x}\right)\right] + \left[\frac{\partial}{\partial y} \cdot \left(H \cdot \frac{\partial (kH)}{\partial y} + H \cdot \frac{\partial (kc)}{\partial y}\right)\right]\right\} \tag{2.8}$$

(W1) (W2) (W3) (W4)

$$\frac{\partial D}{\partial t} = d \cdot B - \nu \cdot D \cdot f(\phi) \tag{2.9}$$

(D1) (D2)

$$\frac{\partial N}{\partial t} = \frac{N_{in} - \mu \cdot N \cdot B \cdot f[h(H)] + \nu \cdot D \cdot (\frac{\mu}{g}) \cdot f(\phi) - r \cdot N - N \cdot \theta \frac{\partial H}{\partial t}}{H \cdot \theta}$$

(N1)

$$+ D_N \cdot \left[\frac{\partial^2 N}{\partial x^2} + \frac{\partial^2 N}{\partial y^2}\right] + \frac{1}{\theta} \cdot \left\{\left[\frac{\partial}{\partial x} \cdot \left(N \cdot \frac{\partial (kH)}{\partial x} + N \cdot \frac{\partial (kc)}{\partial x}\right)\right] + \left[\frac{\partial}{\partial y} \cdot \left(N \cdot \frac{\partial (kH)}{\partial y} + N \cdot \frac{\partial (kc)}{\partial y}\right)\right]\right\} \tag{2.10}$$

(N2) (N3)

Where D1 represents accumulation of peat. Peat accumulation increases linearly with the amount of dead plant biomass. D2 represents the first order decomposition, where $f(\phi)$ is

soil moisture function that follows *Raich et al.,* [1991]. The dynamics of plant biomass, hydraulic head and nutrient are similar to the baseline NDM.

To simulate topographic effects alone (TC model), we set plant advection of water and nutrient to zero.

$$\frac{\partial H}{\partial t} = \frac{p}{\theta} - \frac{t_v \cdot B \cdot f\left[h(H)\right]}{\theta} - \frac{e \cdot f \cdot \left[h(H)\right]}{\theta} + \frac{1}{\theta} \cdot \left\{ \left[\frac{\partial}{\partial x} \cdot \left(H \cdot \frac{\partial (kH)}{\partial x} + H \cdot \frac{\partial (kc)}{\partial x} \right) \right] + \left[\frac{\partial}{\partial y} \cdot \left(H \cdot \frac{\partial (kH)}{\partial y} + H \cdot \frac{\partial (kc)}{\partial y} \right) \right] \right\} \quad (2.11)$$

$$\frac{\partial N}{\partial t} = \frac{N_{in} - \mu \cdot N \cdot B \cdot f[h(H)] + \nu \cdot D \cdot (\frac{\mu}{g}) \cdot f(\phi) - r \cdot N - N \cdot \theta \frac{\partial H}{\partial t}}{H \cdot \theta}$$

$$+ D_N \cdot \left[\frac{\partial^2 N}{\partial x^2} + \frac{\partial^2 N}{\partial y^2} \right] + \frac{1}{\theta} \cdot \left\{ \left[\frac{\partial}{\partial x} \cdot \left(N \cdot \frac{\partial (kH)}{\partial x} + N \cdot \frac{\partial (kc)}{\partial x} \right) \right] + \left[\frac{\partial}{\partial y} \cdot \left(N \cdot \frac{\partial (kH)}{\partial y} + N \cdot \frac{\partial (kc)}{\partial y} \right) \right] \right\} \quad (2.12)$$

2.2.3 Modification to Investigate Carbon-Nitrogen Cycling in Arctic Ecosystem

In Chapter 7, the impacts of topography and self-organizing feedback on carbon-nitrogen (C-N) dynamics of an arctic ecosystem are examined using the NDM. The baseline NDM is modified such that it simulates the effects of climate warming on ecosystem C storage and the cycling of C and N between plants and a shallow active soil pool. The NDM now describes the dynamics of four state variables: aboveground vegetation biomass carbon (*B*), hydraulic head (*H*), soil carbon including humus and detritus but excluding deep "non-interactive" carbon (D), and plant available soil nitrogen (*N,* also known as dissolved organic nitrogen, *DIN*).

$$\underbrace{\frac{\partial B}{\partial t}}_{\textbf{(B1)}} = \underbrace{g \cdot N \cdot B \cdot f[h(H)]}_{\textbf{(B2)}} - d \cdot B + \underbrace{D_B \cdot \left[\frac{\partial^2 B}{\partial x^2} + \frac{\partial^2 B}{\partial y^2}\right]}_{\textbf{(B3)}} \tag{2.13}$$

$$\underbrace{\frac{\partial H}{\partial t}}_{\textbf{(W1)}} = \underbrace{\frac{p}{\theta}}_{\textbf{(W2)}} - \underbrace{\frac{t_v \cdot B \cdot f\left[h(H)\right]}{\theta}}_{\textbf{(W3)}} - \frac{e \cdot f \cdot \left[h(H)\right]}{\theta}$$

$$+ \underbrace{\frac{1}{\theta} \cdot \left\{\left[\frac{\partial}{\partial x} \cdot \left(H \cdot \frac{\partial (kH)}{\partial x} + H \cdot \frac{\partial (kc)}{\partial x}\right)\right] + \left[\frac{\partial}{\partial y} \cdot \left(H \cdot \frac{\partial (kH)}{\partial y} + H \cdot \frac{\partial (kc)}{\partial y}\right)\right]\right\}}_{\textbf{(W4)}} \tag{2.14}$$

$$\underbrace{\frac{\partial D}{\partial t}}_{\textbf{(D1)}} = \underbrace{d \cdot B - \nu \cdot D \cdot f(T) \cdot f(\phi)}_{\textbf{(D2)}} \tag{2.15}$$

$$\frac{\partial N}{\partial t} = N_{in} - \mu \cdot N \cdot B \cdot f[h(H)] + \frac{1}{\alpha} \cdot \eta \cdot \nu \cdot D \cdot f(T) \cdot f(\phi)$$

(N1)

$$+H \cdot \theta \cdot \left(D_N \cdot \left[\frac{\partial^2 N}{\partial x^2} + \frac{\partial^2 N}{\partial y^2} \right] + \frac{1}{\theta} \cdot \left\{ \left[\frac{\partial}{\partial x} \cdot \left(N \cdot \frac{\partial (kH)}{\partial x} + N \cdot \frac{\partial (kc)}{\partial x} \right) \right] + \left[\frac{\partial}{\partial y} \cdot \left(N \cdot \frac{\partial (kH)}{\partial y} + N \cdot \frac{\partial (kc)}{\partial y} \right) \right] \right\} \right)$$

(N2) **(N3)** (2.16)

D2 represents the first order decomposition, where $f(T)$ is the temperature function and $f(\phi)$ is soil moisture function. The temperature and soil moisture functions shown here in Figure 2.2 follow *Waelbroeck and Louis* [1995], *McKane et al*., [1997] and *Stieglitz et al*., [2000].

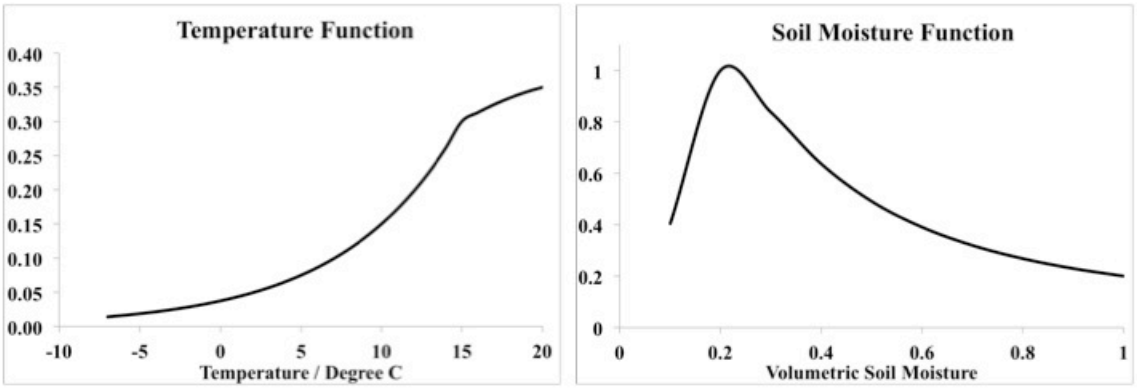

Figure 2.2. Temperature and soil moisture functions used in the calculation of detrital decomposition.

N1 describes the rate of change of nutrient availability due to anthropogenic input, uptake by plants and peat decomposition. η represents the fraction of peat that decomposes into plant available soil N. The remaining fraction represents ecosystem loss of the recalcitrant form of nitrogen, dissolved organic nitrogen (DON). The soil column is assumed to have a single C:N ratio [*Gough et al*., 2002; *Schmidt et al*., 2002; *Shaver et*

al., 2001; *Shaver and Chapin*, 1991], defined as α. For all simulations, α is held constant at 33 [*Stieglitz et al*, 2000]. N2 is the advection of dissolved nutrients due to local hydraulic head gradient (plant induced) and global hydraulic head gradient (topographically induced).

To simulate topographic effects alone (TC model), we set plant advection of water and nutrient to zero.

$$\frac{\partial H}{\partial t} = \frac{p}{\theta} - \frac{t_v \cdot B \cdot f\left[h(H)\right]}{\theta} - \frac{e \cdot f \cdot \left[h(H)\right]}{\theta}$$

$$+\frac{1}{\theta}\cdot\left\{\left[\frac{\partial}{\partial x}\cdot\left(H\cdot\frac{\partial(kH)}{\partial x}+H\cdot\frac{\partial(kc)}{\partial x}\right)\right]+\left[\frac{\partial}{\partial y}\cdot\left(H\cdot\frac{\partial(kH)}{\partial y}+H\cdot\frac{\partial(kc)}{\partial y}\right)\right]\right\} \quad (2.17)$$

$$\frac{\partial N}{\partial t} = N_{in} - \mu \cdot N \cdot B \cdot f[h(H)] + \frac{1}{\alpha}\cdot\eta\cdot\nu\cdot D\cdot f(T)\cdot f(\phi) - r\cdot N$$

$$+H\cdot\theta\cdot\left(D_N\cdot\left[\frac{\partial^2 N}{\partial x^2}+\frac{\partial^2 N}{\partial y^2}\right]+\frac{1}{\theta}\cdot\left\{\left[\frac{\partial}{\partial x}\cdot\left(N\cdot\frac{\partial(kH)}{\partial x}+N\cdot\frac{\partial(kc)}{\partial x}\right)\right]+\left[\frac{\partial}{\partial y}\cdot\left(N\cdot\frac{\partial(kH)}{\partial y}+N\cdot\frac{\partial(kc)}{\partial y}\right)\right]\right\}\right)$$

(2.18)

2.3 Computational Methods

Over the last decade, researchers have begun utilizing the processors of desktop video cards to solve computationally intensive problems in various fields [*Owens et al,* 2008]. Modern-day video cards, known as Graphics Processing Units (GPU's), have anywhere from a few dozen to more than a hundred processors. The computational capacity of GPUs is higher than many of the fastest multi-core CPUs. The use of GPUs

for general purpose computation is known as GPGPU (general-purpose GPU) programming. Some of the earliest GPGPU programming tools are Sh, Brooks, and Scout [*McCool et al,* 2004*; Buck et al,* 2004*; McCormick et al,* 2004]. More recently, NVIDIA Corporation developed a computing architecture named Compute Unified Device Architecture (CUDA). CUDA is designed to reduce overheads to learning and provide easier access to GPU programming. CUDA has been used in many fields of science, including NCAR's Weather Research and Forecast (WRF) model [*Michalakes & Vachharajani,* 2008], advection-reaction-diffusion [*Sanderson et al,* 2009], and computational fluid dynamics [*Crane et al,* 2007]. In this thesis, all the above described versions of NDM have been implemented in CUDA. However, in this section, only the implementation of the baseline NDM is discussed.

The equations of the baseline NDM were each discretized and run using a forward Euler finite difference method. The baseline NDM is an advection-diffusion-reaction system. This system is a good candidate for implementation in CUDA, since CUDA is best suited for problems that can be split into different parts that can be evaluated independently (parallelized). Operator splitting is performed to separate out the different terms that appear in the governing partial differential equations. Specifically, the baseline NDM can be divided into three components: advection, diffusion, and reaction. For each process, a function/kernel is invoked to compute the change in values as a result of the process. Instances of the kernel, each representing a grid point in the spatial domain, can be launched in parallel, thus speeding up the computation by orders of magnitude. A high level overview of the model is described below:

Step 1. Initialize all parameters
Step 2. Biomass Solver: reaction (equation 2.1, B1 – B3) and diffusion (equation 2.1, B4)
Step 3. Hydraulic Head Solver: reaction (equation 2.2, W1 – W3) and advection (equation 2.2, W4)
Step 4. Nutrient Solver: reaction (equation 2.3, N1), diffusion (equation 2.3, N2) and advection (equation 2.3, N3)
Step 5. Update variables
Step 6. Repeat from Step 2

Several types of memory are available in CUDA: global memory, shared memory, constant memory and texture memory. The global memory is the random access video memory on the graphics card. Data stored in global memory can be read or written by any of the threads. Shared memory can also be read or written by threads. However, since it is on-chip, shared memory is much faster than global memory. In contrast to global and shared memories, constant memory and texture memories are read-only memories. The model performance is affected by the type of memory used. In this work, the diffusion and advection processes are represented as spatial derivatives in the equation. For example, the diffusion process is represented by a Laplacian differential operator. In diffusion, the new concentration of a variable (e.g. biomass and nutrient) in a grid will be calculated as the sum of differences between the concentration within the grid and the concentration of the four surrounding neighbors. The computation stencil for the diffusion process is shown in Figure 2.3 (right). For this type of computation, the memory access pattern is such that a thread is reading from an address that nearby threads are reading (Figure 2.3, left). This type of memory access pattern implies that the addresses accessed are not consecutive and therefore cannot be cached together in a conventional CPU caching scheme. In this type of situation, since the texture memory is

already cached on chip, memory requests to off-chip DRAM is greatly reduced, thereby providing higher effective bandwidth.

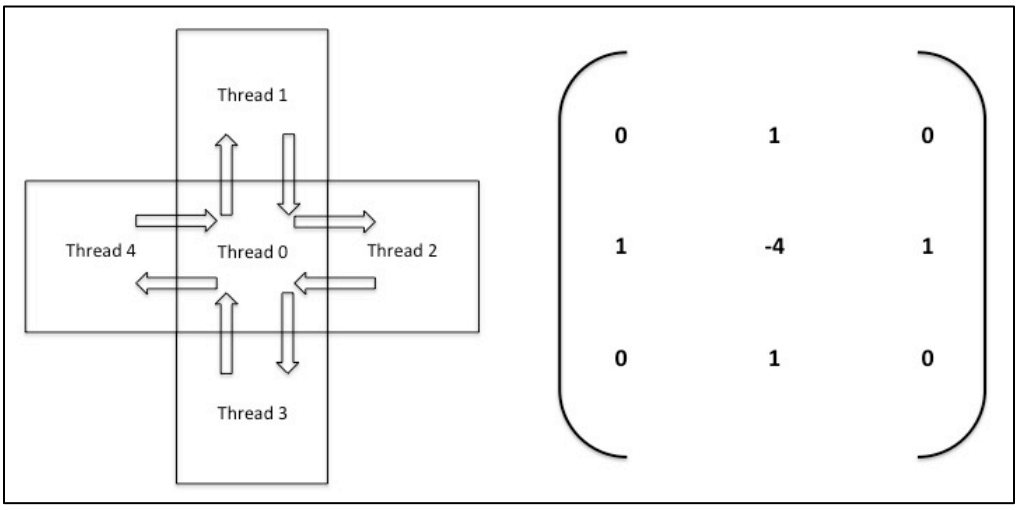

Figure 2.3: (Left) Representation of the diffusion process and mapping of the threads in two-dimensions. (Right) Computational stencil for the diffusion process.

For the reasons explained above, texture memory is used in both the diffusion and advection solvers. Unlike the diffusion and the advection processes, in the reaction processes, the update in value of the variable does not involve values from the surrounding neighbors. As such, global memory is used in the calculations. Biomass, hydraulic head and nutrient each have their own reaction processes.

In the baseline NDM, some parameters are constant and do not change during the execution of the model. Examples are the growth and death rate of the biomass, the diffusion coefficients, and the hydraulic conductivity. CUDA has another type of memory that can be utilized: constant memory. Like texture memory, constant memory is

also cached and is a read-only memory. Since the memory is cached, successive reading from same addresses does not incur additional memory traffic. Further, the NVIDIA GPU is designed such that only single memory read from a constant memory is needed for a group of 16 threads. Compared to global memory, which requires 16 memory read requests for the 16 respective threads, constant memory generates only 1/16 the amount of memory traffic.

2.3.1 Comparison of Computational Speed Between GPU and CPU Version of NDM

To put the processing power of GPU acceleration in perspective, a comparison study on the processing speed of the model coded in the GPU framework and the same model coded in the CPU framework is conducted. The experiment is conducted on a Macbook Pro with standard specs (Intel Core i7, Duo Cores, Processor Speed: 2.66 GHz, L2 Cache (per core): 256 KB, L3 Cache: 4 MB, Memory: 8GB, Graphics Card: NVIDIA GeForce GT 330M). The performance of the model is evaluated based on the total number of iterations simulated per minute for four different simulation grid sizes: (1) 64 x 64 pixels, (2) 128 x 128 pixels, (3) 256 x 256 pixels and (4) 512 x 512 pixels. A total of eight simulation scenarios are explored: four for the GPU based model and four for the CPU based model. For each scenario, the simulation is run three times and the mean model performance is calculated. Results are shown in Table 2.1.

Table 2.1: Performance analysis of the baseline NDM coded in CPP and CUDA. Values in the two rightmost columns are iterations per minutes (larger numbers indicate faster speed).

Domain Size	**Trials**	**C++**	**CUDA**
64 x 64	1	12690	190280
	2	12420	192480
	3	12610	192140
	Mean	12573	191633
128 x 128	1	3140	58040
	2	3420	57620
	3	3160	58050
	Mean	3240	57903
256 x 256	1	840	42150
	2	840	42370
	3	850	41870
	Mean	843	42130
512 x 512	1	180	13240
	2	170	13230
	3	180	13220
	Mean	177	13230

Results depict a general trend: the bigger the domain size, the slower the processing speed (the fewer iterations per minute). Most importantly, the results also show that for all simulations, the GPU framework has higher processing speed than the CPU framework by at least two orders of magnitude for all domain sizes (Figure 2.4). The bigger the domain size, the greater the performance increases of the GPU framework over the CPU framework. In the simulations, each iteration/time step represents a day. Based on the speeds derived from the comparison study, the amount of time needed to complete a 100-year simulation is calculated, for a simulation grid of 512 x 512 in size where each pixel represents 20 x 20 m (total area simulation ~105 km^2). The simulation took 3 minutes to complete on a GPU and 206 minutes using on the CPU (75 times longer).

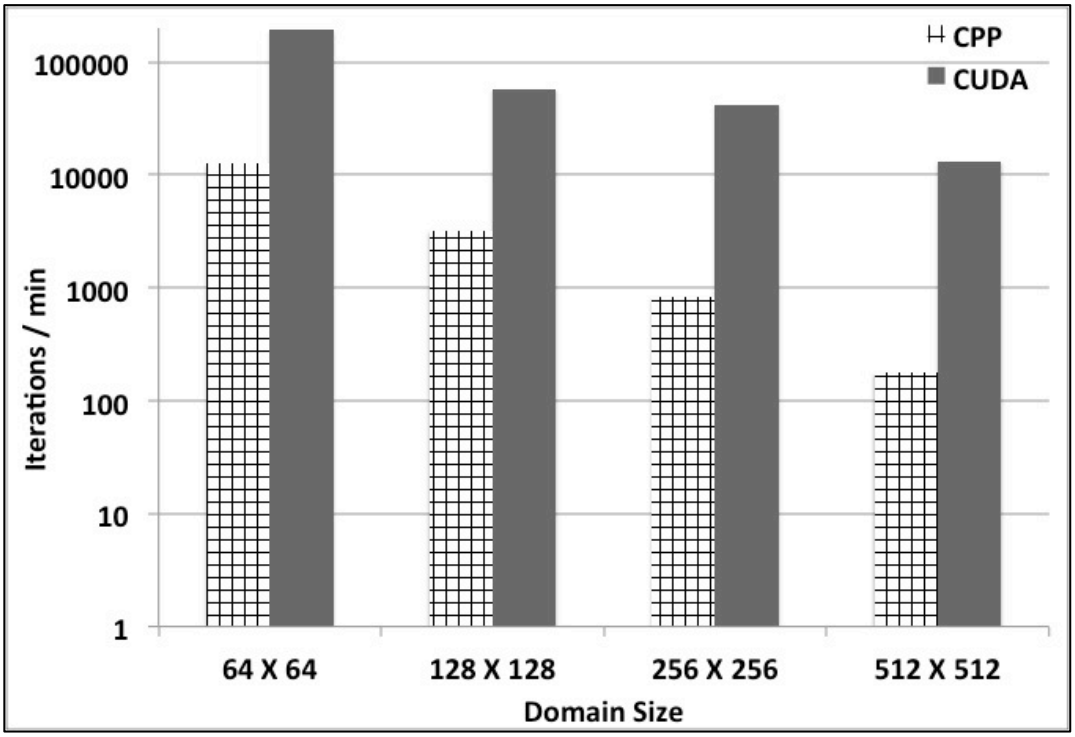

Figure 2.4: Performance analysis of the baseline NDM coded in CPP (CPU, gridded bars) and CUDA (GPU, solid bars). Y-axis shows the mean total number of frames simulated per min for five different simulation grid sizes. The y-axis is logarithmic.

These results are comparable to recent studies that have utilized the processing power of GPU's in order to explore large-scale dynamics in ecosystems [*van de Koppel et al,* 2011*; Hajnal and Bajzat,* 2011]. *van de Koppel et al* [2011] implemented three spatially explicit ecological models in CUDA C [*NVIDIA Corporation* 2009]. They achieved speedup of up to two orders of magnitude (100X) using NVIDIA Telsla C1060 (in comparison to the CPU). *Hajnal and Bajzat* [2011] implemented an *cellular automata* of freshwater phytoplankton community dynamics in GPU and achieved speedup of up to 50X in comparison to CPU. To date, no study exists in the field of eco-hydrology that has investigated the magnitude of speedup that can be achieved when implementing a spatially explicit eco-hydrological model in multiple GPUs.

2.4 References

Buck, I., Foley, T., Horn, D., Sugerman, J., Fatahalian, K., Houston, M. & Hanrahan, P. (2004) Brook for GPUs: stream computing on graphics hardware. *ACM SIGGRAPH 2004*, pp. 777-786. ACM.

Cheng, Y., M. Stieglitz, G. Turk, and V. Engel, 2011. Effects of anisotropy on pattern formation in wetland ecosystems, *Geophys. Res. Lett.*, 38, L04402, doi:10.1029/2010GL046091.

Crane, K., Llamas, I. & Tariq, S. (2007) Real-time simulation and rendering of 3D fluids. *GPU Gems 3*. Addison-Wesley, New York, New York, USA.

Gough, L., P. A. Wookey, and G. R. Shaver (2002), Dry heath arctic tundra responses to long-term nutrient and light manipulation, *Arct Antarct Alp Res*, *34*(2), 211-218.

Hajnal, E., T. Bajzat. 2011. Ecological modeling with Cellular Automaton software implemented in GPU system. *Obuda University e-Bulletin*, Vol. 2, No. 1, 499 – 508.

McCool, M., Du Toit, S., Popa, T., Chan, B. & Moule, K. (2004) Shader algebra. *ACM Transactions on Graphics,* **23,** 787-795.

McCool, A., Meyer, M., Kirby, R. & Johnson, C. (2009) A framework for exploring numerical solutions of advection-reaction-diffusion equations using a GPU-based approach. *Computing and Visualization in Science,* **12,** 155-170.

McCormick, P. S., Inman, J., Ahrens, J. P., Hansen, C. & Roth, G. (2004) Scout: A hardware-accelerated system for quantitatively driven visualization and analysis. *IEEE Visualization 2004*, pp. 171-178.

McKane, R. B., E. B. Rastetter, G. R. Shaver, K. J. Nadelhoffer, A. E. Giblin, J. A. Laundre, and F. S. Chapin (1997), Climatic effects on tundra carbon storage inferred from experimental data and a model, *Ecology*, *78*(4), 1170-1187.

Michalakes, J. & Vachharajani, M. (2008) GPU acceleration of numerical weather prediction. *Parallel Processing Letters,* **18,** 531-548.

NVIDIA Corporation, NVIDIA CUDA Programming Guide, http://www.nvidia.com/object/cuda_develop.html, 2009.

Owens, J. D., Houston, M., Luebke, D., Green, S., Stone, J. E. & Phillips, J. C. (2008) Gpu Computing. *Proceedings of the IEEE,* **96,** 879-899.

Rietkerk, M., Dekker, S. C., Wassen, M. J., Verkroost, A. W. M. & Bierkens, M. F. P. (2004) A putative mechanism for bog patterning. *American Naturalist,* **163,** 699-708.

Stieglitz, M., A. Giblin, J. Hobbie, M. Williams, and G. Kling (2000), Simulating the effects of climate change and climate variability on carbon dynamics in Arctic tundra, *Global Biogeochem Cy*, *14*(4), 1123-1136.

Van de Koppel, J., R. Gupta, C. Vuik. (2011). Scaling up spatially explicit ecological models using graphic processors. *Ecological Modeling*., 222, 3011 – 3019.

Waelbroeck, C., and J. F. Louis (1995), Sensitivity Analysis of a Model of Co2 Exchange in Tundra Ecosystems by the Adjoint Method, *J Geophys Res-Atmos*, *100*(D2), 2801-2816.

3. STUDY SITES AND DATA

3.1 Introduction

In this chapter, the study sites and data utilized in this thesis are described. Studies conducted in chapters 5 and 6 utilized data from the Great Vasyugan Bog in Siberia. Studies conducted in Chapter 7 utilized data from the Arctic Long Term Ecological Research Station (LTER) located in North Slope of Arctic Alaska.

3.2 Great Vasyugan Bog

3.2.1 Site Description and Data

The Great Vasyugan Bog (55 - 59° N, 76 - 83° E) is located in the West Siberian plain and is the largest peatland system in the northern hemisphere. The region has deglaciated 11,000 years ago and permafrost is no longer present [*Lapshina et al*, 2001]. Climate of the region can be categorized as continental. Mean monthly air temperature range from -20°C to 18°C [*Lapshina et al*, 2001]. Other key characteristics of this peatland are shown in Table 3.1.

Table 3.1. Ecosystem characteristics of the Great Vasyugan Bog.

Ecosystem Characteristics	Range of Values From Literature	References
Plant biomass (gB m^{-2})	100 – 2000	*Rietkerk et al* [2004b]
Periodic spacing between vegetation patches/stripes (m)	10 – 50	*Rietkerk et al* [2004a], [2004b], *Eppinga et al* [2009]
Atmospheric input of nutrient (gN m^{-2} yr^{-1})	0 – 5	*Lapshina et al,* [2001], *Rietkerk et al* [2004b], *Eppinga et al* [2009]
Annual Precipitation (mm yr^{-1})	250 – 500	*Frey and Smith,* [2003]

3.3 North Slope, Arctic Alaska

3.3.1 Site Description

Study site chosen in Chapter 7 is located within the Kuparuk Basin in North Slope, Alaska (69°35'48.74"N, 149°26'47.60"W, elevation = ~700 ft), where vegetation stripes (width of ~ 15 – 30 m) that are parallel to the slope direction have been observed (darker green vegetation stripes in Figure 3.2). These distinct bands of vegetation are known as water tracks. The vegetation species of the water tracks are similar to the surrounding tundra. Dominant vegetation species in the region are rhizomatous sedges (*Eriophorum vaginaturm*), deciduous shrubs (*Betula nana*), evergreens (*Ledum palustre*), and mosses (*Sphagnum spp.*) [*Shaver and Chapin*, 1991]. Vegetation in the water tracks are more productive than the surrounding vegetation since water flow and nutrient fluxes in the water tracks are faster than the surrounding area [*Chapin et al*., 1988]. Analysis of the water tracks using digital elevation models have suggested that the water tracks are

channel networks that have not developed into mature channel networks as the presence of permafrost have limited the rate of channel erosion [*McNamara et al.,* 1999]. Digital Elevation Map (DEM) for the terrain was obtained from Artic LTER GIS database (http://toolik.alaska.edu/gis/data) (Figure 3.2).

For this study site, summer precipitation and integrated ground temperature (mean of ground surface and soil temperature 5, 10, 20 and 30 cm) are 100 mm and 4°C respectively. Temperature and precipitation data for this site are obtained from a nearby MET station in Sagwon Alaska (69°25' 27.5''N, 148°41' 45.1'' W, elevation = ~1000 ft). The Sagwon station was set up as part of the North Slope Hydrology Research Projects by the Water and Environmental Research Center of the University of Alaska Fairbanks (http://ine.uaf.edu/werc/projects/NorthSlope/e_kuparuk/sagwon/sagwon.html).

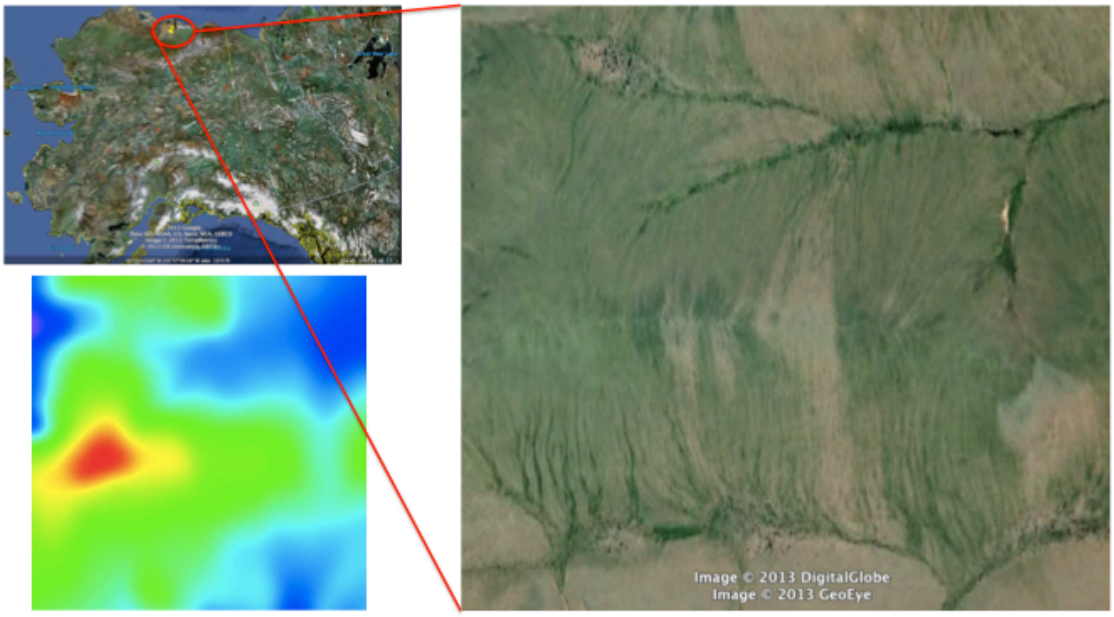

Figure 3.1. Location of study site with reference to Alaska. Image at the bottom left shows the DEM of the region. Images from Google map. © 2013 Google, © 2013 TerraMetrics, © 2013 GIS Innovatsia, DATA+, © 2013 DigitalGlobe and © 2013 GeoEye.

Ecological data used in model calibration are obtained from the Arctic Long Term Ecologic Research (LTER) Station. The Arctic LTER is located in the northern foothills of the Brooks Range, Alaska (68°38′N, 149°34′W, elevation 780m). Dominant vegetations at the site are a mix of rhizomatous sedges (*Eriophorum vaginaturm*), deciduous shrubs (*Betula nana*), evergreens (*Ledum palustre*), and mosses (*Sphagnum spp.*). Field experiments have been conducted and maintained at the LTER since 1981. In designated experimental plots the following treatments were applied during the growing season: N fertilization, P fertilization N+P, N+P fertilization, warming with field greenhouses, warming + N+P fertilization, and light reduction. Aboveground and belowground plant biomass measurements were conducted regularly during the growing

seasons in both the experimental plots and the corresponding control plots [*Bret-harte et al*., 2001; *Shaver et al*., 2001; *Mack et al*., 2004].

3.3.2 Data

3.3.2.1 Data Used in Model Calibration

Table 3.2. Ecosystem characteristics of a typical arctic tundra ecosystem. Based on data from Arctic LTER.

Ecosystem Characteristics	Range of Observed Values	References
Plant Carbon (gC m^{-2})	108 – 938	*Shaver and Chapin*, [1991]
Detrital Carbon (gC m^{-2})	10,000 - 26,400	*Giblin et al*. [1991]
Net Primary Productivity (gC m^{-2} yr^{-1})	16 – 152	*Shaver and Chapin*, 1991]
DIN Loss (gN m^{-2} yr^{-1})	0.003 – 0.008	*Peterson et al*. [1992]
DON Loss (gN m^{-2} yr^{-1})	0.1	*Peterson et al*. [1992]
Width of vegetation stripes (m)	~ 15 – 30	Calculated from image obtained from Google Earth

3.3.2.2 Data Used in Climate Change Simulations

Projected monthly temperature and precipitation of Global Climate Model (GCM) outputs used in this study are downloaded from the Scenarios Network for Alaska and Arctic Planning (SNAP) data site (http://www.snap.uaf.edu/data.php). SNAP houses downscaled and bias corrected historical and projected monthly climate data across Alaska and parts of Western Canada. More details on their downscaling and bias

correction technique can be found in SNAP site (http://www.snap.uaf.edu/downscaling.php). The five GCMs that SNAP has selected have been shown to have the best predictability over the Arctic region based on the results of the Coupled Model Inter-comparison Project (CMIP) [*Walsh et al*., 2008]. The GCMs are: Canadian Centre for Climate Modeling and Analysis General Circulation Model version 3.1 – t47 (CCCMA_GCGM31), Max Planck Institute for Meteorology European Centre Hamburg Model 5 (MPI_ECHAM5), Geophysical Fluid Dynamics Laboratory Coupled Climate Model 2.1 (GFDL_CM21), UN Met Office Hadley Centre Coupled Model 3.0 (UKMO_HADCM3) and Center for Climate System Research Model for Inter-disciplinary Research on Climate (MIROC3_2_MEDRES). For this study, the ensemble mean of the five models are downloaded. Specifically, the downscaled projections of monthly mean temperatures (°C) and precipitation (mm) for each month of every year from January 2001 – December 2100, and decadal means of annual length of growing season (number of days in a year) for each decade from 2010 – 2100 for the site within the Kuparuk Basin (69°35'48.74"N, 149°26'47.60"W).

For SRESB1, the increase in summer (JJA) air temperature from 2001 – 2100 is 0.019 °C/yr and increase in summer precipitation is 0.17 mm/yr. For SRESA2, the increases in temperature and precipitation are higher than those of the SRESB1. The increase in summer (JJA) air temperature from 2001 – 2100 is 0.036 °C/yr and increase in summer precipitation is 0.266 mm/yr (Figure 3.3).

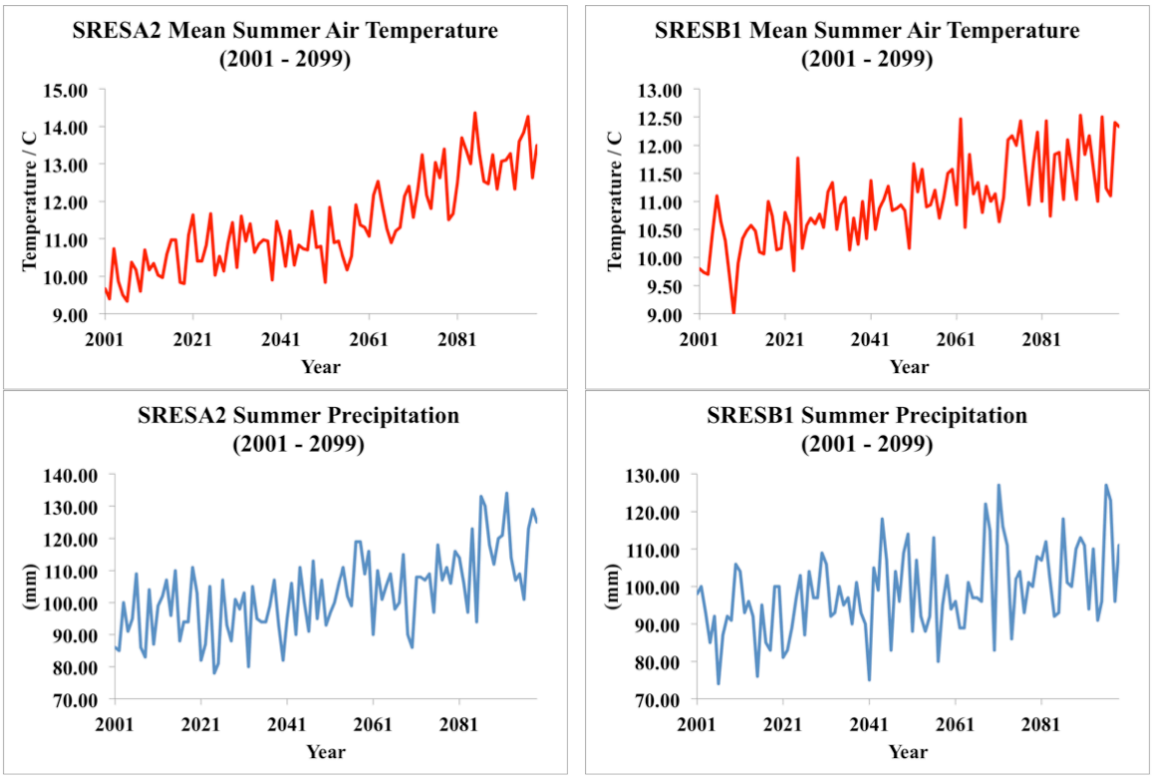

Figure 3.3. Projected mean summer air temperature and total summer precipitation for the study site for two emission scenarios, SRESA2 and SRESB1.

Next, projected daily temperature and precipitation data are constructed from a composite of the historical daily meteorological data from the MET station at Sagwon and monthly temperature and precipitation GCM outputs (2000 – 2099). Data sets from the Sagwon MET station comprised of mean summer (JJA) daily precipitation and temperature (2001 – 2008). Projected daily precipitation is calculated first. For example, to calculate precipitation on 01 Jun 2020, the historical daily site precipitation data on 01 June is divided by its corresponding monthly mean and multiplied by the projected monthly mean from the GCM output. The constructed projected daily precipitation data to be used for climate change simulation in Chapter 7 are shown on Figure 3.5.

However, since an integrated ground temperature (mean of ground surface temperature and soil temperature 5, 10, 20 and 30 cm) is utilized in in the study conducted in Chapter 7, construction of projected integrated ground temperature data requires additional thought. Base on the understanding that ground temperature signals are the phase shifted and amplitude attenuated version of the corresponding air temperature signals from a study conducted by *Cheng et al* [2010] (see Appendix Chapter), an empirical relationship between surface air temperature and the integrated air-soil temperature based on 2000 – 2008 temperature data at Sagwon for the summer growing season is derived.

The analytical solution to a sinusoidal signal of mean temperature, $\overline{T}$, and amplitude A_o applied at the surface of a homogenous infinite half-space is [*Carslaw and Jaeger* 1959]:

$$T(z,t) = \overline{T} + A\sin(\omega t - \phi(z)) \tag{3.1}$$

where z is distance from the surface of the half space. ω is the radial frequency, which is 2π times the actual frequency of the signal. A is the signal attenuation of the form:

$$A = A_o \cdot e^{-k \cdot z} \tag{3.2}$$

and ϕ is the phase lag:

$$\phi = k \cdot z \tag{3.3}$$

k is the wave vector

$$k = \frac{1}{\lambda} = \sqrt{\left(\frac{\pi}{D \cdot \tau}\right)} \tag{3.4}$$

and λ, D, τ, are the damping depth for the ground, defined as the characteristic depth at which the temperature signal is attenuated to *1/e* of the surface, the thermal diffusivity of the ground, and the period of the forcing, respectively.

To calculate the integrated ground temperature from air temperature, equation (3.1) is modified such that $\overline{T} = \overline{T}_g$, where $\overline{T}_g$ is the observed mean summer integrated ground temperature, $A_0 = SAT(t) - \overline{T}_a$, where $\overline{T}_a$ is the observed mean summer air temperature and SAT represents surface air temperature. Analysis of air temperature and integrated ground temperature shows no phase lag between the two temperature signals (Figure 3.4). As such, integrated ground temperature can be calculated from air temperature using the following equation:

$$T_g(t) = \overline{T} + A_0(t) \cdot \varepsilon \qquad (3.5)$$

where ε is an attenuation factor. Optimal values of ε are derived through calibration. From the Sagwon data, $\overline{T}_a$ = 8.2 C, $\overline{T}_g$ = 4 C and ε = 0.525. A root mean square error of 0.84 demonstrates that the simulated integrated ground temperature is in good agreement with the observed integrated ground temperature (Figure 3.4).

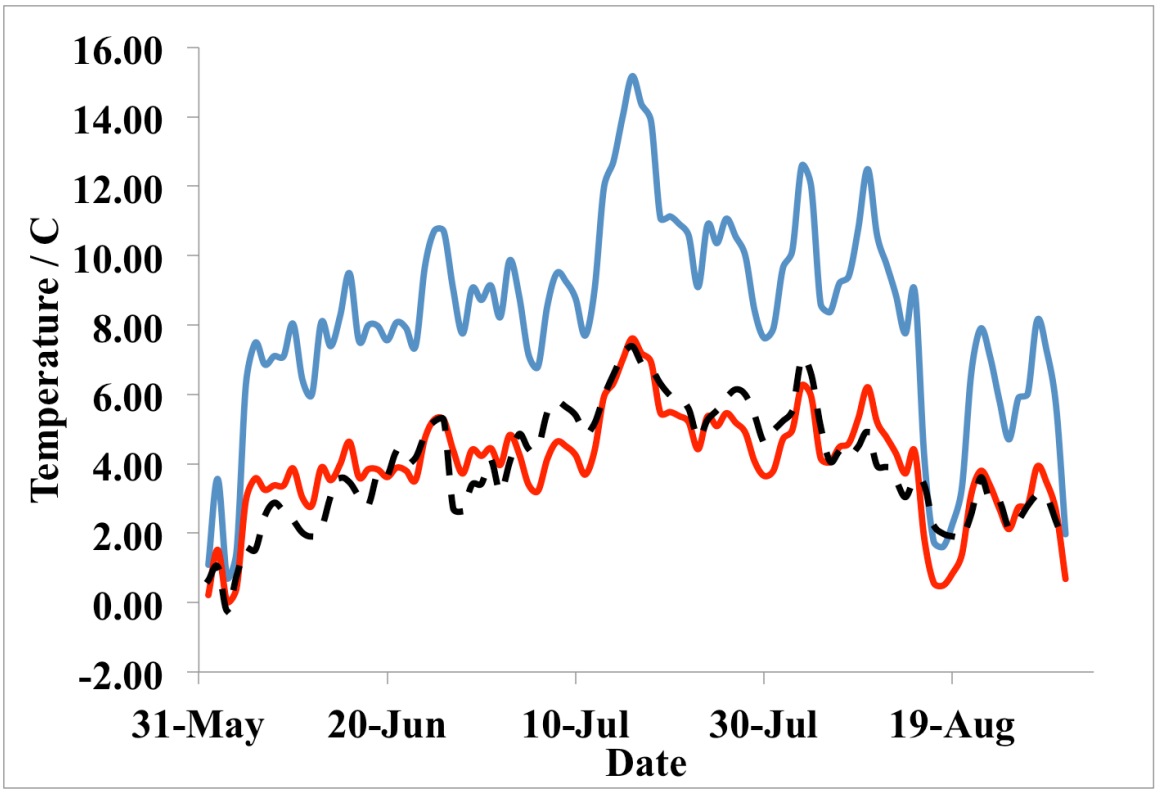

Figure 3.4. Blue line represents observed air temperature at Sagwon site. Dashed black line represent integrated ground temperature at the Sagwon site. Solid red line represents simulated integrated ground temperature at Sagwon site.

Next, equation 3.5 is applied in the calculation of the projected daily integrated ground temperature for both the SRESB1 and SRESA2 scenarios. For example, to calculate integrated ground temperature on 01 Jun 2020, the historical daily site air temperature data on 01 June is divided by its corresponding monthly mean and multiplied by the projected monthly mean from the GCM output. Subsequent application of equation 3.5 to the projected daily air temperature value yields the corresponding daily integrated ground temperature. The constructed projected daily integrated ground temperature data to be used for climate change simulation in Chapter 7 are shown on Figure 3.5.

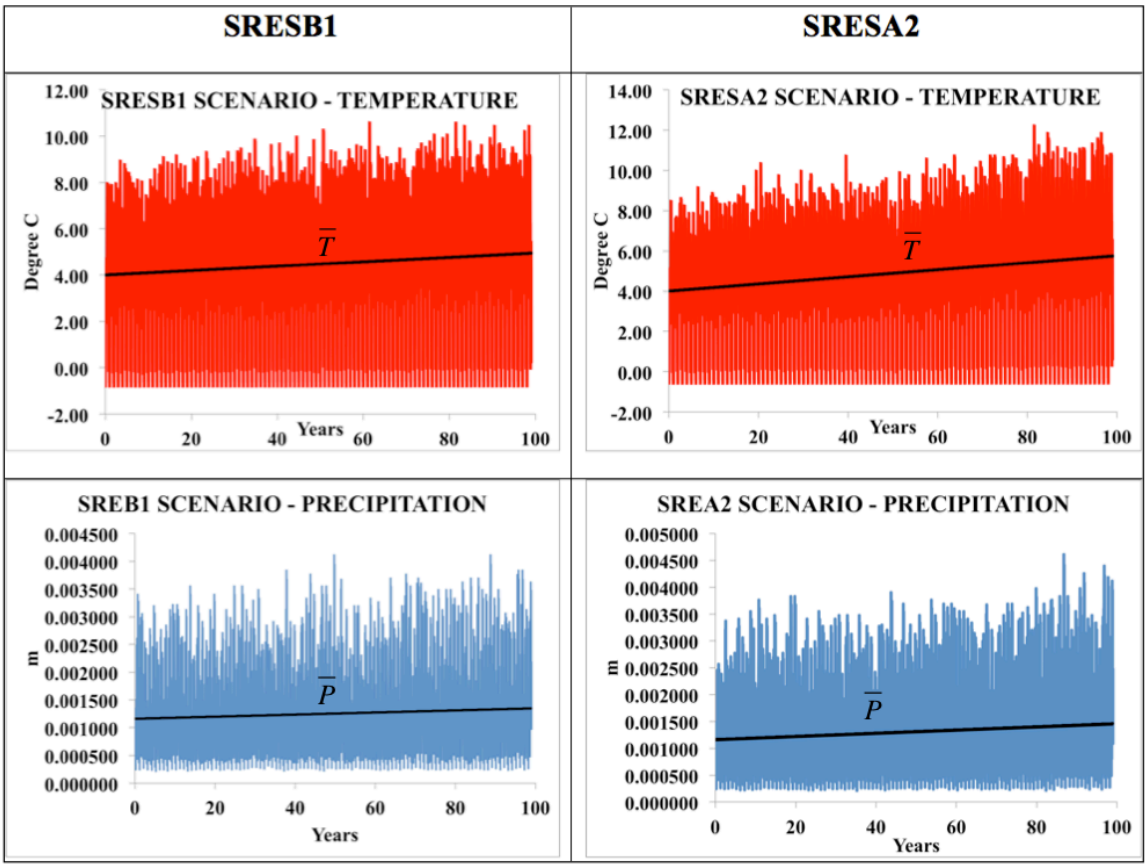

Figure 3.5. Projected daily temperature and precipitation data for both the SRESB1 and SRESA2 scenarios. These data sets are used in climate change simulations in Chapter 7.

3.4 References

Belyea, L. R. (2007), Climatic and topographic limits to the abundance of bog pools, *Hydrol Process*, *21*(5), 675-687.

Bret-Harte, M. S., G. R. Shaver, J. P. Zoerner, J. F. Johnstone, J. L. Wagner, A. S. Chavez, R. F. Gunkelman, S. C. Lippert, and J. A. Laundre (2001), Developmental plasticity allows Betula nana to dominate tundra subjected to an altered environment, *Ecology*, *82*(1), 18-32.

Carslaw, H. S., Jaeger, J. C., 1959: *Conduction of Heat in Solids*. 2nd ed. Oxford University Press, 510 pp.

Chapin, F. S. (1991), Integrated Responses of Plants to Stress, *Bioscience*, *41*(1), 29-36.

Chapin, F. S., and G. R. Shaver (1996), Physiological and growth responses of arctic plants to a field experiment simulating climatic change, *Ecology*, *77*(3), 822-840.

Chapin, F. S., G. R. Shaver, A. E. Giblin, K. J. Nadelhoffer, and J. A. Laundre (1995), Responses of Arctic Tundra to Experimental and Observed Changes in Climate, *Ecology*, *76*(3), 694-711.

Cheng, Y., Stieglitz, M., Pan, F. 2010. Simple Method to Evolve Daily Ground Temperatures From Surface Air Temperatures in Snow Dominated Regions. *Journal of Hydrometeorology*. **11**, 1395 – 1404.

Eppinga, M. B., P. C. de Ruiter, M. J. Wassen, and M. Rietkerk (2009), Nutrients and Hydrology Indicate the Driving Mechanisms of Peatland Surface Patterning, *Am Nat*, *173*(6), 803-818.

Giblin, A. E., K. J. Nadelhoffer, G. R. Shaver, J. A. Laundre, and A. J. Mckerrow (1991), Biogeochemical Diversity Along a Riverside Toposequence in Arctic Alaska, *Ecol Monogr*, *61*(4), 415-435.

Gough, L., P. A. Wookey, and G. R. Shaver (2002), Dry heath arctic tundra responses to long-term nutrient and light manipulation, *Arct Antarct Alp Res*, *34*(2), 211-218.

Hinzman, L. D., D. L. Kane, R. E. Gieck, and K. R. Everett (1991), Hydrologic and Thermal-Properties of the Active Layer in the Alaskan Arctic, *Cold Reg Sci*

Technol, *19*(2), 95-110.

Lapshina, E.D., E. Y. Mouldiyarov, S. V. Vasiliev (2001), Analyses of key area studies. In: Bleuten W, Lapshina ED, Eds. Carbon storage and atmospheric exchange by West Siberian peatlands. Utrecht: Department of Physical Geography, Utrecht University pp 23 – 37.

Mack, M. C., E. A. G. Schuur, M. S. Bret-Harte, G. R. Shaver, and F. S. Chapin (2004), Ecosystem carbon storage in arctic tundra reduced by long-term nutrient fertilization, *Nature*, *431*(7007), 440-443.

McKane, R. B., E. B. Rastetter, G. R. Shaver, K. J. Nadelhoffer, A. E. Giblin, J. A. Laundre, and F. S. Chapin (1997), Climatic effects on tundra carbon storage inferred from experimental data and a model, *Ecology*, *78*(4), 1170-1187.

McKane, R. B., E. B. Rastetter, G. R. Shaver, K. J. Nadelhoffer, A. E. Giblin, J. A. Laundre, and F. S. Chapin (1997), Reconstruction and analysis of historical changes in carbon storage in arctic tundra, *Ecology*, *78*(4), 1188-1198.

McNamara, J. P., D. L. Kane, J. E. Hobbie, and G. W. Kling (2008), Hydrologic and biogeochemical controls on the spatial and temporal patterns of nitrogen and phosphorus in the Kuparuk River, arctic Alaska, *Hydrol Process*, *22*(17), 3294-3309.

Peterson, B. J., R. M. Holmes, J. W. McClelland, C. J. Vorosmarty, R. B. Lammers, A. I. Shiklomanov, I. A. Shiklomanov, and S. Rahmstorf (2002), Increasing river discharge to the Arctic Ocean, *Science*, *298*(5601), 2171-2173.

Ping, C. L., G. J. Michaelson, M. T. Jorgenson, J. M. Kimble, H. Epstein, V. E. Romanovsky, and D. A. Walker (2008), High stocks of soil organic carbon in the North American Arctic region, *Nat Geosci*, *1*(9), 615-619.

Rastetter, E. B., G. I. Agren, and G. R. Shaver (1997), Responses of N-limited ecosystems to increased CO2: A balanced-nutrition, coupled-element-cycles model, *Ecol Appl*, *7*(2), 444-460.

Rastetter, E. B., B. L. Kwiatkowski, S. Le Dizes, and J. E. Hobbie (2004), The role of down-slope water and nutrient fluxes in the response of Arctic hill slopes to climate change, *Biogeochemistry*, *69*(1), 37-62.

Rastetter, E. B., S. S. Perakis, G. R. Shaver, and G. I. Agren (2005), Terrestrial C sequestration at elevated-CO2 and temperature: The role of dissolved organic N loss, *Ecol Appl*, *15*(1), 71-86.

Rietkerk, M., S. C. Dekker, M. J. Wassen, A. W. M. Verkroost, and M. F. P. Bierkens (2004), A putative mechanism for bog patterning, *Am Nat*, *163*(5), 699-708.

Shaver, G. R., W. D. Billings, F. S. Chapin, A. E. Giblin, K. J. Nadelhoffer, W. C. Oechel, and E. B. Rastetter (1992), Global Change and the Carbon Balance of Arctic Ecosystems, *Bioscience*, *42*(6), 433-441.

Shaver, G. R., S. M. Bret-Harte, M. H. Jones, J. Johnstone, L. Gough, J. Laundre, and F. S. Chapin (2001), Species composition interacts with fertilizer to control long-term change in tundra productivity, *Ecology*, *82*(11), 3163-3181.

Shaver, G. R., F. Chapin, and B. L. Gartner (1986), Factors Limiting Seasonal Growth and Peak Biomass Accumulation in Eriophorum-Vaginatum in Alaskan Tussock Tundra, *J Ecol*, *74*(1), 257-278.

Shaver, G. R., and F. S. Chapin (1980), Response to Fertilization by Various Plant-Growth Forms in an Alaskan Tundra - Nutrient Accumulation and Growth, *Ecology*, *61*(3), 662-675.

Shaver, G. R., and F. S. Chapin (1986), Effect of Fertilizer on Production and Biomass of Tussock Tundra, Alaska, USA, *Arctic Alpine Res*, *18*(3), 261-268.

Shaver, G. R., and F. S. Chapin (1991), Production - Biomass Relationships and Element Cycling in Contrasting Arctic Vegetation Types, *Ecol Monogr*, *61*(1), 1-31.

Stieglitz, M., A. Giblin, J. Hobbie, M. Williams, and G. Kling (2000), Simulating the effects of climate change and climate variability on carbon dynamics in Arctic tundra, *Global Biogeochem Cy*, *14*(4), 1123-1136.

Stieglitz, M., R. B. McKane, and C. A. Klausmeier (2006), A simple model for analyzing climatic effects on terrestrial carbon and nitrogen dynamics: An arctic case study, *Global Biogeochem Cy*, *20*(3).

Walsh, J. E., W. L. Chapman, V. Romanovsky, J. H. Christensen, and M. Stendel (2008), Global Climate Model Performance over Alaska and Greenland, *J Climate*,

21(23), 6156-6174.

Williams, M., E. B. Rastetter, G. R. Shaver, J. E. Hobbie, E. Carpino, and B. L. Kwiatkowski (2001), Primary production of an arctic watershed: An uncertainty analysis, *Ecol Appl*, *11*(6), 1800-1816.

4. SIMULATIONS

In this chapter, the simulations conducted in this thesis are described in details.

4.1 Simulations to Study the Impact of Vegetation Self-Organization and Topography on Vegetation Patterning

In Chapter 5, the goal is to examine the impact of vegetation self-organization and topography on wetland vegetation patterning using the baseline Nutrient Depletion Model (NDM). The baseline NDM is described by equations 2.4 – 2.6 in Chapter 2. For all simulations conducted in Chapter 5, the original parameter values (Table 4.1), and the initial and boundary conditions employed by *Rietkerk et al.* [2004] are used.

Table 4.1: Model parameters and values used to generate maze pattern, string pattern and vegetation bands parallel to flow direction. Parameter values from *Rietkerk et al*. [2004].

Symbol	Interpretation	Unit	Value
g	Plant growth parameter	$m^3\ g_N^{-1}\ day^{-1}$	5.48×10^{-4}
μ	Plant uptake parameter	$m^3\ g_B^{-1}\ day^{-1}$	5.48×10^{-6}
d	Recycling parameter	day^{-1}	2.74×10^{-4}
b	Plant loss parameter	day^{-1}	5.48×10^{-4}
D_B	Diffusion coefficient for biomass	$m^2\ day^{-1}$	5.48×10^{-3}
p	Precipitation	$m\ day^{-1}$	1.37×10^{-3}
t_v	Plant transpiration parameter	$m^3\ g_B^{-1}\ day^{-1}$	1.4×10^{-5}
e	Evaporation parameter	$m\ day^{-1}$	8.22×10^{-4}
k	Hydraulic conductivity	$m\ day^{-1}$	1.37
N_{in}	Nutrient input	$g_N^{-1}\ m^{-2}\ day^{-1}$	4.1×10^{-3}
r	Nutrient loss parameter	day^{-1}	2.74×10^{-4}
D_N	Diffusion coefficient for nutrient	$m^2\ day^{-1}$	2.74×10^{-2}

First, the baseline NDM is employed to simulate three vegetation patterns that are characteristics of wetland ecosystem: maze pattern, perpendicular string pattern and parallel string pattern. To simulate a maze pattern on flat ground, dc = 0 m, and k_x/k_y = 1. To simulate perpendicular string patterns, dc = 0.015 m to simulate moderate regional hydraulic gradient and introduce anisotropic hydraulic conductivity by setting k_x/k_y = 0.75. To simulate parallel string, a similar degree of anisotropy in hydraulic conductivity is retained and k_x/k_y = 0.75. However, the magnitude of the regional hydraulic gradient is increased and dc = 0.025 m.

Next, sensitivity analysis on pertinent hydrologic parameters of the model is conducted by performing two sets of simulations to study sequences of vegetation states that accompany gradual changes in plant transpiration rate, regional hydraulic gradient that is oriented in the y-direction and degree of anisotropy in hydraulic conductivity. The first set of simulations demonstrates how changes in plant transpiration and regional hydraulic gradient affect vegetation patterning. The main parameters varied are the plant transpiration parameter, t_v, and dc. t_v varies between 50% and 200% of 1.4 x 10^{-5} m^3 g_B^{-1} day^{-1} (a value used in the earlier simulations following *Rietkerk et al.*, 2004). dc varies from 0 to 0.025 m. The values of regional hydraulic gradient are constrained to below 0.03 to maintain consistency with observed values. *Belyea* [2007] has shown that surface gradients in northern peatlands can range from 0 to 0.03 m m^{-1}. The second set of simulations demonstrates the interactive effects of anisotropic hydraulic conductivity and regional hydraulic gradient on vegetation patterns. The main parameters of interest are k_x/k_y and dc, which are gradually increased from 0 to 1 and 0 to 0.025 m, respectively. t_v is kept constant at 1.4 x 10^{-5} m^3 g_B^{-1} day^{-1}.

4.2 Simulations to Study the Impact of Vegetation Self-Organization and Topography on Biomass Growth Dynamics

In Chapter 6, the goal is to examine the impact of vegetation self-organization and watershed topography over ecosystems biomass growth dynamics using the modified NDM. The modified NDM is described by equations 2.7 – 2.12 in Chapter 2. We simulate steady state and transient dynamics of a western Siberian peatland (see Chapter 3, section 3.1 for site description). The two questions to address are: (1) how do watershed topography and vegetation self-organizing feedbacks together and separately impact equilibrium plant biomass stocks across nutrient input and rainfall gradients, and (2) under similar initial and environmental conditions, will the transient response of a system with self-organizing feedback differ from a system without self-organizing feedback.

To explicitly tease apart the impacts of topographic control and self-organizing control, paired simulations by (a) the modified NDM that includes for both topographic control and self-organizing mechanisms together (TC+SO model) (see Chapter 2, equations 2.7, 2.8, 2.9, 2.10), and (b) the modified NDM that includes for topographic control (TC model) alone (see Chapter 2, equations 2.7, 2.9, 2.11, 2.12) are conducted.

In the first set of simulations, the biomass trajectories of both the TC and TC+SO models on flat ground (slope = 0%), under different magnitudes of constant nutrient inputs and rainfall are simulated. The nutrient inputs range from 0.0041 g m^{-2} d^{-1},(1.5g m^{-2} yr^{-1}) to 0.0015 g m^{-2} d^{-1} (0.56g m^{-2} yr^{-1}). All are within the range observed for western Siberia [*Bouwman and van Vuuren*, 1999] and explored in the *Reitkerk et al.* [2004] study. Three rainfall regimes are explored: 250mm yr^{-1} (low rainfall), 375mm yr^{-1}

(intermediate rainfall) and 500mm yr^{-1} (high rainfall). All are within the range observed for western Siberia [*Frey and Smith*, 2003]. In the second set of simulations, the biomass trajectories of both the TC and TC+SO models on a gentle slope (slope = 0.25%), but under similar nutrient inputs and rainfall values as the first set of simulations are simulated. Equilibrium biomass values from these first two sets of simulations will allow us to address the first question posed above.

The final set of simulations is aimed at addressing the last question. First, both TC+SO and TC models build up equal stocks of vegetation biomass, detritus and nutrient under the following environmental condition: nutrient influx = 0.0041gN m^{-2} d^{-1}, annual precipitation = 500 mm and slope = 0%. At 2000 years, when the vegetation biomass is at steady state (<1% of difference in biomass between Year 2000 and Year 1600), the following changes to the current nutrient influx rate are imposed: (1) 50% increase, (2) 50% decrease, and (3) 100% decrease (set to zero).

For all simulations, the model grid consists of 128 x 128 elements that are 3m on each side. For initial condition, we randomly seed 10% of the domain with biomass patches of 100 gB m^{-2}. Parameter values fall within the ranges as discussed by *Reitkerk et al.* [2004] (Table 4.2).

Table 4.2: Model parameters and values of the Nutrient Depletion Model used in the simulations to examine the impact of vegetation self-organization and topography over ecosystems biomass growth dynamics.

Symbol	Interpretation	Unit	Value
g	Plant growth parameter	$m^3\ g_N^{-1}\ day^{-1}$	5.48×10^{-4}
μ	Plant uptake parameter	$m^3\ g_B^{-1}\ day^{-1}$	5.48×10^{-6}
d	Plant mortality	day^{-1}	8.22×10^{-4}
D_B	Diffusion coefficient for biomass	$m^2\ day^{-1}$	5.48×10^{-3}
p	Precipitation	$m\ day^{-1}$	1.37×10^{-3}
t_v	Plant transpiration parameter	$m^3\ g_B^{-1}\ day^{-1}$	1.4×10^{-5}
e	Evaporation parameter	$m\ day^{-1}$	8.22×10^{-4}
k	Hydraulic conductivity	$m\ day^{-1}$	1.37
r	Nutrient loss parameter	day^{-1}	2.74×10^{-4}
ν	Potential peat decay rate	day^{-1}	2.0×10^{-5}
θ	Soil porosity	dimensionless	0.85

4.3 Simulations to Study the Impact of Vegetation Self-Organization and Topography on Arctic Carbon-Nitrogen Dynamics

In Chapter 7, the modified NDM is applied to arctic Alaska to explore the impacts of topography and self-organizing feedback on carbon-nitrogen (C-N) dynamics of an arctic ecosystem. The modified NDM is described by equations 2.13 – 2.18 in Chapter 2. The two questions to be addressed are: (1) how do watershed topography and vegetation self-organizing feedbacks together and separately impact the accumulation of plant and soil carbon stocks since the last glacial maxima, and (2) under similar initial conditions and climate forcings, will the transient response of a system with vegetation self-organizing feedbacks differ from a system without said feedback (topography only).

Similar to Chapter 6, to explicitly tease apart the impacts of topographic control and self-organizing control, paired simulations by (a) the modified NDM that includes for

both topographic control and self-organizing mechanisms together (TC+SO model) (see Chapter 2, equations 2.13, 2.14, 2.15, 2.16), and (b) the modified NDM that includes for topographic control (TC model) alone (see Chapter 2, equations 2.13, 2.15, 2.17, 2.18) are conducted.

Two sets of simulations are conducted: (1) an arctic growing season (June, July and August) baseline simulation that simulates the accumulation of present day plant and soil C-N stocks, and (2) climate change scenarios for the period of 2000 – 2099 to explore the potential changes to the arctic C-N dynamics.

4.3.1 Baseline Simulations

An arctic growing season (June, July and August) baseline simulation that simulate the accumulation of present day plant and soil C-N stocks from the beginning of the current postglacial period (10,000 yr BP) is conducted. Both the TC and TC+SO models are calibrated based on the long-term soil and plant C and N measurements from the Arctic LTER (see Chapter 3, section 3.3 for data description). For initial condition, we randomly seed 5% of a bare hill slope with biomass patches of 100 gC m^{-2}. Initially, the landscape is uniformly covered with detritus C of 50 gC m^{-2}, nutrient of 1.5 gN m^{-2} and hydraulic head of 1 m. For this study site, summer precipitation and integrated ground temperature (mean of ground surface and soil temperature 5, 10, 20 and 30 cm) are 100 mm and 4°C respectively (see Chapter 3, section 3.3 for data description). Input of N into the system was set at 0.115 gN m^{-2} yr^{-1}. Inputs of N into the ecosystem around Arctic LTER are mainly through N fixation and atmospheric deposition and can range between 0.1 – 0.2 gN m^{-2} yr^{-1}.

Table 4.3. Model parameters and values of the Nutrient Depletion Model used in the simulations to examine the impact of vegetation self-organization and topography over ecosystems arctic carbon-nitrogen dynamics.

	Interpretation	Unit	Value	References
g	Plant growth parameter	$m^3\ g_N^{-1}\ day^{-1}$	2.63×10^{-3}	*Shaver and Chapin* [1991]
μ	Plant uptake parameter	$m^3\ g_B^{-1}\ day^{-1}$	2.63×10^{-5}	*Shaver and Chapin* [1991]
d	Plant mortality	day^{-1}	1.85×10^{-4}	*Shaver and Chapin* [1991]
D_B	Biomass diffusion coefficient	$m^2\ day^{-1}$	5.48×10^{-3}	*Rietkerk et al*. [2004]
p	Precipitation	$m\ day^{-1}$	1.16×10^{-3}	*Kane and Hinzman* [2013]
t_v	Plant transpiration parameter	$m^3\ g_B^{-1}\ day^{-1}$	1.4×10^{-5}	Back-calculated
e	Evaporation parameter	$m\ day^{-1}$	0.82×10^{-4}	Back-calculated
k	Hydraulic conductivity	$m\ day^{-1}$	1.37	*Reeve et al*. [2001], *Givnish et al*. [2008
η	Peat fraction decomposed into N	dimensionless	0.31	Back-calculated
α	C:N ratio	dimensionless	33	*McKane et al*. [1997]
ν	Potential peat decay rate	day^{-1}	2.6×10^{-3}	Back-calculated
D_N	Nutrient diffusion coefficient	$m^2\ day^{-1}$		*Rietkerk et al*. [2004]
θ	Soil porosity	dimensionless	0.85	*Hinzman et al*. [1991]

4.3.2 Climate Change Simulations

To examine the effects of climate change on the arctic ecosystem, we conducted the following climate change scenarios on both the SO+TC and TC models as described in Table 4.4. We chose two emission scenarios from the International Panel on Climate Change (IPCC) Fourth Assessment Report (AR4). There have been four assessment reports from the IPCC since 1990. With the AR4 being the latest released in 2007. The Special Report on Emission Scenario B1 (SRESB1) represents the future scenario that will result in the lowest warming, while Special Report on Emission Scenario A2 (SRESA2) will result in a much warmer climate.

Table 4.4. Summary table of climate change scenarios investigated. Effects of change in temperature: mean(T_M), and variability (T_V), change in precipitation: mean (P_M) and variability (P_V).

SRESB1	**SRESA2**
T_M	T_M
P_M	P_M
T_M + P_M	T_M + P_M
T_M + T_V	T_M + T_V
P_M + P_V	P_M + P_V
(T_M + T_V) + (P_M + P_V)	(T_M + T_V) + (P_M + P_V)

The simulated results from year 10,000 of the baseline simulations of the TC+SO and TC models are utilized as initial conditions for all subsequent climate change scenario simulations. For the climate change simulations, we focus on the center region (size = 512 x 512 grid cells) of the original landscape (size = 1024 x 1024 grid cells). Baseline simulation results of this region are similar to the baseline simulation results of the original 1024 x 1024 landscape. For the TC+SO model, at equilibrium, simulated biomass C is 600 gC m^{-2} and detrital C is 16,193 gC m^{-2}. Simulated loss of dissolved

nitrogen from the ecosystem is ~0.115 gN m^{-2} yr^{-1}. Simulated NPP equal to ~104 gC m^{-2} yr-1, and is balanced by detrital decomposition. For the TC model, at equilibrium, simulated biomass C is 597 gC m^{-2} and detrital C is 16,091 gC m^{-2}. Simulated loss of dissolved nitrogen from the ecosystem is ~0.115 gN m^{-2} yr^{-1}. Simulated NPP equal to ~103 gC m^{-2} yr^{-1}, and is balanced by detrital decomposition.

For all combinations of T_V and P_V scenarios, projected daily temperature and precipitation data constructed in Chapter 3 (see section 3.3.2.2) are used as forcing data. For all T_M scenarios (Table 4.4), temperature is linearly increased by 0.95°C (SRESB1) and 1.8°C (SRESA2) from a baseline temperature of 4°C over a hundred years. For all P_M scenarios (Table 4.4), precipitation is linearly increased by 17 mm (SRESB1) and 26.6 mm (SRESA2) over a hundred years. For a baseline integrated ground temperature of 4°C, warming of 0.95°C and 1.8°C, soil respiration will increase by 15% and 30% for the SRESB1 and SRESA2 scenario respectively. It is reasonable to assume that plant uptake will keep up with soil decomposition; the plant growth parameter was incremented linearly over the 100-year warming [*Stieglitz et al*., 2006]. In contrast, there is no response in plant growth to increase in precipitation. In arctic Alaska, water is not known to be a growth-limiting factor [*Oberbauer and Miller*, 1982]. Further, field studies have shown minimal impact of increase summer precipitation on total tundra productivity [*Keuper et al*., 2012].

4.4 References

Belyea, L. R. (2007), Climatic and topographic limits to the abundance of bog pools, *Hydrological Processes*, *21*(5), 675-687.

Givnish, T. J., J. C. Volin, V. D. Owen, V. C. Volin, J. D. Muss, and P. H. Glaser (2008), Vegetation differentiation in the patterned landscape of the central Everglades: importance of local and landscape drivers, *Global Ecol Biogeogr*, *17*(3), 384-402.

Hinzman, L. D., D. L. Kane, R. E. Gieck, and K. R. Everett (1991), Hydrologic and Thermal-Properties of the Active Layer in the Alaskan Arctic, *Cold Reg Sci Technol*, *19*(2), 95-110.

Keuper, F., F. J. W. Parmentier, D. Blok, P. M. van Bodegom, E. Dorrepaal, J. R. van Hal, R. S. P. van Logtestijn, and R. Aerts (2012), Tundra in the Rain: Differential Vegetation Responses to Three Years of Experimentally Doubled Summer Precipitation in Siberian Shrub and Swedish Bog Tundra, *Ambio*, *41*, 269-280.

McKane, R. B., E. B. Rastetter, G. R. Shaver, K. J. Nadelhoffer, A. E. Giblin, J. A. Laundre, and F. S. Chapin (1997), Climatic effects on tundra carbon storage inferred from experimental data and a model, *Ecology*, *78*(4), 1170-1187.

Oberbauer, S., and P. C. Miller (1982), Growth of Alaskan Tundra Plants in Relation to Water Potential, *Holarctic Ecol*, *5*(2), 194-199.

Reeve, A. S., D. I. Siegel, and P. H. Glaser (2001), Simulating dispersive mixing in large peatlands, *J Hydrol*, *242*(1-2), 103-114.

Rietkerk, M., S. C. Dekker, M. J. Wassen, A. W. M. Verkroost, and M. F. P. Bierkens (2004), A putative mechanism for bog patterning, *Am Nat*, *163*(5), 699-708.

Shaver, G. R., and F. S. Chapin (1991), Production - Biomass Relationships and Element Cycling in Contrasting Arctic Vegetation Types, *Ecol Monogr*, *61*(1), 1-31.

Stieglitz, M., R. B. McKane, and C. A. Klausmeier (2006), A simple model for analyzing climatic effects on terrestrial carbon and nitrogen dynamics: An arctic case study, *Global Biogeochem Cy*, *20*(3).

5. THE INFLUENCE OF TOPOGRAPHY AND VEGETATION SELF-ORGANIZATION OVER PATTERN FORMATION IN WETLAND ECOSYSTEMS

5.1 Introduction

Wetland ecosystems are often characterized by vegetation patterns. For instance, maze patterns are commonly observed in northern bogs. These patterns consist of interconnected hummock forming ridges that are slightly elevated above wetter hollows. Another pattern characteristic of the northern bogs is the string pattern [*Sakaguchi,* 1980*; Foster et al.,* 1983], which consists of elevated vegetation bands that are orientated perpendicular to the water flow direction and which are separated by waterlogged sloughs (hereafter this type of pattern will be referred to as *perpendicular strings*). Vegetation bands orientated parallel to the prevailing flow direction have also been observed in wetland ecosystems [*Ellery et al.,* 2003*; Ogden.,* 2005*; San José et al.,* 2001] (hereafter this type of pattern will be referred to as *parallel strings*). The ridge and slough ecosystem of the Florida Everglades is one such example of a parallel string pattern.

A number of conceptual and simulation models have been proposed to explain the formation of maze and string patterns in wetland ecosystems [*Swanson and Grigal,* 1988; *Hilbert et al.,* 2000; *Rietkerk et al.,* 2004; *Eppinga et al.,* 2009; *Larsen and Harvey,* 2010]. For example, *Hilbert et al.* [2000] invoked a peat accumulation mechanism to explain the formation of maze patterns on flat ground. The Hilbert model describes the interaction between peat production and depth to water table. At sites where the peat

surface is sufficiently above the water table, vegetation growth is near optimal, the rate of organic matter input into the soil is higher than the rate of decomposition, and thus peat accumulates. On the other hand, at saturated sites, vegetation growth is limited, the rate of organic matter input into the soil is lower than the rate of decomposition, and thus peat depth decreases. With time, sites with moderate soil wetness connect and form maze-like structures that surround waterlogged hollows.

A ponding mechanism has been invoked to explain the development of perpendicular strings [*Swanson and Grigal,* 1988] in bogs. Specifically, a vegetation patch impedes the downslope flow of water. This then leads to ponding of upslope water, which locally increases hydroperiod and water depth and which can inhibits the upslope expansion of emergent vegetation. At a distance further upslope the water surface is lower which provides favorable conditions for patch growth. At the same time that the alternating conditions lead to growth or inhibition along the hydrologic gradient, individual patches may expand in the direction perpendicular to the hydrologic gradient. Together, these processes ultimately yield strings of vegetation perpendicular to the prevailing flow.

Nutrient accumulation has also been proposed as a mechanism for vegetation pattern formation [*Rietkerk et al.,* 2004]. *Rietkerk et al.* [2004] developed a spatially explicit, advection-reaction-diffusion type model (henceforth called the Rietkerk model) to describe the formation of maze and perpendicular string patterns. Specifically, a scale dependent feedback between the plant biomass, transpiration and nutrient accumulation drives the formation of the vegetation patterns. Vegetation induces subsurface water and nutrient fluxes towards itself through transpiration, activating further growth, which

increases transpiration and nutrient accumulation. In this positive feedback, the plants function as activators that promote additional growth within short distances, leading to patches of relatively higher vegetation densities than the surrounding environment (short distance facilitation). The nutrient accumulation caused by plant growth also acts as an inhibitor of growth at a distance by depleting the available nutrients for other plants or patches (long distance inhibition).

In a recent modeling study, *Eppinga et al.* [2009] identified three important pattern-structuring mechanisms in wetland ecosystems: peat accumulation [*Hilbert et al.,* 2000*; Belyea and Clymo,* 2001], water ponding [*Swanson and Grigal,* 1988*; Couwenberg,* 2005*; Couwenberg and Joosten,* 2005] and nutrient accumulation [*Rietkerk et al.,* 2004b]. *Eppinga et al.* [2009] incorporated these processes into a single modeling framework that describes vegetation patterning as a result of interactions between four state variables: plant biomass, peat thickness, groundwater table, and nutrient availability. *Eppinga et al.* [2009] use this model to conduct a factorial analysis to explore how these mechanisms affect the resulting pattern formation on both flat ground and a synthetic straight slope. Their results provided the first insight as to how topography and self-organizing mechanisms can together impact the form and orientation of the resulting vegetation pattern on the landscape. However, to date no other studies have been conducted to elucidate the impacts of topography and self-organizing mechanism on form and orientation of wetland vegetation patterns.

In this chapter, the goal is to examine the impact of vegetation self-organization and topography on wetland vegetation patterning using the baseline Nutrient Depletion Model (NDM). The baseline NDM is described by equations 2.4 – 2.6 in Chapter 2.

Simulations conducted in this chapter are described in details in Chapter 4 (see Section 4.1). Simulation results are presented and discussed in details in this chapter.

5.2 Simulation Results

Modeling results show that in the absence of a regional hydraulic gradient (i.e. dc = 0), a maze pattern develops with time (Figure 5.1a). In the presence of a moderate regional hydraulic gradient and when $k_x/k_y < 1$, the vegetation patches aggregate and spread in the direction perpendicular of the downhill flow, leading to the formation of the perpendicular string pattern (Figure 5.1b). However, in the presence of a larger regional hydraulic gradient, vegetation patches aggregate and spread in the direction of the downhill flow, leading to the formation of regular vegetated bands oriented parallel to the flow direction (Figure 5.1c). For all three vegetation patterns, the spatial distribution of dissolved nutrient matches the distribution of biomass.

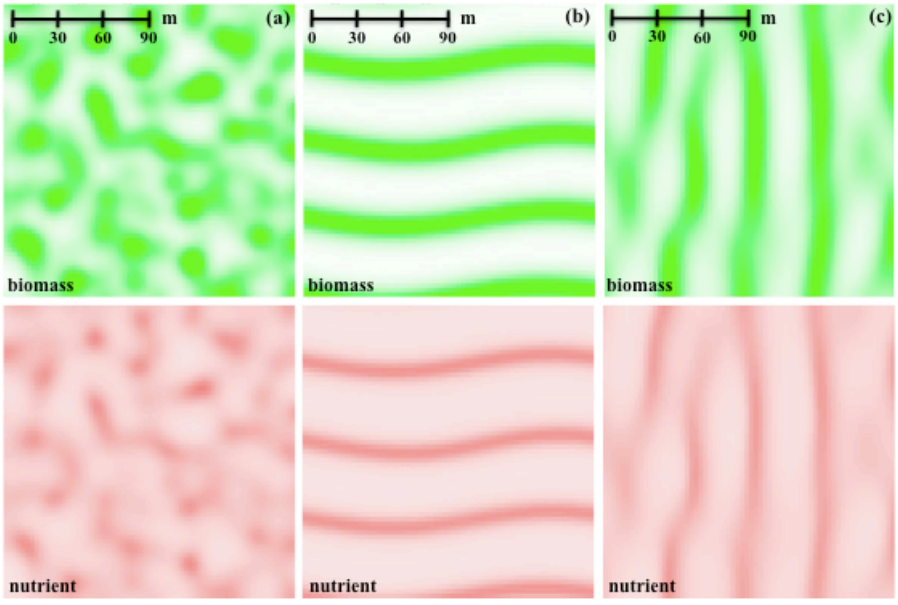

Figure 5.1: Simulated vegetation patterns. (1a) Maze pattern on flat ground. (1b) String pattern on slope. (1c) Vegetation bands parallel to prevailing flow direction. Plant biomass are shown by green colors; darker green color indicate a higher biomass. Values range from 0 g m^{-2} (white color) to 1,500 g m^{-2} (dark green).

Figure 5.2a shows the resulting vegetation states from the sensitivity analysis of plant transpiration rate and regional hydraulic gradient (selected results shown). The model predicts homogenous distribution of plant biomass at a low plant transpiration rate of $t_v = 0.7 \times 10^{-5}$ m^3 g_B^{-1} day^{-1}, independent of c (Figure 5.2a, first row). In the absence of a regional hydraulic gradient, as plant transpiration rate increases, maze patterns form first, then patch patterns start to emerge. (Figure 5.2a, first column). In the presence of a large regional hydraulic gradient ($dc = 0.025$ m), and as plant transpiration rate increases, parallel strings start to form. As t_v continues to increase, the distance between the vegetation bands increases, suggesting that spatial distance of inhibition is proportional to t_v (Figure 5.2a, last column).

Sensitivity analyses demonstrate the vegetation patterning which results from variable degrees of anisotropy in the hydraulic conductivities and regional hydraulic gradients (Figure 5.2b, selected results shown). For $k_x/k_y \leq 0.5$, the model predicts the formation of perpendicular strings for $dc = 0$ to 0.015 (Figure 5.2b). However, for $dc > 0.015$, and with $k_x/k_y \leq 0.5$, homogenous distributions of plant biomass are produced. At $k_x/k_y = 1$, patch patterns form in the presence of small regional hydraulic gradients, while parallel string patterns form (Figure 5.2b, last column) in the presence of a large regional hydraulic gradient ($dc = 0.025$m).

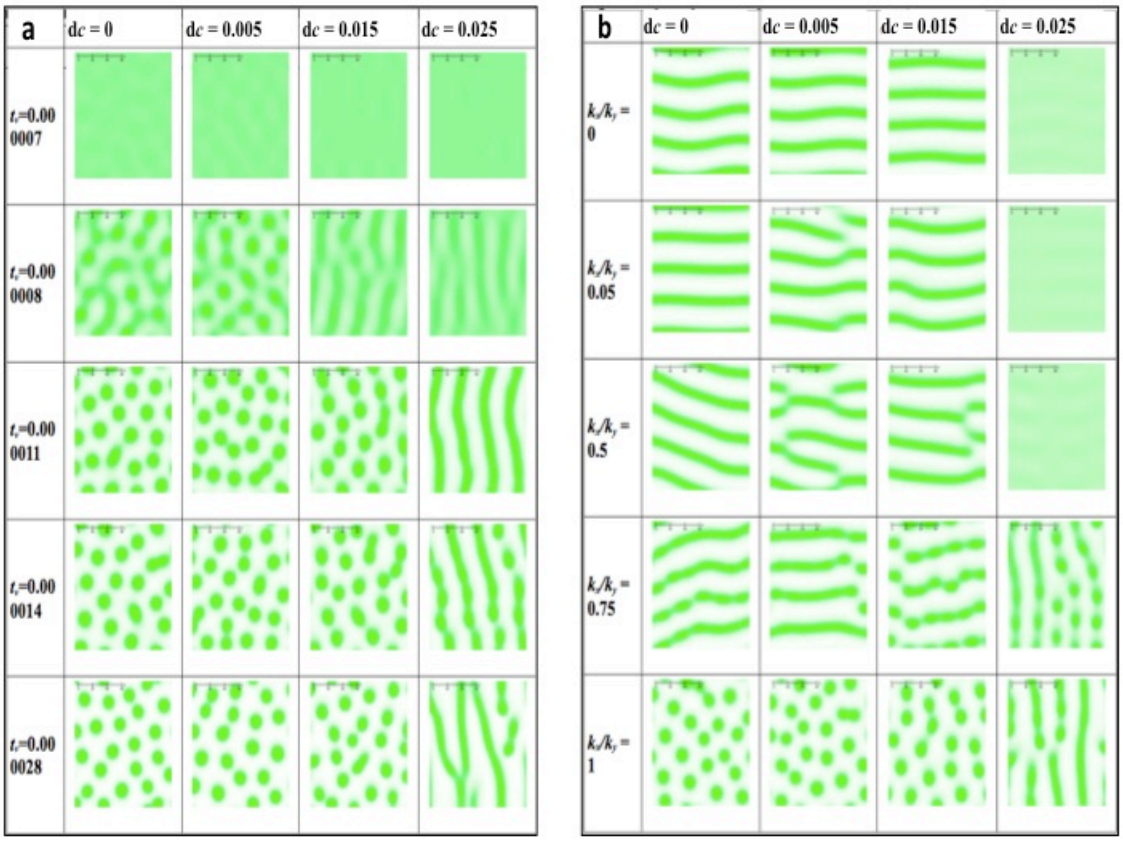

Figure 5.2: (a) Spatial patterns of plant biomass for $0.000007 < t_v < 0.000028$ m^3 g_B^{-1} day^{-1} and $0 < dc < 0.025$ m. (b) Spatial patterns of plant biomass for $0 < k_x/k_y < 1$ and $0 < dc < 0.025$ m. Plant biomass are shown by green colors; darker green color indicate a higher biomass. Values range from 0 g m^{-2} (white color) to 1,500 g m^{-2} (dark green).

5.3 Discussion

Simulation results demonstrate that the relative magnitude of the *x*-*y* advection rates as represented through anisotropy in the regional hydraulic gradient (i.e. $dc/dy \neq 0$) or hydraulic conductivity (i.e. $k_x/k_y \neq 1$), determine the landscape-scale vegetation patterns in nutrient-limited wetland ecosystems. In the absence of anisotropy, the advection of water and dissolved nutrients towards the vegetation (local advection) are uniform in both *x*-*y* directions and results in maze patterns. In the presence of a regional hydraulic gradient, fluxes of water and dissolved nutrients flow in the direction of the

gradient. When the regional advection of water and dissolved nutrients is smaller than the local advection of water and dissolved nutrients, the nutrients released from the turnover of vegetation is retained locally for growth, allowing patch patterns to form and which are maintained at steady state (Figure 5.2a, first three columns for $t_v > 0.7 \times 10^{-5}$ m^3 g_B^{-1} day^{-1}). On the other hand, when the regional advection of water and dissolved nutrients is greater than the local fluxes, nutrients released from the turnover of vegetation are transported in the direction of the regional hydraulic gradient. For example, in the presence of a regional hydraulic gradient in the *y*-direction, the advection of water and nutrients towards vegetation in the *x*-direction inhibits the growth of perpendicular strings, while the flux of nutrients in the *y*-direction promotes the growth of parallel strings. The effect of the regional hydraulic gradient on the resulting patterns is clearly shown in the last row of Figure 5.2b.

Simulation results suggest that the strength of the regional gradient and the effective anisotropy in hydraulic conductivities affect the resulting configuration of the vegetation pattern. In the NDM, the k_x/k_y ratio determines the relative strength of the long distance inhibition in the *x* and *y* directions of the domain. For example, when $k_x/k_y < 1$ and the regional hydraulic gradient in the *y*-direction is moderate (i.e. d$c < 0.015$), the advection of water and nutrients induced by transpiring vegetation in the *x*-direction is much lower than advection of water and nutrients along the longitudinal axis (*y*-direction). Biomass then grows laterally toward zones of relatively higher nutrients, and thus, perpendicular vegetation bands form. However, beyond a certain upper threshold value of the regional gradient (d$c > 0.015$), the high flux of available nutrients entering the domain in this direction and from decay in incipient vegetation patches already within

the domain causes biomass to grow preferentially in the direction of the regional hydraulic gradient, and vegetation bands oriented parallel to the prevailing flow develop.

The ponding mechanism as proposed by *Swanson and Grigal* [1988] induces a negative feedback between vegetation patches caused by flooding stress in the upslope direction. This negative feedback, in turn, drives the formation of perpendicular stripes. We envision that upslope ponding also results in a localized hydraulic gradient caused by the downstream resistance of the emergent vegetation, which is oriented in the direction perpendicular to the regional hydraulic gradient (y-direction). This then results in the advection of water and nutrients towards the patch margins, which reduces the long-distance inhibition of vegetation growth in the x-direction. Specifically, this advection of water and nutrients in the x-direction reduces the impact of the transpiration driven local hydraulic gradient in the x-direction. In our model, we therefore subsume the combined effects of the transpiration driven flow (explicitly represented) and the flow due to ponding (implicitly represented) into our k_x term such that $k_x/k_y < 1$. By doing so, we capture the first order effects of ponding as espoused by *Swanson and Grigal* [1988].

The modeling framework proposed here differs from other modeling approaches. *Eppinga et al.* [2009] suggest that nutrient accumulation alone can drive the formation of parallel strings on a slope and maze patterns on relatively flat ground, but is not sufficient to form perpendicular strings. The *Eppinga et al.* [2009] model can only produce perpendicular string patterns when either peat accumulation or water ponding is explicitly invoked in addition to the nutrient accumulation mechanism. In another recent modeling study, *Larsen and Harvey* [2010] have demonstrated that sediment transport feedback can be an important pattern-structuring mechanism in wetland landscapes. Using a cellular

automata model that describes sediment transport and vegetation dynamics, *Larsen and Harvey* [2010] have also reproduced the various vegetation patterns observed in wetland ecosystems. While we believe that both the nutrient accumulation and sediment transport feedback mechanisms are important, at present we do not yet understand the degree to which these two mechanisms operate independently or separately in patterned wetlands.

5.4 Conclusion

This chapter demonstrates that by representing the main effect of ponding implicitly through an effective anisotropy in hydraulic conductivity, the various patterns in wetland ecosystems can be reproduced. Simulation results demonstrate that the relative magnitude of the *x*-*y* advection rates as represented through effective anisotropy governs pattern evolution in wetland ecosystems. We contend that the effective anisotropy in hydraulic conductivity adequately represents the mechanisms that lead to the emergence of perpendicular vegetation patterns in wetland habitats. This modeling approach thus provides an improvement in the intuitive understanding of the controls governing pattern formation in wetland ecosystems.

5.5 References

Belyea, L. R. (2007), Climatic and topographic limits to the abundance of bog pools, *Hydrological Processes*, *21*(5), 675-687.

Belyea, L. R., and R. S. Clymo (2001), Feedback control of the rate of peat formation., *Proceedings of the Royal Society B: Biological Sciences*, *268*, 1315-1321.

Couwenberg, J. (2005), A simulation model of mire patterning - revisited, *Ecography*, *28*, 653-661.

Couwenberg, J., and H. Joosten (2005), Self-organization in raised bog patterning: the origin of microtope zonation and mesotope diversity, *Journal of Ecology*, *93*, 1238-1248.

Ellery, W. N., T. S. McCarthy, and N. D. Smith (2003), Vegetation, hydrology, and sedimentation patterns on the major distributary system of the Okavango Fan, Botswana, *Wetlands*, *23*(2), 357-375.

Eppinga, M. B., P. C. de Ruiter, M. J. Wassen, and M. Rietkerk (2009), Nutrients and Hydrology Indicate the Driving Mechanisms of Peatland Surface Patterning, *Am Nat*, *173*(6), 803-818.

Foster, D. R., G. A. King, P. H. Glaser, and H. E. Wright (1983), Origin of string patterns in boreal peatlands, *Nature*, *306*, 256-258.

Hilbert, D. W., N. Roulet, and T. Moore (2000), Modelling and analysis of peatlands as dynamical systems, *Journal of Ecology*, *88*(2), 230-242.

Larsen, L. G., and J. W. Harvey (2010), Modeling of hydroecological feedbacks predicts distinct classes of landscape pattern, process, and restoration potential in shallow aquatic ecosystems, *Geomorphology*.

Larsen, L. G., J. W. Harvey, and J. P. Crimaldi (2007), A delicate balance: Ecohydrology feedbacks governing landscape morphology in a lotic peatland, *Ecological Monograph*, *77*(4), 591-614.

Ogden, J. C. (2005), Everglades ridge and slough conceptual ecological model, *Wetlands*, *25*(4), 810-820.

Rietkerk, M., S. C. Dekker, M. J. Wassen, A. W. M. Verkroost, and M. F. P. Bierkens (2004), A putative mechanism for bog patterning, *The American Naturalist*, *163*(5), 699-708.

Sakaguchi, Y. (1980), On the genesis of banks and hollows in peat bogs: an explanation by a thatch line theory., *Bulletin of the Department of Geography University of Tokyo*, *12*, 35-58.

San Jose, J. J., M. L. Meirelles, R. Bracho, and N. Nikonova (2001), A comparative analysis of the flooding and fire effects on the energy exchange in a wetland community (Morichal) of the Orinoco Llanos, *J Hydrol*, *242*(3-4), 228-254.

Swanson, D. K., and D. F. Grigal (1988), A simulation model of mire patterning, *Oikos*, *53*, 309-314.

6. THE INFLUENCE OF TOPOGRAPHY AND VEGETATION SELF-ORGANIZATION OVER BIOMASS GROWTH DYNAMICS IN WETLAND ECOSYSTEMS

6.1 Introduction

Understanding the first order controls over resource cycling and limitation in ecosystem is critical for predicting ecosystems functioning and response to disturbances. For example, process-based eco-hydrological models have been utilized extensively to elucidate the first order controls over resource cycling in ecosystems. Spatially distributed and process oriented models such as DHSVM [*Wigmosta et al.,* 2002], VELMA [*Abdelnour et al.,* 2011] and RHESSys [*Tague and Band*, 2001] have been used to study how logging practices and climate change affect the hydrologic and carbon (C) and nitrogen (N) cycling of the old growth forests of the Pacific Northwest. The DHSVM has also been applied to a forested catchment in British Columbia to investigate the effects of clear cutting on peak flow sensitivity [*Whitaker et al*., 2002]. A distributed hydrological model, OHDIS-KWMSS [*Tachikawa et al.,* 2004] has been applied to investigate the interaction between sources and age of flow within forested catchments in the Pacific Northwest [*Sayama and McDonnell,* 2009]. Another distributed model, HillVi has been utilized to investigate the impact of porosity and soil depth variability on flow and transport processes [*Weiler and McDonnell*, 2004]. SWAT-N model [*Pohlert et al*., 2007] has been employed to study discharge and N loading of German forests. ELM [*Fitz and Trimble*, 2006] has been used to study the response of the ridge and slough habitat to water management and climate changes in the Florida Everglades. Another

distributed model, the Soil and Water Integrated Model (SWIM), has been utilized to investigate different fertilization strategies and N leaching associated with each strategy [*Krysanova and Haberlandt,* 2002]. A common concept shared by these models is that topography exerts primary control over ecosystem resource fluxes.

Modeling studies of wetland ecosystems demonstrate how the topographic control of water and nutrient flows to impact spatial distribution of water table depth and soil moisture, and subsequently affect ecosystem productivity [*Sonnentag et al.,* 2008] and carbon balance [*Govind et al.,* 2009]. *Sonnentag et al.* [2008] employed a spatially distributed model, the Boreal Ecosystem Productivity Simulator (BEPS), to examine the effects of topography on wetness (water table depth and soil moisture content), evapotranspiration and gross ecosystem productivity in the Mer Bleue peatland, Canada. Their results showed that the model tended to underestimate daily evapotranspiration and gross ecosystem productivity by ~10 – 12% when topographically driven lateral fluxes were neglected from the model framework.

Another group of models have been developed to describe large-scale vegetation patterning in resource limited wetland ecosystems [*Swanson and Grigal,* 1988; *Rietkerk et al.,* 2004; *Eppinga et al.,* 2009; *Larsen and Harvey,* 2010]. *Swanson and Grigal* [1988] developed a mathematical model to present a ponding mechanism to explain the formation of perpendicular strings in bogs. Specifically, a vegetation patch impedes the downslope flow of water. This then leads to ponding of upslope water, which locally increases hydroperiod and water depth and which can inhibit the upslope expansion of emergent vegetation. At a distance further upslope the water surface is lower which provides favorable conditions for vegetation growth. At the same time that the

alternating conditions lead to growth or inhibition along the hydrologic gradient, individual patches may expand in the direction perpendicular to the hydrologic gradient. Together, these processes result in strings of vegetation parallel to the contours of the slope. *Rietkerk et al.* [2004b] developed a model that incorporates a positive feedback between the plant biomass, transpiration, and nutrient accumulation that describes the formation of the vegetation patterns in the northern bogs (a.k.a nutrient accumulation mechanism). Specifically, vegetation induces water and nutrient fluxes towards itself through transpiration, activating further growth, which increases transpiration and nutrient accumulation locally. Thus plants deplete nutrients from their surrounding, inhibiting plant growth in the area where nutrients are depleted. A concept demonstrated by the *Rietkerk et al.* [2004b] model is that vegetated patches facilitate local growth by developing mechanisms to concentrate resources in the near field while depleting them at distance. Where resources are depleted away from, or between vegetated patches growth is inhibited. These simulation studies demonstrate the strong control that vegetation exerts over modifying the resource fluxes in the environment.

To date, the impacts of topography and self-organizing mechanisms on wetland ecosystem dynamics have been largely investigated separately [*Rietkerk et al.,* 2004; *Govind et al*., 2009]. Recent studies that explicitly explore at the combined effects of topographic and self organizing mechanisms on ecosystem dynamics are *Eppinga et al.* [2009], *Larsen and Harvey* [*2010*] and *Cheng et al.* [2011], who have shown that self-organizing mechanisms and topography operate together to impact orientation of wetland vegetation stripes. Nevertheless, how self-organizing mechanisms and topography

operate together to affect vegetative biomass growth dynamics under various degrees of resource availability has not been rigorously studied.

In this chapter, the goal is to demonstrate how topography and self-organizing mechanisms together and separately impact vegetative growth dynamics of wetland ecosystems using the modified Nutrient Depletion Model (NDM). The modified NDM is described by equations 2.7 – 2.12 in Chapter 2. Simulations conducted in this chapter are described in details in Chapter 4 (see Section 4.2). Simulation results are presented and discussed in details in this chapter.

6.2 Simulations Results

In the first set of simulations, for the TC+SO model, small vegetation patches grow, connect, and organize into maze/spot patterns on the landscape. At equilibrium spatially-averaged biomass values range from 125 g m^{-2} to 428 g m^{-2} for low rainfall, 284 g m^{-2} to 672 g m^{-2} for intermediate rainfall and 461 g m^{-2} to 912 g m^{-2} for high rainfall (Figure 6.1, left panel). On the other hand, for the TC model, vegetation patches grow and diffuse, until at equilibrium the landscape is uniformly covered with vegetation. Equilibrium biomass values range from 124 g m^{-2} to 429 g m^{-2} for low rainfall, 214 g m^{-2} to 672 g m^{-2} for intermediate rainfall and 305 g m^{-2} to 913 g m^{-2} for high rainfall (Figure 4.1, left panel).

In the second set of simulations, for the TC+SO model, equilibrium biomass values range from 123 g m^{-2} to 424 g m^{-2} for low rainfall, 257 g m^{-2} to 666 g m^{-2} for intermediate rainfall and 410 g m^{-2} to 894 g m^{-2} for high rainfall (Figure 6.1, right panel). On the other hand, for the TC model, equilibrium biomass values range from 123 g m^{-2} to

425 g m^{-2} for low rainfall, 212 g m^{-2} to 664 g m^{-2} for intermediate rainfall and 300 g m^{-2} to 898 g m^{-2} for high rainfall (Figure 6.1, right panel).

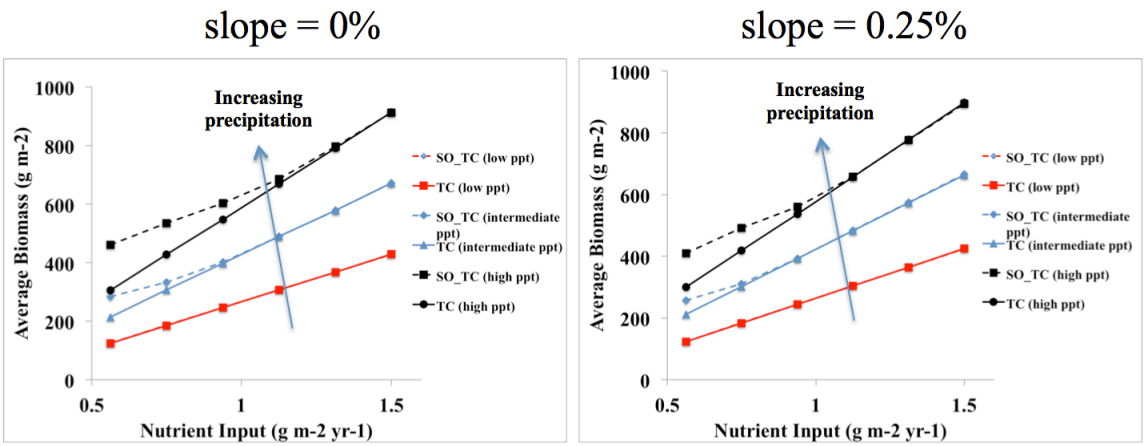

Figure 6.1. Equilibrium spatially average biomass for the TC+SO system (dotted lines) and the TC system (solid lines) for flat ground (left panel) and slope = 0.25% (right panel). Black lines represent annual rainfall of 500 mm, blue lines represent annual rainfall of 375 mm and red lines represent annual rainfall of 250 mm.

In the final set of simulations, the TC+SO and TC models respond similarly to the 50% increase in nutrient influx, at Year 4000 plant biomass of both models is at ~1400 gB m^{-2}. However, the trajectories of the models differ in response to reductions in nutrient influx. Plant biomass of the TC+SO model decreased at a slower rate than that of the TC model. For a 50% reduction in nutrient influx, plant biomass of the TC+SO model at Year 4000 is ~12% higher than plant biomass of the TC model. For a 100% reduction in nutrient influx, plant biomass of the TC model decrease drastically and die out by Year 3200. On the other hand, plant biomass of the TC+SO system persist longer and only die out by Year 4400 (Figure 6.2).

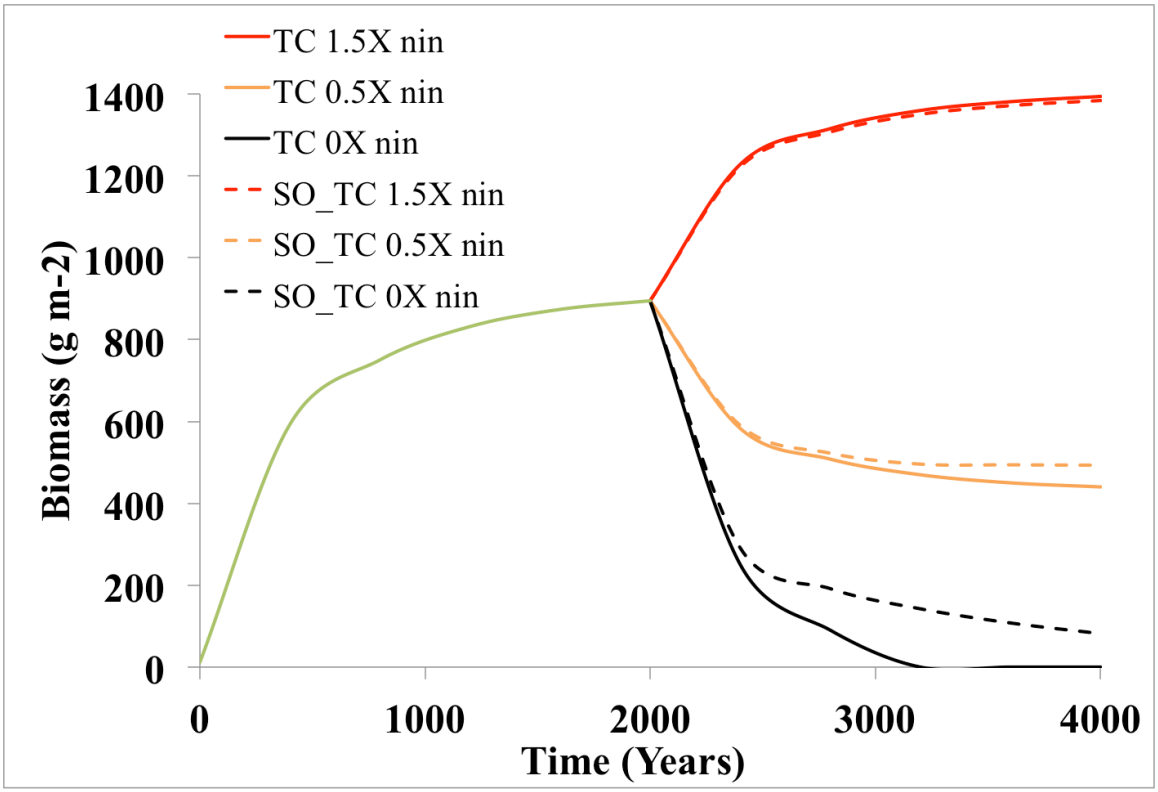

Figure 6.2: Results of the transient simulation. Both TC and TC+SO models build up equal stocks of vegetation biomass under the following environmental condition: nutrient influx = 0.0041gN m^{-2} d^{-1}, annual precipitation = 500 mm and slope = 0%. At 2000 years, when the vegetation biomass is at steady state, the following changes to the nutrient influx rate are imposed: (Case 1) 50% increase, (Case 2) 50% decrease, and (Case 3) 100% decrease (set to zero). For Case 1, the biomass trajectories of both systems are the same. For Cases 2 and 3, the biomass for the TC+SO model decreases at a slower rate than the biomass of the TC model.

6.3 Discussion

We conduct a number of simulations to understand how spatial self-organizing mechanisms and topography together and separately impact vegetation dynamics of peatlands in western Siberia. We find that: (1) Self-organizing mechanisms result in a more efficient capture and retention of resources. As a result, a model that includes for

self-organizing mechanisms (TC+SO model) can yield higher equilibrium biomass than a model that excludes for self-organizing mechanisms (TC model). (2) However, when resources or topographic gradients increase or annual rainfall decrease, the vegetation growth dynamics of the TC+SO and TC converge. (3) Even when both TC+SO and TC models have accumulated equal stocks of plant biomass at steady state under similar environmental conditions, transient responses of the systems to nutrient reduction can still differ.

The dynamics of the TC+SO and TC models converge when either (1) topographic gradient is increased or (2) nutrient inputs to the system are increased or (3) rainfall is decreased (Figure 6.1). As topographic gradient is increased, topography has more dominant control over nutrient flows. On the other hand, on the flat ground, self-organizing mechanism has dominant control over nutrient flows (Figure 6.1). For the same nutrient input, the dynamics of TC+SO and TC models become similar at the steep slope, instead of the flat ground. The convergence of dynamics in response to nutrient addition can be interpreted as such: with the rise in nutrient inputs to the system, nutrient availability becomes greater than demand, and as such the depletion of nutrient to levels below that which will support plants does not occur, and long range inhibition between vegetation decreases. With time, vegetation patches grow closer to one another, eventually covering the whole landscape. When vegetation covers the landscape uniformly, effects of self-organizing mechanisms diminish and topographic controls dominate. These results suggest that topographically driven models may sufficiently represent growth dynamics of ecosystems in areas with (1) high nutrient inputs and/or (2) terrains with topographic gradients that fall on the high end of the observed values (0 -

0.03 m m^{-1}) for northern peatlands [*Belyea*, 2007] or in regions experiencing low annual rainfall.

In this study, the transient simulations of system response to nutrient alterations highlight the importance of incorporating transient dynamics into the analysis of complex systems, so as to provide a complete picture on the response of systems to perturbations [*Hastings*, 2004; *Suding et al*., 2009]. In particular, while it is clear that both the TC+SO and TC systems will eventually die out in response to 100% reduction in nutrient influx, the trajectories of both systems will not be elucidated without the transient simulations. Theoretical studies as exemplified by *von Hardenberg et al*. [2001], *Rietkerk et al*. [2002], *Lejeuene et al*. [2004], *Rietkerk et al*. [2004a] and *Rietkerk et al*. [2004], tend to place emphasis on long term asymptotic behavior of the system, as reflected by their use of steady state analysis to characterize the systems. Transient simulations, on the other hand, take into account memory of the system and add a temporal dimension of system behavior; which can be an important measure of the success during ecosystem management.

Finally, we offer a number of caveats. This study has focused on the self-organizing dynamics of vascular plant biomass. We recognize that ecosystems comprise a number of species, each occupying a respective niche. The inclusion of multiple species will likely yield a different set of dynamic responses to nutrient and topographic controls. These new dynamics may include greater stability of the ecosystem due to greater biodiversity [*Tilman et al*., 2006], and shifts in community composition in response to increasing variability in resource input [*Knapp et al.*, 2002]. In grassland species manipulation experiment, *Tilman et al.* [2006] found a similar positive

relationship between biodiversity and ecosystem stability. *Knapp et al*. [2002] manipulated the temporal distribution and size of rainfall in a grassland experiment and examined subsequent shifts in plant community composition. They observed increased plant species diversity as precipitation variability is increased.

In order to maintain the simplicity of the model and highlight the effects of a spatial self-organizing mechanism, this study has focused on the response of periodic vegetation patterns. Another class of vegetation patterns: scale-free patterns, was not taken into consideration. In contrast to the periodic patterns, scale free patterns lack distinct characteristic lengths and cluster analysis revealed these patterns to follow power-law distribution [*Scanlon et al*., 2007]. Recent analysis of satellite imageries of the vegetation covers across South African landscapes has revealed that scale free patterns persist across a range of rainfall gradients (~200 – 900 mm yr^{-1}) [*Scanlon et al*., 2007]. Recent model studies have attributed the formation of scale free patterns to local facilitation in growth between neighboring vegetation, and global scale resource competition through processes such as fast overland flow [*von Hardenberg et al*., 2010; *Manor and Shnerb*, 2008]. Specifically, *von Hardenberg et al.* [2010] showed that when the rate at which the resource is dispersed or distributed in the environment becomes higher relative to the depletion rate, scale free patterns can result. Therefore, to gain a complete picture of how spatial organization of vegetation impact ecosystem function, it is important to understand how resource dynamics are influenced by scale free patterns and during transition from scale free to periodic patterns.

6.4 Conclusion

In this study, we show how self-organizing mechanism and topography operate together to affect vegetation growth dynamics in a wetland ecosystem. Results from this study show that the incorporation of vegetation self-organizing feedbacks can capture the spatial heterogeneity as observed in natural patterned ecosystems, and yield higher vegetation biomass under strong resource limiting conditions. For example, in the case of high rainfall, low nutrient, and flat ground, plant biomass is ~50% higher for the TC+SO model than the TC model. Therefore, results from this study suggest that self-organizing processes can impact regional scale vegetation growth dynamics of a nutrient limited ecosystem where terrain is flat or the topographic gradient is gentle.

However, when the topographic gradient becomes steep, topographic control dominates and self-organizing control becomes insignificant. As such, the incorporation of a self-organizing processes (a nutrient accumulation mechanism in this study) may not be necessary when dealing with large-scale climate models, such as global climate models (GCMs), that operate at spatial resolutions that are orders of magnitude coarser than the spatial resolution that the vegetation self-organizing feedbacks operate. Since simulation results obtained through aggregation (e.g. spatially averaged plant biomass) over such large spatial extent that includes a wide range of topographic gradients can diminish the effects of self-organizing feedbacks. GCMs typically operate at coarser spatial resolutions. For example, the United Kingdom Hadley Centre's HadCM3 [*Cox et al.*, 1999] has a spatial resolution of approximately 300km x 300km. Recent computational advancement has allowed GCMs to move to finer resolution of 100km x 100km [*Le Treut et al.*, 2007]. A common technique employed to represent spatial heterogeneity on the land surface due to different vegetation covers and land uses is to

discretize a GCM cell into finer tiles. Each tile will represent a different land cover, and surface energy, water and carbon fluxes from each of the tiles will be aggregated and passed onto the GCM cell [*Pitman*, 2003]. However, the tiles are still orders of magnitude coarser than the spatial resolution that the vegetation self-organizing feedbacks operate ($10^0 – 10^1$ m). To discretize a GCM cell to the resolution that the self-organizing feedbacks operate will be computationally expensive. For example, a GCM cell of 300km x 300km will consist of 10^{10} 3m x 3m tiles. Given such technical challenges, and as the results from this study indicate, self-organizing feedbacks are only important in regions of with low topographic gradients, we feel that the incorporation of such fine scale feedback into the land surface schemes coupled to the GCM is not realistic at present.

6.5 References

Abdelnour, A., M. Stieglitz, F. Pan, and R. McKane (2011), Catchment hydrological responses to forest harvest amount and spatial pattern, *Water Resour. Res.*, *47*.

Belyea, L. R. (2007), Climatic and topographic limits to the abundance of bog pools, *Hydrological Processes*, *21*(5), 675-687.

Cheng, Y., M. Stieglitz, G. Turk, and V. Engel (2011), Effets of anisotropy on pattern formation in wetland ecosystems, *Geophysical Research Letter*.

Cox, P. M., R. A. Betts, C. B. Bunton, R. L. H. Essery, P. R. Rowntree, and J. Smith (1999), The impact of new land surface physics on the GCM simulation of climate and climate sensitivity, *Clim. Dyn.*, 15, 183 – 203.

Eppinga, M. B., P. C. de Ruiter, M. J. Wassen, and M. Rietkerk (2009), Nutrients and hydrology indicate the driving mechanisms of peatland surface patterning, *The American naturalist*, *173*(6), 803-818.

Gilad, E., J. von Hardenberg, A. Provenzale, M. Shachak, and E. Meron (2004), Ecosystem engineers: from pattern formation to habitat creation, *Physical review letters*, *93*(9), 098105.

Govind, A., J. M. Chen, and W. Ju (2009), Spatially explicit simulation of hydrologically controlled carbon and nitrogen cycles and associated feedback mechanisms in a boreal ecosystem, *J. Georphys Res.*, *114*.

Hastings, A. (2004), Transients: the key to long-term ecological understanding?, *Trends in ecology & evolution*, *19*(1), 6.

Klausmeier, C. A. (1999), Regular and irregular patterns in semiarid vegetation, *Science*, *284*(5421), 1826-1828.

Knapp, A. K., Fay, P. A., Blair, J. M., Collins, S. L., Smith, M. D., Carlisle, J. D., Harper, C. W., Danner, B. T., Lett, M. S. & McCarron, J. K. (2002) Rainfall variability, carbon cycling, and plant species diversity in a mesic grassland. *Science,* 298, 2202-2205.

Krysanova, V., and U. Haberlandt (2002), Assessment of nitrogen leaching from arable land in large river basins:: Part I. Simulation experiments using a process-based model, Ecological Modelling, 150(3), 255-275.

Lejeune, O., M. Tlidi, and P. Couteron (2002), Localized vegetation patches: a self-organized response to resource scarcity, *Physical review. E, Statistical, nonlinear, and soft matter physics*, *66*(1 Pt 1), 010901.

Lejeune, O., M. Tlidi, and R. Lefever (2004), Vegetation spots and stripes: Dissipative structures in arid landscapes, *International Jounal of Quantum Chemistry*, *98*, 10.

Le Treut, H., R. Somerville, U. Cubasch, Y. Ding, C. Mauritzen, A. Mokssit, T. Peterson and M. Prather, 2007: Historical Overview of Climate Change. In: Climate Change 2007: The Physical Science Basis. Contribution of Working Group I to the Fourth Assessment Report of the Intergovernmental Panel on Climate Change [Solomon, S., D. Qin, M. Manning, Z. Chen, M. Marquis, K.B. Averyt, M. Tignor and H.L. Miller (eds.)]. Cambridge University Press, Cambridge, United Kingdom and New York, NY, USA.

Manor, A., and N. M. Shnerb (2008), Facilitation, competition, and vegetation patchiness: from scale free distribution to patterns, *Journal of theoretical biology*, *253*(4), 838-842.

Pitman, A. J. (2003), The evolution of, and revolution in, land surface schemes designed for climate models, *Int. J. Climatol*., 23, 479 – 510.

Raich, J., E. Rastetter, J. Melillo, D. Kicklighter, P. Steudler, B. Peterson,A. Grace, B. Moore III, and C. Vorosmarty (1991), Potential net primary productivity in South America: Application of a global model, Ecol. Appl., 1(4), 399–429.

Rietkerk, M., M. C. Boerlijst, F. van Langevelde, R. Hillerislambers, J. de Koppel, L. Kumar, H. H. Prins, and A. M. de Roos (2002), Self-organization of vegetation in arid ecosystems, *The American naturalist*, *160*(4), 524-530.

Rietkerk, M., S. C. Dekker, P. C. de Ruiter, and J. van de Koppel (2004a), Self-organized patchiness and catastrophic shifts in ecosystems, *Science*, *305*(5692), 1926-1929.

Rietkerk, M., S. C. Dekker, M. J. Wassen, A. W. Verkroost, and M. F. Bierkens (2004b), A putative mechanism for bog patterning, *The American naturalist*, *163*(5), 699-708.

Rietkerk, M., and J. van de Koppel (2008), Regular pattern formation in real ecosystems, *Trends in ecology & evolution*, *23*(3), 169-175.

Sayama, T., and J. McDonnell (2009), A new time-space accounting scheme to predict stream water residence time and hydrograph source components at the watershed scale, Water Resources Research, 45, W07401, doi:07410.01029/02008WR007549.

Scanlon, T. M., K. K. Caylor, S. A. Levin, and I. Rodriguez-Iturbe (2007), Positive feedbacks promote power-law clustering of Kalahari vegetation, *Nature*, *449*(7159), 209-212.

Sonnentag, O. J., J. M. Chen, N. T. Roulet, and W. Ju (2008), Spatially explicit simulation of peatland hydrology and carbon dioxide exchange: Influence of mesoscale topography, *J. Georphys Res.*, *113*.

Stieglitz, M., D. Rind, J. Famiglietti, and C. Rosenzweig (1997), An efficient approach to modeling the topographic control of surface hydrology for regional and global climate modeling, *J. of Climate*, *10*(1), 19.

Suding, K. N., and R. J. Hobbs (2009), Threshold models in restoration and conservation: a developing framework, *Trends in ecology & evolution*, *24*(5), 271-279.

Tachikawa, Y., G. Nagatani, and K. Takara (2004), Development of stage discharge relationship equation incorporating saturated-unsaturated flow mechanism, Annual Journal of Hydraulic Engineering, Japan. Society of Civil Engineers, 48, 7-12.

Tague, C. L., and L. E. Band (2004), RHESSys: Regional Hydro-Ecologic Simulation System - An object-oriented approach to spatially distributed modeling of carbon, water and nutrient cycling, *Earth Interact*, *8*, 42.

Tilman, D., Reich, P.B., Knops, J.M.H. (2006). Biodiversity and ecosystem stability in a decade long grassland experiment. Nature. Vol 441, 1:629-632.

van de Koppel, J., and M. Rietkerk (2004), Spatial interactions and resilience in arid ecosystems, *The American naturalist*, *163*(1), 113-121.

Vitousek, P. M., and R. W. Howarth (1991), Nitrogen Limitation on Land and in the Sea - How

Can It Occur, *Biogeochemistry*, *13*(2), 87-115.

von Hardenberg, J., A. Y. Kletter, H. Yizhaq, J. Nathan, and E. Meron (2010), Periodic versus scale-free patterns in dryland vegetation, *Proceedings. Biological sciences / The Royal Society*, *277*(1688), 1771-1776.

von Hardenberg, J., E. Meron, M. Shachak, and Y. Zarmi (2001), Diversity of vegetation patterns and desertification, *Physical review letters*, *87*(19), 198101.

Weiler, M. and J.J. McDonnell 2004. Virtual experiments: A new approach for improving process conceptualization in hillslope hydrology. Journal of Hydrology, 285: 3-18, doi:10.1016/S0022 1694(03)00271-3

Whitaker, A., Y. Alila, J. Beckers, and D. Toews (2002), Evaluating peak flow sensitivity to clear-cutting in different elevation bands of a snowmelt-dominated mountainous catchment, Water Resources Research, 38(9), 1172, doi:1110.1029/2001WR000514.

7. THE IMPACT OF TOPOGRAPHY AND VEGETATION SELF-ORGANIZATION ON PRESENT AND FUTURE C-N DYNAMICS OF ARCTIC TERRESTRIAL ECOSYSTEMS

7.1 Introduction

Warming in the Arctic over the past century has been well documented, with the warming trend expected to continue into the next century [*Serreze et al*., 2000; Intergovernmental Panel on Climate Change, 2007]. Changes that have been observed in the past decades in response to this warming include increased precipitation [*Dai et al*., 1997; *Ye et al*., 1998], decreased snow cover duration and extent [*Dye* 2002; *Stone et al*., 2002], increased river discharge [*Peterson et al*., 2002], increased ground temperature [*Osterkamp and Romanovsky*, 1999; *Romanovsky et al*., 2002; *Stieglitz et al*., 2003] and increased growing season length [*Foster*, 1989; *Foster et al*., 1992; *Smith et al*., 2004].

The Arctic climate has been conducive for net C sequestration during the past 10,000 years. As a result, the Arctic peatlands have been a sink for atmospheric CO_2 through the Holocene [*Billings*, 1987; *Gorham*, 1991]. At present, the tundra soils hold up between 43 to 200 gigatons of soil organic carbon [*Post et al*, 1982; *Shaver et al*., 1992]. However, this may no longer be the case as the subsurface warms. An increase in subsurface temperature can stimulate soil organic matter decomposition, increase the corresponding CO_2 efflux into the atmosphere and induce a positive feedback to climate warming. However, whether the Arctic becomes a source or sink for the atmospheric

CO_2 is dependent on the balance between soil decomposition and vegetation productivity of the Arctic ecosystem.

Changes in the structure and productivity of arctic vegetation under a warmer climate can also impact global carbon (C) cycling. As temperature increases, nitrogen mineralization rates can also increase, resulting in increasing plant available nitrogen (N), a growth-limiting nutrient in arctic ecosystems [*Shaver and Chapin*, 1986; *Chapin* 1991]. The increase in N availability, coupled with longer growing season length, lead to higher plant productivity. Studies have revealed shifts in biomass, species and productivity of terrestrial arctic vegetation [*Bret-Harte et al*., 2001; *Hollister et al*., 2005; *Chapin and Shaver*, 1996; *Hobbie and Chapin*, 1998; *Natali et al*., 2011; *Sturm et al*., 2005; *Tape et al*., 2006; *Myneni et al*., 1997; *Nemani et al*., 2003; *Jia et al*., 2003]. Multispectral remote sensing studies have provided evidence for increased plant productivity [*Myeni et al*., 1997; *Nemani et al*., 2003; *Jia et al*., 2003] in arctic Alaska. Repeat photography of areas throughout North Slope of Alaska revealed an expansion of deciduous shrubs such as willow and birch over the past few decades [*Tape et al*., 2006]. Soil warming experiments conducted in arctic tundra have reported increase in aboveground biomass and productivity, and a general shift in plant species from graminoids towards deciduous shrubs [*Bret-Harte et al*., 2001; *Hollister et al*., 2005; *Chapin and Shaver*, 1996; *Hobbie and Chapin*, 1998; *Natali et al*., 2011]. The increase in plant productivity is expected to increase photosynthetic C uptake of atmospheric CO_2.

Given the important role that vegetation productivity plays in the determining net ecosystem productivity (NEP, NEP = net primary productivity – heterotrophic respiration), modeling studies have been conducted to understand changes in arctic

vegetation productivity under a warming climate, and subsequent impact on carbon cycling [*McKane et al*., 1997a, 1997b; *Stieglitz et al*., 2000; *Rastetter et al*., 2004; *Stieglitz et al., 2006*; *Euskirchen et al*., 2009]. *Stieglitz et al* [2000] simulated climatic effects on carbon dynamics of Arctic tundra using a hydrologic model that includes topographic effects, soil freeze-thaw dynamics, and snow physics, coupled with a plant-soil model that includes for soil decomposition processes and aboveground net primary productivity. By allowing leaf nitrogen to increase by 20% over the period of simulation (1960 – 2060), they found NPP increases from 140 to 200 gC m^{-2} yr^{-1} in response to a 5°C increase in mean annual air temperature. *Euskirchen et al* [2009] examined shifts in vegetation species and productivity in arctic Alaska in response to climate change, using the Terrestrial Ecosystem Model (TEM) that includes for vegetation dynamics of various plant functional types (e.g. grasses, shrubs, trees). They forced the model with nine climatic simulations from the Intergovernmental Panel on Climate Change (IPCC). Simulation results show increased NPP for all plant functional types, with the birch having the highest increase in NPP than the rest.

Recently, models that incorporated vegetation-resource feedbacks demonstrated the ability of vegetation to reorganize spatially to optimally utilize resources under nutrient limitation. *Gilad et al.* [2004] developed a model to describe the formation of patterns in semi-arid and arid ecosystems. The model incorporated local positive feedback due to increased infiltration within vegetated patches and long distance inhibition to vegetation growth due to competition for water. *Rietkerk et al.* [2004] developed a model that incorporates a positive feedback between the plant biomass, transpiration, and nutrient accumulation that describes the formation of the vegetation

patterns in the northern bogs (a.k.a nutrient accumulation mechanism). Specifically, vegetation induces water and nutrient fluxes towards itself through transpiration, activating further growth, which increases transpiration and nutrient accumulation locally. Thus plants deplete nutrients from their surrounding, inhibiting plant growth in the area where nutrients are depleted. A concept shared by the *Rietkerk et al.* [2004] and *Gilad et al*. [2004] models is that vegetation facilitates local growth by developing mechanisms to extract resources at-distance. As such, at-distance, where resources are extracted and depleted, growth is inhibited. These simulation studies demonstrate the strong control that vegetation exerts over modifying the resource fluxes to their advantage.

In this chapter, we seek to understand how the incorporation of a vegetation self-organizing mechanism, a mechanism that has been excluded from previous modeling studies [*Stieglitz et al*., 2000; *Rastetter et al*., 2004; *Stieglitz et al*., 2006; *Euskirchen et al.*, 2009], will impact productivity of the Arctic ecosystem. Using the Northern peatlands as an example, in the previous chapter we showed that a model that includes for spatial self-organizing dynamics yields higher biomass productivity than a model that omit the dynamics. Specifically, in regions where growth limiting resources or topographic gradients are low or annual rainfall are high, the model that incorporated spatial self-organizing dynamics can support higher biomass than a model that omit the dynamics. Given the high degree of nutrient limitation in arctic tundra ecosystems [*Shaver et al*., 1991] and the presence of spatial vegetation patterns in parts of northern Alaska, we seek to understand if the incorporation of a vegetation self-organizing mechanism will impact vegetation growth dynamics and the subsequent prediction of net

primary productivity of arctic ecosystems under changing climate. The two questions we seek to address are: (1) how do watershed topography and vegetation self-organizing feedbacks together and separately impact the accumulation of arctic plant and soil carbon stocks, and (2) under similar initial and future climate forcings, will the transient response of a system with vegetation self-organizing feedbacks differ from a system without said feedback (topography only). The NDM is first modified to include for more realistic peat decomposition functions. The modified NDM is described by equations 2.13 – 2.18 in Chapter 2. An arctic baseline simulation that simulates the accumulation of present day plant and soil C-N stocks is first conducted. Next, climate change simulations based on the International Panel on Climate Change (IPCC) Fourth Assessment Report (AR4) Special Report on Emission Scenario B1 (SRESB1) and SRESA2 are conducted. Simulations are discussed in details in Chapter 3 (see section 3.3). In the following sections, simulation results are described and discussed in detail.

7.2 Simulation Results

7.2.1 Baseline Simulation

After 7000 years of ecosystem buildup, the arctic ecosystem achieves steady state. For the TC+SO simulation, small vegetation patches grow, connect, and organize into stripes (width of ~20m) that are parallel to the slope direction. In addition, biomass growth is also higher in regions of low topographic gradient, where nutrients and water converge. At equilibrium, simulated biomass C is 640 gC m^{-2} and detrital C is 17,100 gC m^{-2}. Simulated loss of dissolved nitrogen from the ecosystem is ~0.115 gN m^{-2} yr^{-1}. Simulated NPP equal to ~110 gC m^{-2} yr^{-1}, and is balanced by detrital decomposition. For the TC simulation, vegetation patches grow and diffuse. Similar to the TC+SO simulation, vegetation growth is higher in the regions of low topographic gradient, where nutrients and water converge. However, unlike the TC+SO simulations, no vegetation stripes form along the slopes (Figure 7.1). At equilibrium, simulated biomass C, detrital C, loss of dissolved N from the ecosystem, NPP and detrital decomposition of the TC system is similar to the values from the TC+SO system (Figure 7.2).

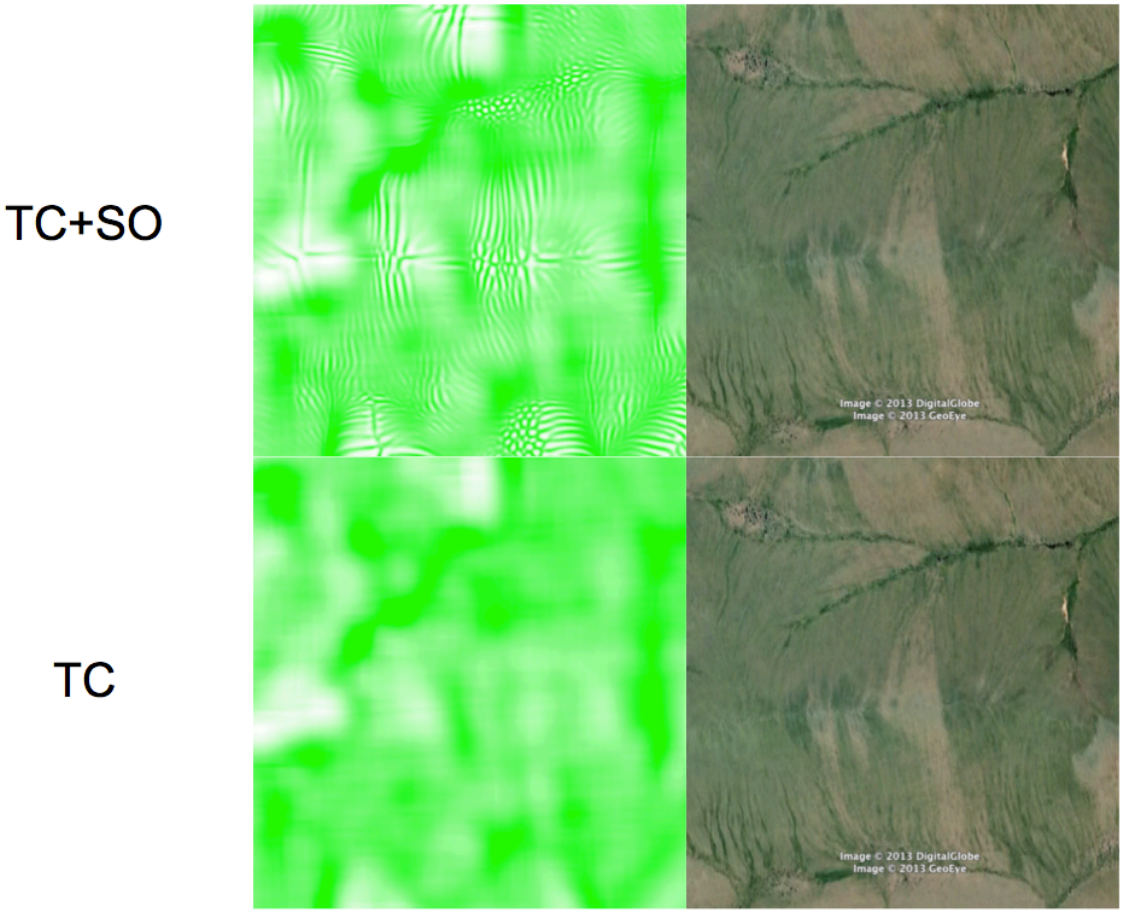

Figure 7.1. Top: Simulated spatial distribution of plant biomass from the TC+SO model in comparison to the aerial map of the study site. Bottom: Simulated spatial distribution of plant biomass from the TC model in comparison to the aerial map of the study site.

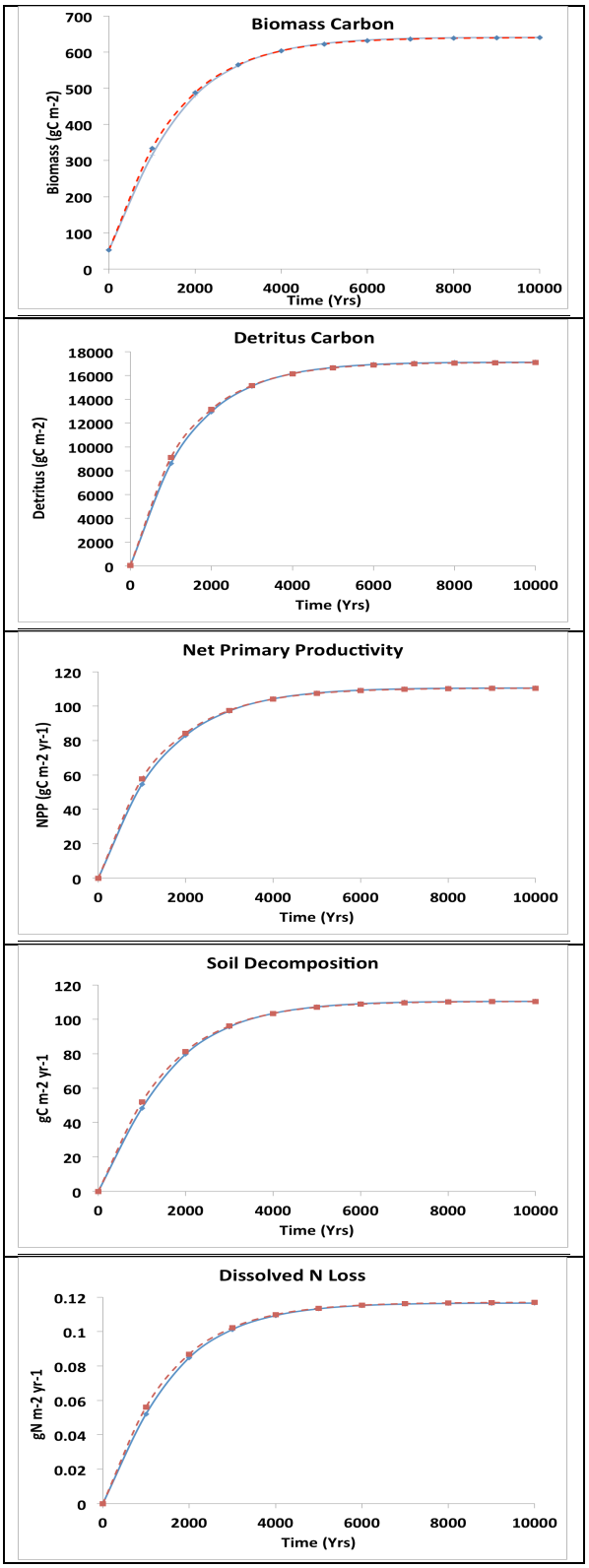

Figure 7.2. Simulated results from the baseline simulation. Dashed dotted lines represent simulation results of the TC+SO model, while solid lines represent simulation results of the TC model.

Table 7.1. Comparison of simulated output values against observed values.

Output	Simulated Value	Range of Observed Values	References
Plant Carbon (gC m^{-2})	640	108 – 938	*Shaver and Chapin*, [1991]
Detrital Carbon (gC m^{-2})	17,100	10,000 - 26,400	*Giblin et al*. [1991]
Net Primary Productivity (gC m^{-2} yr^{-1})	110	16 – 152	*Shaver and Chapin*, 1991]
DIN Loss (gN m^{-2} yr^{-1})	0.006	0.003 – 0.008	*Peterson et al*. [1992]
DON Loss (gN m^{-2} yr^{-1})	0.111	0.1	*Peterson et al*. [1992]
Width of vegetation stripes (m)	20	~ 15 – 30	Calculated from image from Google Earth

7.2.2 Climate Change Simulations

We categorize the climate change scenarios into two groups: (1) increase in mean, and (2) increase in mean and variability.

7.2.2.1 Increase in Mean

7.2.2.1.1 Increase in Temperature Only

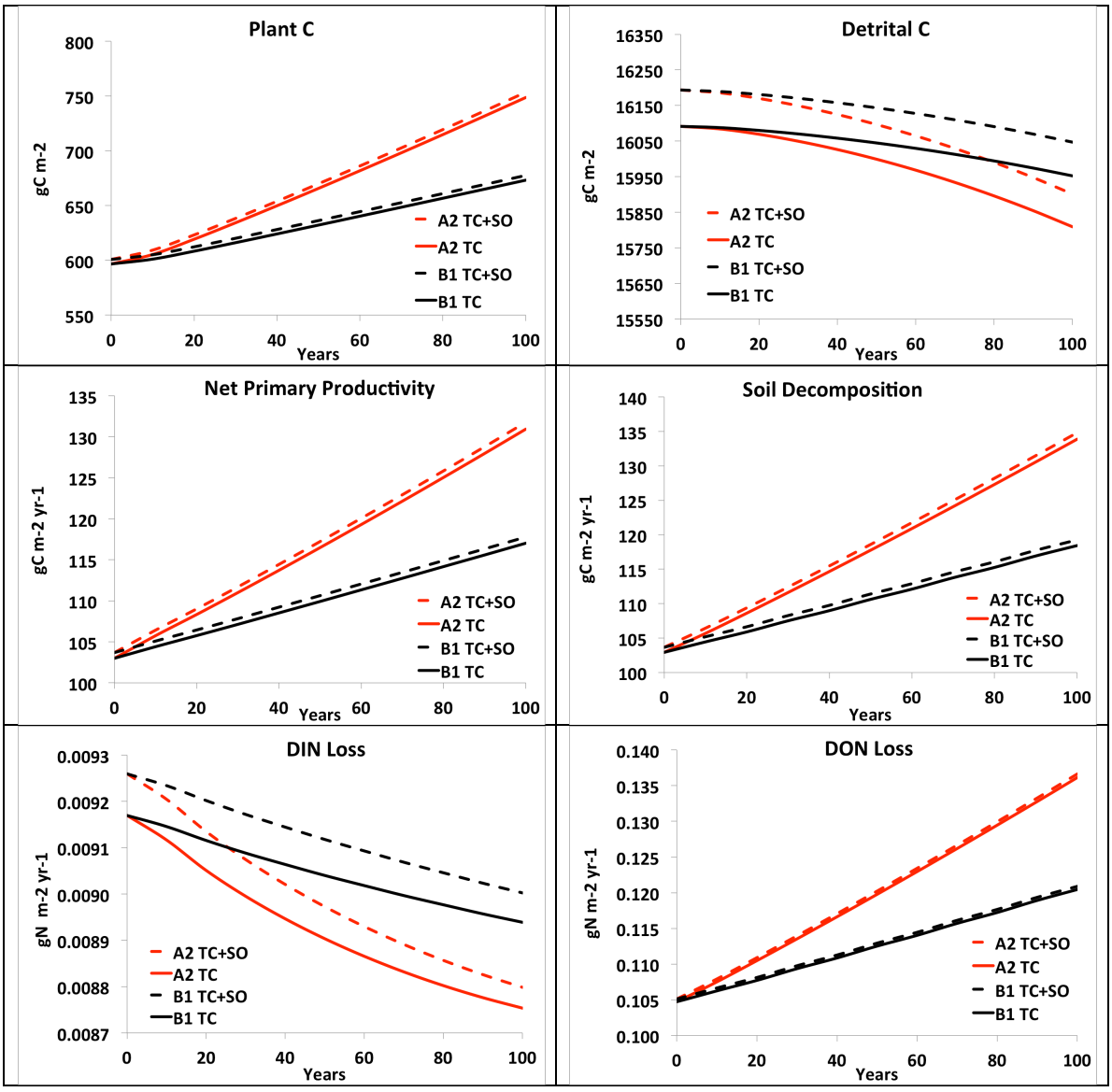

Figure 7.3. Simulated plant C, detrital C, net primary productivity, soil decomposition, DIN loss and DON loss for the T_M case. Red lines represent results for the SRESA2 scenario. Black lines represent results for the SRESB1 scenario. Solid lines represent TC+SO results. Dashed lines represent TC results.

For all T_M scenarios (Chapter 4, Table 4.4), temperature is linearly increased by 0.95°C (SRESB1) and 1.8°C (SRESA2) from a baseline temperature of 4°C over a hundred years. Similar to the baseline simulations, there are no significant differences in dynamics between the TC+SO and the TC models. For both the SRESB1 and SRESA2 scenarios, the general behaviors of the models can are: (1) increase in NPP causes an increase in biomass C which reduces loss of DIN from the systems, and (2) increase in soil decomposition in response to rise in temperature causes soil C to decrease but increases rate of DON loss from the systems. Specifically, for the SRESB1 scenario, NPP increases by 14 gC m^{-2} yr^{-1}, causing biomass C to increase by 70 gC m^{-2} and DIN loss to reduce by 0.0003 gN m-2 yr^{-1}. Soil decomposition rate increases by 15 gC m^{-2} yr^{-1}, causing soil C to decrease by 140 gC m^{-2} and DON loss to increase by 0.019 gN m^{-2} yr^{-1}. At the end of one hundred years, net ecosystem C storage decreased by 0.4% from the present day ecosystem C stocks. For the SRESA2, NPP increases by 29 gC m^{-2} yr^{-1}, causing biomass C to increase by 150 gC m^{-2} and DIN loss to reduce by 0.0005 gN m^{-2} yr^{-1}. Soil decomposition rate increases by 31 gC m^{-2} yr^{-1}, causing soil C to decrease by 290 gC m^{-2} and DON loss to increase by 0.032 gN m^{-2} yr^{-1}. At the end of one hundred years, net ecosystem C storage decreased by 0.8% from the present day ecosystem C stocks (Figure 7.3).

7.2.2.1.2 Increase in Precipitation Only

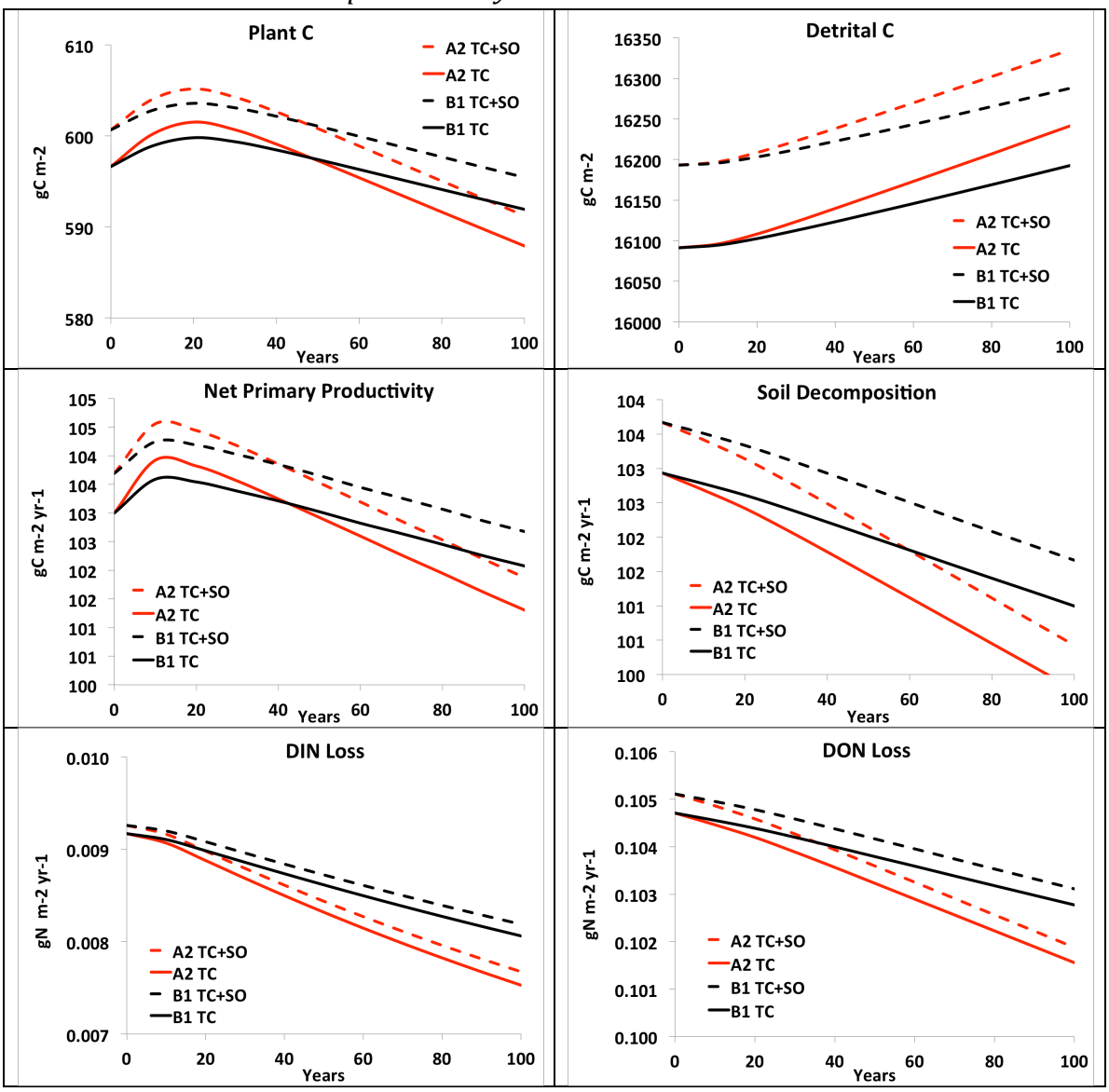

Figure 7.4. Simulated plant C, detrital C, net primary productivity, soil decomposition, DIN loss and DON loss for the P_M case. Red lines represent results for the SRESA2 scenario. Black lines represent results for the SRESB1 scenario. Solid lines represent TC+SO results. Dashed lines represent TC results.

For all P_M scenarios (Chapter 4, Table 4.4), precipitation is linearly increased by 17 mm (SRESB1) and 26.6 mm (SRESA2) over a hundred years. Similar to earlier simulations, there are no significant differences in the transient dynamics between the TC+SO and the TC models. In contrast to increase in temperature, increase in precipitation has minimal impact on the C-N dynamics of both the TC+SO and TC models, in that plant C, soil C, NPP, soil decomposition, DIN loss and DON losses all vary within 2% of their original values. Results show that increase in precipitation decreases soil decomposition rate, causing soil C to increase but all other processes (i.e. DIN loss, DON loss and NPP) and plant C to decrease. After one hundred years, net ecosystem C storage varied less than 0.2% from the present day ecosystem C stocks for both SRESB1 and SRESA2 scenarios (Figure 7.4).

7.2.2.1.3 Increase in Temperature and Precipitation

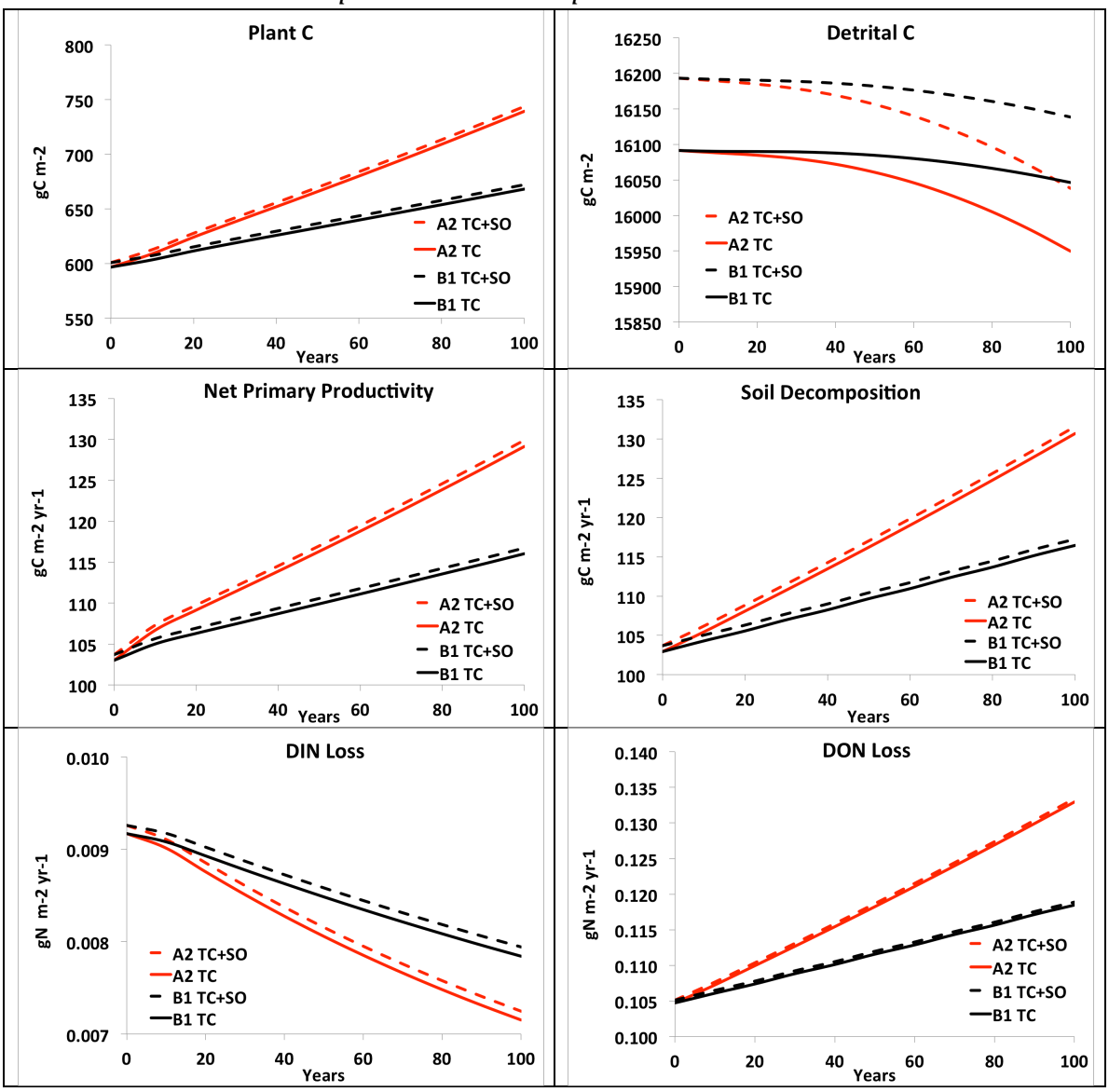

Figure 7.5. Simulated plant C, detrital C, net primary productivity, soil decomposition, DIN loss and DON loss for the T_M + P_M case. Red lines represent results for the SRESA2 scenario. Black lines represent results for the SRESB1 scenario. Solid lines represent TC+SO results. Dashed lines represent TC results.

For all T_M + P_M scenarios (Chapter 4, Table 4.4), temperature is linearly increased by 0.95°C (SRESB1) and 1.8°C (SRESA2) from a baseline temperature of 4°C, while precipitation is linearly increased by 17 mm (SRESB1) and 26.6 mm (SRESA2) over a hundred years. Over the hundred years, there are no significant differences in dynamics between the TC+SO and the TC models. For both the SRESB1 and SRESA2 scenarios, the general behaviors of the models can are similar to the T_M scenarios: (1) increase in NPP causes an increase in biomass C which reduces loss of DIN from the systems, and (2) increase in soil decomposition in response to rise in temperature causes soil C to decrease but increases rate of DON loss from the systems. However, the corresponding increase in precipitation moderates the impact of temperature on soil decomposition rate. As a result, soil decomposition rates for the T_M + P_M scenario is lower than the decomposition rates for the T_M scenario. Specifically, for the SRESB1 scenario, NPP increases by 13 gC m^{-2} yr^{-1}, causing biomass C to increase by 70 gC m^{-2} and DIN loss to reduce by 0.0014 gN m^{-2} yr^{-1}. Soil decomposition rate increases by 13 gC m^{-2} yr^{-1}, causing soil C to decrease by 50 gC m^{-2} and DON loss to increase by 0.014 gN m^{-2} yr^{-1}. For the SRESA2, NPP increases by 26 gC m^{-2} yr^{-1}, causing biomass C to increase by 144 gC m^{-2} and DIN loss to reduce by 0.0021 gN m^{-2} yr^{-1}. Soil decomposition rate increases by 28 gC m^{-2} yr^{-1}, causing soil C to decrease by 155 gC m^{-2} and DON loss to increase by 0.028 gN m^{-2} yr^{-1}. After one hundred years, net ecosystem C storage varied less than 0.2% from the present day ecosystem C stocks for both SRESB1 and SRESA2 scenarios (Figure 7.5).

7.2.2.2 Increase in Mean and Variability

7.2.2.2.1 Increase in Temperature Only

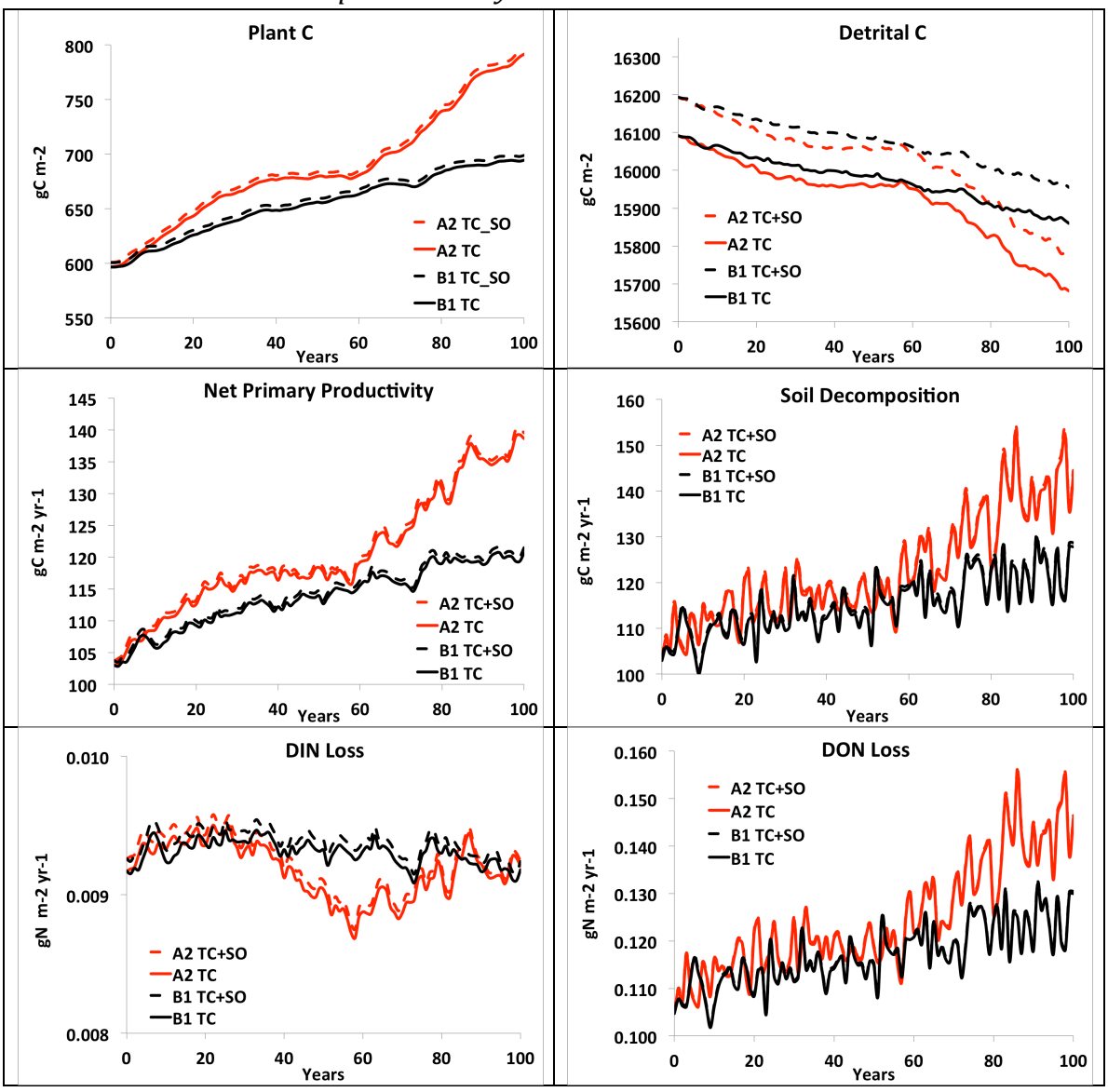

Figure 7.6. Simulated plant C, detrital C, net primary productivity, soil decomposition, DIN loss and DON loss for the T_V case. Red lines represent results for the SRESA2 scenario. Black lines represent results for the SRESB1 scenario. Solid lines represent TC+SO results. Dashed lines represent TC results.

For all T_V scenarios (SRESB1 and SRESA2, see Chapter 4, Table 4.4), there are no significant differences in dynamics between the TC+SO and the TC models. For both the SRESB1 and SRESA2 scenarios, the general behaviors of the models can are: (1) increase in NPP causes an increase in biomass C, and (2) increase in soil decomposition in response to rise in temperature causes soil C to decrease but increases rate of DON loss from the systems. Specifically, for the SRESB1 scenario, NPP increases by 17 gC m^{-2} yr^{-1}, causing biomass C to increase by 99 gC m^{-2}. Soil decomposition rate increases by 25 gC m^{-2} yr^{-1}, causing soil C to decrease by 231 gC m^{-2} and DON loss to increase by 0.025 gN m^{-2} yr^{-1}. At the end of one hundred years, net ecosystem C storage decreased by 0.8% from the present day ecosystem C stocks. For the SRESA2, NPP increases by 36 gC m^{-2} yr^{-1}, causing biomass C to increase by 197 gC m^{-2}. Soil decomposition rate increases by 41 gC m^{-2} yr^{-1}, causing soil C to decrease by 410 gC m^{-2} and DON loss to increase by 0.041 gN m^{-2} yr^{-1}. At the end of one hundred years, net ecosystem C storage decreased by 1.3% from the present day ecosystem C stocks (Figure 7.6).

7.2.2.2.2 Increase in Precipitation Only

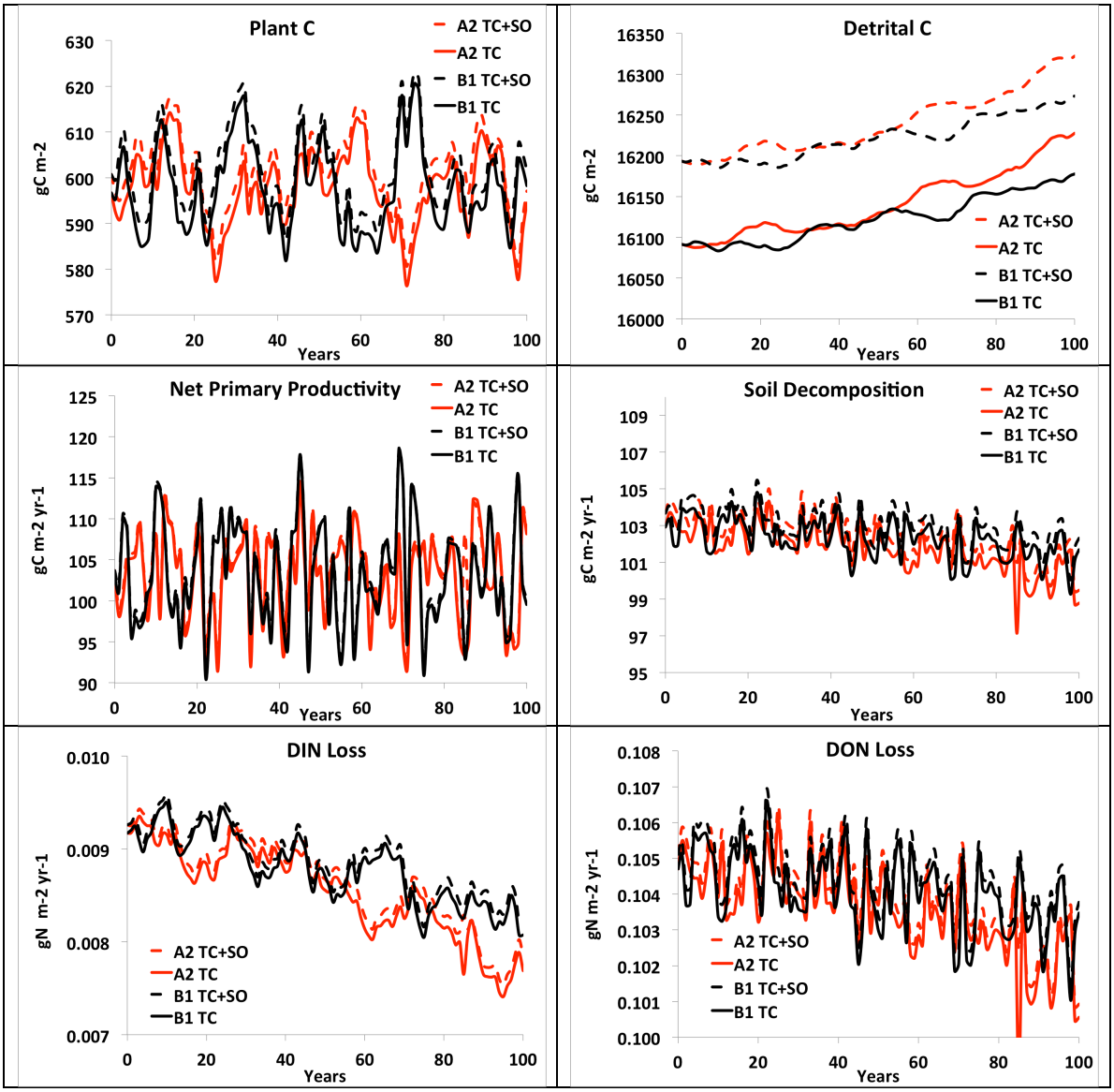

Figure 7.7. Simulated plant C, detrital C, net primary productivity, soil decomposition, DIN loss and DON loss for the P_V case. Red lines represent results for the SRESA2 scenario. Black lines represent results for the SRESB1 scenario. Solid lines represent TC+SO results. Dashed lines represent TC results.

For all P_V scenarios (SRESB1 and SRESA2, see Chapter 4, Table 4.4), there are no significant differences in dynamics between the TC+SO and the TC models. In contrast to increase in temperature, increase in precipitation has minimal impact on the C-N dynamics of both the TC+SO and TC models. NPP oscillates between 90 and 120 gC m^{-2} yr^{-1}, causing plant C to oscillate within ± 20 gC m-2 of the baseline values. Soil decomposition rates oscillate within 2 gC m^{-2} yr^{-1} of the mean values, with the mean values decreasing by 2 -3 gC m^{-2} yr^{-1} over the course of one hundred years. As a result, soil C shows an overall increase in one hundred years (50 gC m^{-2} for SRESB1 and 100 gC m^{-2} for SRESA2). DIN loss decreased by ~0.001 gN m^{-2} yr^{-1} over a hundred years. DON loss rates behave in a similar manner to soil decomposition rates, oscillating within 0.0015 gN m^{-2} yr^{-1} of the mean value, with the mean values decreasing by 0.002 – 0.003 gN m^{-2} yr^{-1} over one hundred years. At the end of one hundred years, net ecosystem C storage increased by ~0.5% and 0.8% from the present day ecosystem C stocks for SRESB1 and SRESA2 scenario respectively (Figure 7.7).

7.2.2.2.3 Increase in Temperature and Precipitation

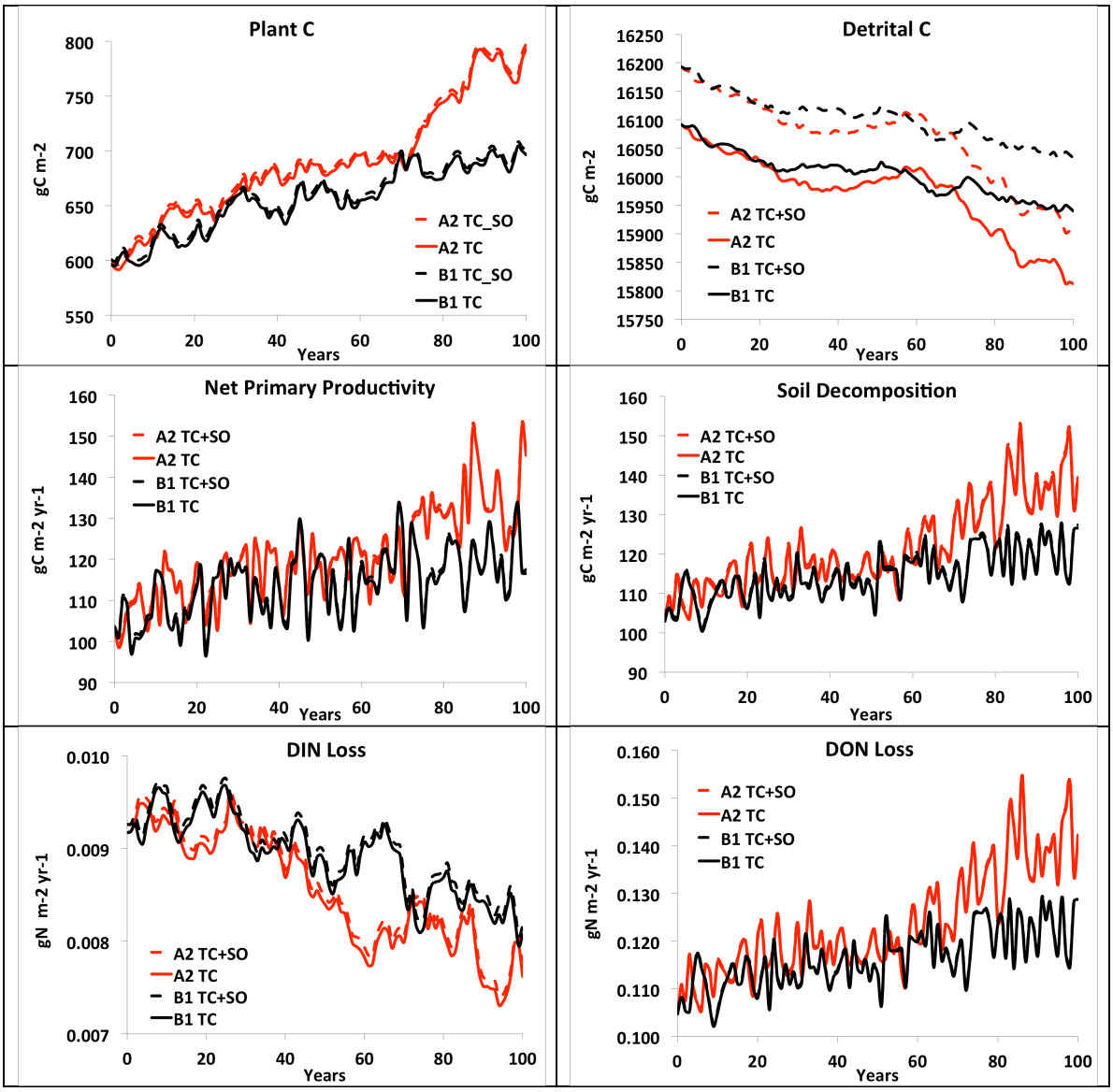

Figure 7.8. Simulated plant C, detrital C, net primary productivity, soil decomposition, DIN loss and DON loss for the T_V + P_V case. Red lines represent results for the SRESA2 scenario. Black lines represent results for the SRESB1 scenario. Solid lines represent TC+SO results. Dashed lines represent TC results.

For all T_V + P_V scenarios (SRESB1 and SRESA2, see Chapter 4, Table 4.4), there are no significant differences in dynamics between the TC+SO and the TC models. For both the SRESB1 and SRESA2 scenarios, the general behaviors of the models can are similar to the T_V scenarios: (1) increase in NPP causes an increase in biomass C which reduces loss of DIN from the systems, and (2) increase in soil decomposition in response to rise in temperature causes soil C to decrease but increases rate of DON loss from the systems. However, the corresponding increase in precipitation moderates the impact of temperature on soil decomposition rate. As a result, soil decomposition rates for the T_V + P_V scenario is lower than the decomposition rates for the T_V scenario. Specifically, for the SRESB1 scenario, NPP increases by 13 gC m^{-2} yr^{-1}, causing biomass C to increase by 100 gC m^{-2} and DIN loss to decrease by 0.001 gN m^{-2} yr^{-1}. Soil decomposition rate increases by 23 gC m^{-2} yr^{-1}, causing soil C to decrease by 152 gC m^{-2} and DON loss to increase by 0.024 gN m^{-2} yr^{-1}. At the end of one hundred years, net ecosystem C storage decreased by ~0.33% from the present day ecosystem C stocks. For the SRESA2, NPP increases by 42 gC m^{-2} yr^{-1}, causing biomass C to increase by 198 gC m^{-2} and DIN loss to decrease by ~0.002 gN m^{-2} yr^{-1}. Soil decomposition rate increases by 36 gC m^{-2} yr^{-1}, causing soil C to decrease by 279 gC m^{-2} and DON loss to increase by 0.037 gN m^{-2} yr^{-1}. At the end of one hundred years, net ecosystem C storage decreased by ~0.53% from the present day ecosystem C stocks (Figure 7.8).

7.3 Discussion

We conducted a number of simulations to investigate the following: (1) how do watershed topography and vegetation self-organizing feedbacks together and separately impact the accumulation of arctic plant and soil carbon stocks, and (2) under similar

initial and future climate forcings, will the transient response of a system with vegetation self-organizing feedbacks differ from a system without said feedback (topography only).

For the baseline simulations, results show that under similar environmental conditions, both the SO+TC and TC models accumulate similar amounts of plant biomass and soil C, with similar rates of NPP, soil decomposition, dissolved nitrogen losses. However, the SO+TC model is able to better capture the spatial distribution of biomass across the landscape than the TC model. Similarity in the C-N dynamics of the SO+TC and TC models suggest the dominance of topography over the control of water and resource fluxes on this landscape. In the previous chapter, we investigated the shift in dominance between self-organizing control and topographic control over resource fluxes of a high latitude wetland ecosystem in response to shift in topographic gradients. The results show that self-organizing mechanisms result in a more efficient capture and retention of resources, which result in higher equilibrium biomass, on terrains that are flat or where topographic gradients are gentle. However, when topographic gradients increase, the vegetation growth dynamics of the TC+SO and TC models converge. The average slope of this landscape is ~2%, with steep slopes of 12% in many parts. Climate change simulations also show that similarity in dynamics between the TC+SO and TC models. Results suggest that the increase in temperature and precipitation that are characteristic of climate change of region are associated with increase in N availability through increase soil decomposition. Results from the previous chapter (Chapter 6) showed that when nutrient availability is increased, the dynamics of the TC and TC+SO converge. Hence, both baseline and climate change simulations from this study suggest

that for the arctic region, topographically driven models can adequately simulate present and future C-N dynamics of the terrestrial ecosystem.

Simulation results depict a general response of the ecosystem to an increase in temperature: increase in net primary productivity, which increases plant C accumulation and decreases DIN loss. On the other hand, increases in temperature increase soil decomposition, reducing soil C storage and increasing DON loss. In contrast, an increase in precipitation increases soil moisture and reduces soil decomposition rates. Simulation results in this study are similar to to earlier modeling studies [*Stieglitz et al*., 2000] and field studies [*Kwon et al., 2006*; *Olivas et al*., 2010]. *Stieglitz et al* [2000] simulated future climatic impacts on carbon dynamics of Arctic tundra using a hydrologic model that includes topographic effects, coupled with a plant-soil model that includes for soil decomposition processes and aboveground net primary productivity. Their results showed that dry conditions favor aerobic soil decomposition, resulting in larger CO_2 efflux and net ecosystem loss of carbon. On the other hand, wetter soil conditions favor slower anaerobic decomposition; resulting in smaller CO_2 efflux and net ecosystem gain of carbon. *Kwon et al* [2006] measured net ecosystem CO_2 exchange (NEE) of Alaskan wet sedge and moist tussock tundra ecosystems during summer months from 1999 to 2003. They found that the moist tussock tundra is relatively warmer and drier than the wet sedge tundra. As a result, over the five-year period, the drier moist tussock tundra was losing carbon while the wetter wet sedge tundra was gaining carbon [*Kwon et al*., 2006]. *Olivas et al* [2010] manipulated water levels in a drained thaw lake basin in Barrow, Alaska, to study the effects of water table on CO_2 exchange of the ecosystem.

They found that increasing the subsurface water level decreased soil oxygen availability and consequently decreased soil decomposition, and reducing CO_2 efflux.

The climate change simulation results from this study are consistent with other modeling results:

(1) Increased loss of DON will continue to constrain biomass growth during warming [*Rastetter et al*., 2005; *Stieglitz et al*., 2006]. DON represents the form of nitrogen that plants are unable to utilize for their growth and maintenance. Hence unlike DIN, plants are not able to reduce DON losses from terrestrial ecosystems by increasing their nitrogen demand. Observed DON losses of terrestrial ecosystem have been found to represent 20 – 80% of the total N loss from ecosystems [*Perakis and Hedin*, 2002; *Qualls et al*., 2002]. In their warming simulations, *Stieglitz et al* [2006] showed that a 5°C warming can result in increase in plant biomass by ~300 gC m^{-2} and reduce DIN losses by ~0.003 gN m^{-2} yr^{-1}, DON losses increase and are four times greater than present day losses. In this study, simulated DON increased for all warming scenarios and by as much 46% under the T_V SRESA2 (warmest) scenario (Figure 7.6).

(2) No significant net loss of ecosystem C for all climate change scenarios examined in this study. In this study, under the T_V SRESA2 (warmest) scenario, net ecosystem C stock decreased by 1.3% (Figure 7.6). This magnitude of change is smaller than the changes in model outputs when model parameters are varied, as revealed by sensitivity analysis of model parameters (see Appendix section). As such, changes in ecosystem C for all climate change scenarios can be considered as insignificant. The idea that we will get much beyond a small change in system dynamics in this study can also

be understood by examining the relationship between plant growth and soil decomposition. In this study we have assumed that as temperature rises, plant uptake will keep up with increasing soil decomposition rate. This implies that plant growth is tightly coupled to soil decomposition and associated release of plant available N. This result is similar to findings from earlier modeling studies [*McKane et al.*, 1997a; *Stieglitz et al*., 2006]. *Mckane et al* [1997a] applied a process-based model, MBL-GEM (Marine Biological Laboratory General Ecosysem Model; *Rastetter et al*., 1991] to simulate response of tussock tundra to manipulations of environmental factors such as CO_2, temperature, light and soil nutrients. They found that 2X current CO_2 and N fertilization increased ecosystem C stocks by 1.4 and 2.9% respectively. Warming of 3.5°C decreased ecosystem C stock by 1.9%.

Finally, simulation results from this study show that changes in daily variability in temperature and precipitation can impact ecosystem dynamics as much as the changes in mean temperature and precipitation. For example, comparison between simulation results of T_M SRESA2 and T_V SRESA2 show that the inclusion of daily variability in temperature increases NPP by 24%, soil decomposition by 32%, DON losses by 28%, biomass C accumulation by 31% and soil C loss by 42%. The increase in variability in temperature from 2060 to 2099 as shown in the T_V SRESA2 temperature data drives the more rapid accumulation of plant C and corresponding loss of soil C (Figure 7.6). Impacts of changes in variability of meteorological variables on form and function of terrestrial ecosystems have also been demonstrated through modeling study [*Medvigy et al*., 2010] and field experiments [*Knapp et al*., 2002]. *Medvigy et al* [2010] compared simulation outputs of the Ecosystem Demography Model version 2 (ED2) [*Medvigy et*

al., 2009] when forced with hourly, daily and monthly meteorological data. They found that high frequency variations in solar insolation and precipitation significantly control ecosystem function through the process of leaf-level photosynthesis. Results generated by the hourly meteorological data defer from results generated using lower frequency meteorological datasets with same mean values. *Knapp et al*. [2002] increased intra-annual variability of precipitation by altering the temporal distribution and size of rainfall events in a grassland, and examined subsequent shifts in plant community composition. They observed increased plant species diversity as precipitation variability is increased.

7.4 Conclusion

A simple modeling framework has been applied to understand how do watershed topography and vegetation self-organizing feedbacks together and separately impact the accumulation of arctic plant and soil carbon stocks, and (2) under similar initial and future climate forcings, will the transient response of a system with vegetation self-organizing feedbacks differ from a system without said feedback (topography only). Simulation results suggest that for this arctic region, topographically driven models can adequately simulate present and future C-N dynamics of the terrestrial ecosystem. The climate change simulation results from this study are consistent with other modeling results: (1) Increased loss of DON will continue to constrain biomass growth during warming [*Rastetter et al*, 2005; *Stieglitz et al*; 2006]. (2) No significant net loss of ecosystem C for all climate change scenarios examined in this study [*McKane et al*., 1997; *Stieglitz et al*., 2006].

Results from this study are applicable to the North Slope region. The characteristics of the study site (e.g. vegetation biomass, composition and soil carbon stocks) are representative of the tundra ecosystem throughout the North Slope region. While it is expected that model parameters may need to be recalibrated in order to capture the change in dynamics due to local topography, climate and environmental factors, it is not expected that the newly calibrated parameter values will deviate drastically from parameter values used in this study.

7.5 Appendix For Baseline Simulation: Sensitivity of Model Parameters

Sensitivity analysis was conducted on pertinent parameters in the model. First, a baseline simulation was conducted on a synthetic straight slope (slope = 2%), which consists of 64 x 64 elements that are 3m on each side. Parameter values used in this baseline simulation are similar to those used in the arctic baseline simulation (see Chapter 4, section 4.3). Next, these parameter values were varied by ±10%, and the corresponding output values (such as biomass carbon, detrital carbon, hydraulic head, net primary productivity and soil decomposition rate) were compared against outputs from the baseline simulation. Results show that in general, changes in the majority of the parameters (e.g. biomass and nutrient diffusion, D_B and D_N) have little impact on the output values (less than 5% change). Altering plant mortality rate, d, has the most impact on biomass C. Increasing d by 10% decreases biomass C by 6.3%, decreasing d by 10% increases biomass C by ~10%. Altering the fraction of N released from decomposition of detritus, f_N, greatly impacts the productivity of the system. Decreasing f_N by 10% reduces biomass C by ~44%. Increasing f_N by 10% increases biomass C by ~200%.

Table 7.2. Results of sensitivity analysis for parameters D_B, D_N, f_N and t_v.

Plant biomass diffusion, D_B					
	Baseline	**0.9**	**%Δ**	**1.1**	**%Δ**
Biomass Carbon (gC m^{-2})	**606**	611	0.83	602	-0.66
Detritus Carbon (gC m^{-2})	**16350**	16457	0.65	16267	-0.51
Hydraulic Head (m)	**0.601**	0.605	0.67	0.596	-0.83
Net Primary Productivity (gC m^{-2} yr^{-1})	**105**	105	0.29	104	-0.67
Decomposition (gC m^{-2} yr^{-1})	**105**	105	0.38	104	-0.57
Nutrient diffusion, D_N					
	Baseline	**0.9**	**%Δ**	**1.1**	**%Δ**
Biomass Carbon (gC m^{-2})	**606**	612	0.99	600	-0.99
Detritus Carbon (gC m^{-2})	**16350**	16488	0.84	16225	-0.76
Hydraulic Head (m)	**0.601**	0.604	0.50	0.597	-0.67
Net Primary Productivity (gC m^{-2} yr^{-1})	**105**	106	1.24	104	-0.67
Decomposition (gC m^{-2} yr^{-1})	**105**	106	1.34	104	-0.57
Fraction of peat decomposed into DIN, f_N					
	Baseline	**0.9**	**%Δ**	**1.1**	**%Δ**
Biomass Carbon (gC m^{-2})	**606**	342	-43.56	1833	202.48
Detritus Carbon (gC m^{-2})	**16350**	10315	-36.91	44460	171.93
Hydraulic Head (m)	**0.601**	0.643	6.99	0.548	-8.82
Net Primary Productivity (gC m^{-2} yr^{-1})	**105**	59	-43.65	316	201.81
Decomposition (gC m^{-2} yr^{-1})	**105**	59	-43.59	316	202.10
Plant transpiration parameter, t_v					
	Baseline	**0.9**	**%Δ**	**1.1**	**%Δ**
Biomass Carbon (gC m^{-2})	**606**	624	2.97	600	-0.99
Detritus Carbon (gC m^{-2})	**16350**	17051	4.29	15997	-2.16
Hydraulic Head (m)	**0.601**	0.609	1.33	0.599	-0.33
Net Primary Productivity (gC m^{-2} yr^{-1})	**105**	108	3.15	103	-1.62
Decomposition (gC m^{-2} yr^{-1})	**105**	108	3.25	103	-1.53

Table 7.3. Results of sensitivity analysis for parameters *g*, *d*, *k* and *e*.

Biomass growth rate, *g*					
	Baseline	**0.9**	**%Δ**	**1.1**	**%Δ**
Biomass Carbon (gC m^{-2})	**606**	612	0.99	609	0.50
Detritus Carbon (gC m^{-2})	**16350**	16499	0.91	16443	0.57
Hydraulic Head (m)	**0.601**	0.631	4.99	0.585	-2.66
Net Primary Productivity (gC m^{-2} yr^{-1})	**105**	106	1.24	105	0.29
Decomposition (gC m^{-2} yr^{-1})	**105**	106	1.34	105	0.38
Plant mortality, *d*					
	Baseline	**0.9**	**%Δ**	**1.1**	**%Δ**
Biomass Carbon (gC m^{-2})	**606**	666	9.90	568	-6.27
Detritus Carbon (gC m^{-2})	**16350**	15957	-2.40	17036	4.20
Hydraulic Head (m)	**0.601**	0.579	-3.66	0.634	5.49
Net Primary Productivity (gC m^{-2} yr^{-1})	**105**	104	-0.67	108	3.15
Decomposition (gC m^{-2} yr^{-1})	**105**	104	-0.57	108	3.25
Evaporation parameter, *e*					
	Baseline	**0.9**	**%Δ**	**1.1**	**%Δ**
Biomass Carbon (gC m^{-2})	**606**	606	0.00	606	0.00
Detritus Carbon (gC m^{-2})	**16350**	16355	0.03	16344	-0.04
Hydraulic Head (m)	**0.601**	0.601	0.00	0.6	-0.17
Net Primary Productivity (gC m^{-2} yr^{-1})	**105**	105	0.29	105	0.29
Decomposition (gC m^{-2} yr^{-1})	**105**	105	0.38	105	0.38
Hydraulic conductivity, *k*					
	Baseline	**0.9**	**%Δ**	**1.1**	**%Δ**
Biomass Carbon (gC m^{-2})	**606**	615	1.49	608	0.33
Detritus Carbon (gC m^{-2})	**16350**	16599	1.52	16405	0.34
Hydraulic Head (m)	**0.601**	0.589	-2.00	0.619	3.00
Net Primary Productivity (gC m^{-2} yr^{-1})	**105**	106	1.24	105	0.29
Decomposition (gC m^{-2} yr^{-1})	**105**	106	1.34	105	0.38

7.6 References

Belyea, L. R. (2007), Climatic and topographic limits to the abundance of bog pools, *Hydrol Process*, *21*(5), 675-687.

Billings, W. D. (1987), Carbon Balance of Alaskan Tundra and Taiga Ecosystems - Past, Present and Future, *Quaternary Sci Rev*, *6*(2), 165-177.

Bret-Harte, M. S., G. R. Shaver, J. P. Zoerner, J. F. Johnstone, J. L. Wagner, A. S. Chavez, R. F. Gunkelman, S. C. Lippert, and J. A. Laundre (2001), Developmental plasticity allows Betula nana to dominate tundra subjected to an altered environment, *Ecology*, *82*(1), 18-32.

Chapin, F. S. (1991), Integrated Responses of Plants to Stress, *Bioscience*, *41*(1), 29-36.

Chapin, F. S., and G. R. Shaver (1996), Physiological and growth responses of arctic plants to a field experiment simulating climatic change, *Ecology*, *77*(3), 822-840.

Chapin, F. S., G. R. Shaver, A. E. Giblin, K. J. Nadelhoffer, and J. A. Laundre (1995), Responses of Arctic Tundra to Experimental and Observed Changes in Climate, *Ecology*, *76*(3), 694-711.

Dai, A., I. Y. Fung, and A. D. DelGenio (1997), Surface observed global land precipitation variations during 1900-88, *J Climate*, *10*(11), 2943-2962.

Dye, D. G. (2002), Variability and trends in the annual snow-cover cycle in Northern Hemisphere land areas, 1972-2000, *Hydrol Process*, *16*(15), 3065-3077.

Eppinga, M. B., P. C. de Ruiter, M. J. Wassen, and M. Rietkerk (2009), Nutrients and Hydrology Indicate the Driving Mechanisms of Peatland Surface Patterning, *Am Nat*, *173*(6), 803-818.

Euskirchen, E. S., A. D. McGuire, F. S. Chapin, S. Yi, and C. C. Thompson (2009), Changes in vegetation in northern Alaska under scenarios of climate change, 2003-2100: implications for climate feedbacks, *Ecol Appl*, *19*(4), 1022-1043.

Foster, J. L. (1989), The Significance of the Date of Snow Disappearance on the Arctic

Tundra as a Possible Indicator of Climate Change, *Arctic Alpine Res*, *21*(1), 60-70.

Foster, J. L., J. W. Winchester, and E. G. Dutton (1992), The Date of Snow Disappearance on the Arctic Tundra as Determined from Satellite, Meteorological Station and Radiometric Insitu Observations, *Ieee T Geosci Remote*, *30*(4), 793-798.

Giblin, A. E., K. J. Nadelhoffer, G. R. Shaver, J. A. Laundre, and A. J. Mckerrow (1991), Biogeochemical Diversity Along a Riverside Toposequence in Arctic Alaska, *Ecol Monogr*, *61*(4), 415-435.

Gilad, E., J. von Hardenberg, A. Provenzale, M. Shachak, and E. Meron (2004), Ecosystem engineers: From pattern formation to habitat creation, *Phys Rev Lett*, *93*(9).

Givnish, T. J., J. C. Volin, V. D. Owen, V. C. Volin, J. D. Muss, and P. H. Glaser (2008), Vegetation differentiation in the patterned landscape of the central Everglades: importance of local and landscape drivers, *Global Ecol Biogeogr*, *17*(3), 384-402.

Gorham, E. (1991), Northern Peatlands - Role in the Carbon-Cycle and Probable Responses to Climatic Warming, *Ecol Appl*, *1*(2), 182-195.

Gough, L., P. A. Wookey, and G. R. Shaver (2002), Dry heath arctic tundra responses to long-term nutrient and light manipulation, *Arct Antarct Alp Res*, *34*(2), 211-218.

Hinzman, L. D., D. L. Kane, R. E. Gieck, and K. R. Everett (1991), Hydrologic and Thermal-Properties of the Active Layer in the Alaskan Arctic, *Cold Reg Sci Technol*, *19*(2), 95-110.

Hobbie, S. E., and F. S. Chapin (1998), Response of tundra plant biomass, aboveground production, nitrogen, and CO(2) flux to experimental warming, *Ecology*, *79*(5), 1526-1544.

Hollister, R. D., P. J. Webber, and C. Bay (2005), Plant response to temperature in Northern Alaska: Implications for predicting vegetation change, *Ecology*, *86*(6), 1562-1570.

Jia, G. S. J., H. E. Epstein, and D. A. Walker (2003), Greening of arctic Alaska, 1981-

2001, *Geophys Res Lett*, *30*(20).

Keeling, C. D., J. F. S. Chin and T. P. Whorf (1996), Increased activity of northern vegetation inferred from atmospheric CO2 measurements, Nature, 382(11), 146 – 149.

Keuper, F., F. J. W. Parmentier, D. Blok, P. M. van Bodegom, E. Dorrepaal, J. R. van Hal, R. S. P. van Logtestijn, and R. Aerts (2012), Tundra in the Rain: Differential Vegetation Responses to Three Years of Experimentally Doubled Summer Precipitation in Siberian Shrub and Swedish Bog Tundra, *Ambio*, *41*, 269-280.

Knapp, A. K., P. A. Fay, J. M. Blair, S. L. Collins, M. D. Smith, J. D. Carlisle, C. W. Harper, B. T. Danner, M. S. Lett, and J. K. McCarron (2002), Rainfall variability, carbon cycling, and plant species diversity in a mesic grassland, *Science*, *298*(5601), 2202-2205.

Kwon, H. J., W. C. Oechel, R. C. Zulueta, and S. J. Hastings (2006), Effects of climate variability on carbon sequestration among adjacent wet sedge tundra and moist tussock tundra ecosystems, *J Geophys Res-Biogeo*, *111*(G3).

Mack, M. C., E. A. G. Schuur, M. S. Bret-Harte, G. R. Shaver, and F. S. Chapin (2004), Ecosystem carbon storage in arctic tundra reduced by long-term nutrient fertilization, *Nature*, *431*(7007), 440-443.

McKane, R. B., E. B. Rastetter, G. R. Shaver, K. J. Nadelhoffer, A. E. Giblin, J. A. Laundre, and F. S. Chapin (1997), Climatic effects on tundra carbon storage inferred from experimental data and a model, *Ecology*, *78*(4), 1170-1187.

McKane, R. B., E. B. Rastetter, G. R. Shaver, K. J. Nadelhoffer, A. E. Giblin, J. A. Laundre, and F. S. Chapin (1997), Reconstruction and analysis of historical changes in carbon storage in arctic tundra, *Ecology*, *78*(4), 1188-1198.

McNamara, J. P., D. L. Kane, J. E. Hobbie, and G. W. Kling (2008), Hydrologic and biogeochemical controls on the spatial and temporal patterns of nitrogen and phosphorus in the Kuparuk River, arctic Alaska, *Hydrol Process*, *22*(17), 3294-3309.

Medvigy, D., S. C. Wofsy, J. W. Munger, D. Y. Hollinger, and P. R. Moorcroft (2009), Mechanistic scaling of ecosystem function and dynamics in space and time: Ecosystem Demography model version 2, *J Geophys Res-Biogeo*, *114*.

Medvigy, D., S. C. Wofsy, J. W. Munger, and P. R. Moorcroft (2010), Responses of terrestrial ecosystems and carbon budgets to current and future environmental variability, *P Natl Acad Sci USA*, *107*(18), 8275-8280.

Myneni, R. B., C. D. Keeling, C. J. Tucker, G. Asrar, and R. R. Nemani (1997), Increased plant growth in the northern high latitudes from 1981 to 1991, *Nature*, *386*(6626), 698-702.

Natali, S. M., E. A. G. Schuur, and R. L. Rubin (2012), Increased plant productivity in Alaskan tundra as a result of experimental warming of soil and permafrost, *J Ecol*, *100*(2), 488-498.

Nemani, R. R., C. D. Keeling, H. Hashimoto, W. M. Jolly, S. C. Piper, C. J. Tucker, R. B. Myneni, and S. W. Running (2003), Climate-driven increases in global terrestrial net primary production from 1982 to 1999, *Science*, *300*(5625), 1560-1563.

Oberbauer, S., and P. C. Miller (1982), Growth of Alaskan Tundra Plants in Relation to Water Potential, *Holarctic Ecol*, *5*(2), 194-199.

Oberbauer, S., G. Starr, E. W. Popp (1998), Effects of extended growing season and soil warming on carbon dioxide and methane exchange of tussock tundra in Alaska. *Journal of Geophysical Research*, 103, 29075 – 29082.

Olivas, P. C., S. F. Oberbauer, C. E. Tweedie, W. C. Oechel, and A. Kuchy (2010), Responses of CO2 flux components of Alaskan Coastal Plain tundra to shifts in water table, *J Geophys Res-Biogeo*, *115*.

Osterkamp, T. E., and V. E. Romanovsky (1999), Evidence for warming and thawing of discontinuous permafrost in Alaska, *Permafrost Periglac*, *10*(1), 17-37.

Perakis, S. S. (2002), Nutrient limitation, hydrology and watershed nitrogen loss, *Hydrol Process*, *16*(17), 3507-3511.

Perakis, S. S., and L. O. Hedin (2002), Nitrogen loss from unpolluted South American forests mainly via dissolved organic compounds, *Nature*, *415*(6870), 416-419.

Peterson, B. J., R. M. Holmes, J. W. McClelland, C. J. Vorosmarty, R. B. Lammers, A. I. Shiklomanov, I. A. Shiklomanov, and S. Rahmstorf (2002), Increasing river discharge to the Arctic Ocean, *Science*, *298*(5601), 2171-2173.

Ping, C. L., G. J. Michaelson, M. T. Jorgenson, J. M. Kimble, H. Epstein, V. E. Romanovsky, and D. A. Walker (2008), High stocks of soil organic carbon in the North American Arctic region, *Nat Geosci*, *1*(9), 615-619.

Post, W. M., W. R. Emanuel, P. J. Zinke, and A. G. Stangenberger (1982), Soil Carbon Pools and World Life Zones, *Nature*, *298*(5870), 156-159.

Qualls, R. G., B. L. Haines, W. T. Swank, and S. W. Tyler (2002), Retention of soluble organic nutrients by a forested ecosystem, *Biogeochemistry*, *61*(2), 135-171.

Rastetter, E. B., G. I. Agren, and G. R. Shaver (1997), Responses of N-limited ecosystems to increased CO2: A balanced-nutrition, coupled-element-cycles model, *Ecol Appl*, *7*(2), 444-460.

Rastetter, E. B., B. L. Kwiatkowski, S. Le Dizes, and J. E. Hobbie (2004), The role of down-slope water and nutrient fluxes in the response of Arctic hill slopes to climate change, *Biogeochemistry*, *69*(1), 37-62.

Rastetter, E. B., S. S. Perakis, G. R. Shaver, and G. I. Agren (2005), Terrestrial C sequestration at elevated-CO2 and temperature: The role of dissolved organic N loss, *Ecol Appl*, *15*(1), 71-86.

Rastetter, E. B., M. G. Ryan, G. R. Shaver, J. M. Melillo, K. J. Nadelhoffer, J. E. Hobbie, and J. D. Aber (1991), A General Biogeochemical Model Describing the Responses of the C-Cycle and N-Cycle in Terrestrial Ecosystems to Changes in Co2, Climate, and N-Deposition, *Tree Physiol*, *9*(1-2), 101-126.

Reeve, A. S., D. I. Siegel, and P. H. Glaser (2001), Simulating dispersive mixing in large peatlands, *J Hydrol*, *242*(1-2), 103-114.

Rietkerk, M., S. C. Dekker, M. J. Wassen, A. W. M. Verkroost, and M. F. P. Bierkens (2004), A putative mechanism for bog patterning, *Am Nat*, *163*(5), 699-708.

Schmidt, I. K., S. Jonasson, G. R. Shaver, A. Michelsen, and A. Nordin (2002), Mineralization and distribution of nutrients in plants and microbes in four arctic ecosystems: responses to warming, *Plant Soil*, *242*(1), 93-106.

Schuur, E. A. G., et al. (2008), Vulnerability of permafrost carbon to climate change: Implications for the global carbon cycle, *Bioscience*, *58*(8), 701-714.

Serreze, M. C., J. E. Walsh, F. S. Chapin, T. Osterkamp, M. Dyurgerov, V. Romanovsky, W. C. Oechel, J. Morison, T. Zhang, and R. G. Barry (2000), Observational evidence of recent change in the northern high-latitude environment, *Climatic Change*, *46*(1-2), 159-207.

Shaver, G. R., W. D. Billings, F. S. Chapin, A. E. Giblin, K. J. Nadelhoffer, W. C. Oechel, and E. B. Rastetter (1992), Global Change and the Carbon Balance of Arctic Ecosystems, *Bioscience*, *42*(6), 433-441.

Shaver, G. R., S. M. Bret-Harte, M. H. Jones, J. Johnstone, L. Gough, J. Laundre, and F. S. Chapin (2001), Species composition interacts with fertilizer to control long-term change in tundra productivity, *Ecology*, *82*(11), 3163-3181.

Shaver, G. R., F. Chapin, and B. L. Gartner (1986), Factors Limiting Seasonal Growth and Peak Biomass Accumulation in Eriophorum-Vaginatum in Alaskan Tussock Tundra, *J Ecol*, *74*(1), 257-278.

Shaver, G. R., and F. S. Chapin (1980), Response to Fertilization by Various Plant-Growth Forms in an Alaskan Tundra - Nutrient Accumulation and Growth, *Ecology*, *61*(3), 662-675.

Shaver, G. R., and F. S. Chapin (1986), Effect of Fertilizer on Production and Biomass of Tussock Tundra, Alaska, USA, *Arctic Alpine Res*, *18*(3), 261-268.

Shaver, G. R., and F. S. Chapin (1991), Production - Biomass Relationships and Element Cycling in Contrasting Arctic Vegetation Types, *Ecol Monogr*, *61*(1), 1-31.

Smith, N. V., S. S. Saatchi, and J. T. Randerson (2004), Trends in high northern latitude soil freeze and thaw cycles from 1988 to 2002, *J Geophys Res-Atmos*, *109*(D12).

Stieglitz, M., S. J. Dery, V. E. Romanovsky, and T. E. Osterkamp (2003), The role of snow cover in the warming of arctic permafrost, *Geophys Res Lett*, *30*(13).

Stieglitz, M., A. Giblin, J. Hobbie, M. Williams, and G. Kling (2000), Simulating the effects of climate change and climate variability on carbon dynamics in Arctic tundra, *Global Biogeochem Cy*, *14*(4), 1123-1136.

Stieglitz, M., J. Hobbie, A. Giblin, and G. Kling (1999), Hydrologic modeling of an arctic tundra watershed: Toward Pan-Arctic predictions, *J Geophys Res-Atmos*,

104(D22), 27507-27518.

Stieglitz, M., R. B. McKane, and C. A. Klausmeier (2006), A simple model for analyzing climatic effects on terrestrial carbon and nitrogen dynamics: An arctic case study, *Global Biogeochem Cy*, *20*(3).

Stone, R. S., E. G. Dutton, J. M. Harris, and D. Longenecker (2002), Earlier spring snowmelt in northern Alaska as an indicator of climate change, *J Geophys Res-Atmos*, *107*(D10).

Sturm, M., T. Douglas, C. Racine, and G. E. Liston (2005), Changing snow and shrub conditions affect albedo with global implications, *J Geophys Res-Biogeo*, *110*(G1).

Tape, K., M. Sturm, and C. Racine (2006), The evidence for shrub expansion in Northern Alaska and the Pan-Arctic, *Glob Change Biol*, *12*(4), 686-702.

Van Wijk, M. T., M. Williams, J. A. Laundre and G. R. Shaver (2003), Interannual variability of plant phenology in tussock tundra: modeling interactions of plant productivity, plant phenology, snowmelt and soil thaw, *Global Change Biology*, 9, 743 – 758.

Waelbroeck, C., and J. F. Louis (1995), Sensitivity Analysis of a Model of Co2 Exchange in Tundra Ecosystems by the Adjoint Method, *J Geophys Res-Atmos*, *100*(D2), 2801-2816.

Walsh, J. E., W. L. Chapman, V. Romanovsky, J. H. Christensen, and M. Stendel (2008), Global Climate Model Performance over Alaska and Greenland, *J Climate*, *21*(23), 6156-6174.

Williams, M., E. B. Rastetter, G. R. Shaver, J. E. Hobbie, E. Carpino, and B. L. Kwiatkowski (2001), Primary production of an arctic watershed: An uncertainty analysis, *Ecol Appl*, *11*(6), 1800-1816.

Ye, H. C., H. R. Cho, and P. E. Gustafson (1998), The changes in Russian winter snow accumulation during 1936-83 and its spatial patterns, *J Climate*, *11*(5), 856-863.

8. CONCLUSIONS AND FUTURE RESEARCH

8.1 Conclusions

The Nutrient Depletion Model (NDM) presented in this thesis provides a simple framework to ascertain the relative control of self-organizing feedback and topography over ecosystem dynamics. The shift in dominance between self-organizing control and topographic control in response to shift in topographic gradients provide a more complete picture on controls over vegetation pattern formation, ecosystem nutrient cycling and vegetative growth dynamics. Results from this thesis suggest that self-organizing processes can impact regional scale vegetation growth dynamics of a nutrient limited ecosystem where the terrain is flat or the topographic gradient is gentle. However, incorporation of a self-organizing processes (such as nutrient accumulation mechanism) may not be necessary when dealing with large scale climate model that operate at spatial resolutions that are orders of magnitude coarser than the spatial resolution that the vegetation self-organizing feedbacks operate. Since simulation results obtained through aggregation over such large spatial extent that includes a wide range of topographic gradients will diminish the effects of self-organizing feedbacks.

A number of simulations were conducted to address the research questions presented in Chapter 1. In Chapter 5, forty scenarios where pertinent self-organizing feedback parameters and topography were varied to investigate the impact of the two first order controls on the resulting vegetation pattern on the landscape. In Chapter 6, seventy-two simulations were conducted to examine the impact of the two first order on

the resulting vegetation biomass amount. In Chapter 7, the NDM model was applied to arctic Alaska to explore the impact of the two controls (SO and TC) on carbon nitrogen dynamics of the arctic ecosystem. An arctic baseline simulation was conducted to allow the system accumulate plant and soil carbon that are consistent with present day observed values. Thereafter, twenty-four climate change simulations were conducted to simulate the impact of a wide range of projected changes in air temperature and precipitation on the system with and without self-organizing feedback. The main insights from this study include the following:

(1). By accounting for effective anisotropy in a simple modeling framework that encompasses only a scale dependent feedback between biomass and nutrient flow, the various vegetation patterns observed in wetland ecosystems (maze, and vegetation bands both perpendicular and parallel to prevailing flow directions) can be reproduced.

(2). Self-organizing mechanisms and topography operate together to impact the resulting vegetation patterns on the landscape. On a flat ground, self-organizing mechanisms exert dominant control over water and nutrient fluxes, and maze or spots vegetation patterns result. On a slope, topography also exerts control over water and nutrient fluxes. In the absence of anisotropy, vegetation stripes parallel to the slope direction forms. In contrast, in the presence of anisotropy, vegetation stripes perpendicular to the slope direction forms.

(3). Self-organizing mechanisms result in a more efficient capture and retention of resources. As a result, a model that includes for self-organizing mechanisms (TC+SO model) can yield higher equilibrium biomass than a model that excludes for self-

organizing mechanisms (TC model). However, a model that includes for self-organizing mechanisms (TC+SO model) do not always yield higher equilibrium biomass than a model that excludes for self-organizing mechanisms (TC model). When resources or topographic gradients increase or annual rainfall decrease, the vegetation growth dynamics of the TC+SO and TC models converge.

(4). Results suggest that for the arctic site examined in this thesis, topographically driven models can adequately simulate present and future C-N dynamics of the terrestrial ecosystem.

(5). Climate change simulations showed that increased loss of dissolved organic nitrogen (DON) will continue to constrain biomass growth during warming. DON represents the form of nitrogen that plants are unable to utilize for their growth and maintenance. Hence unlike DIN, plants are not able to reduce DON losses from terrestrial ecosystems by increasing their nitrogen demand. Observed DON losses from streams of terrestrial ecosystem have been found to represent 20 – 80% of the total N loss from ecosystems [*Perakis and Hedin*, 2002; *Qualls et al*., 2002]. This result is similar to earlier modeling studies [*Rastetter et al*., 2005; *Stieglitz et al*., 2006].

(6). Climate change simulations also showed no significant net loss of ecosystem C for all climate change scenarios examined in this study. Results corroborated with results from earlier modeling studies [*McKane et al.*, 1997a; *Stieglitz et al*., 2006].

(7). Simulation results from this thesis show that changes in daily variability in temperature and precipitation can impact ecosystem dynamics as much as the changes in mean temperature and precipitation. Comparison between simulation results of T_M

SRESA2 and T_V SRESA2 show that the inclusion of daily variability in temperature increases NPP by 24%, soil decomposition by 32%, DON losses by 28%, biomass C accumulation by 31% and soil C loss by 42%. The increase in variability in temperature from 2060 to 2099 as shown in the T_V SRESA2 temperature data drives the more rapid accumulation of plant C and corresponding loss of soil C (Figure 7.6).

(8). Results from this thesis are applicable to the North Slope region. The characteristics of the study site (e.g. vegetation biomass, composition and soil carbon stocks) are representative of the tundra ecosystem throughout the North Slope region. While it is expected that model parameters may need to be recalibrated in order to capture the change in dynamics due to local topography, climate and environmental factors, it is not expected that the newly calibrated parameter values will deviate drastically from parameter values used in this study.

8.2 Future Research

Here, some possible extension of this work that will allow for a more robust analysis of the impact of climate change on arctic C-N dynamics are discussed:

(1) **Incorporation of multiple species dynamics.** In this study the integrated vegetation dynamics of the various arctic terrestrial vegetation are simulated. The dynamics of individual vegetation species are not modeled. *Natali et al* [2011] found that increase in summer temperature cause shift in phenology and species level NPP. *Euskirchen et al* [2009] show increased NPP for all plant functional types, with the birch (*Betula spp.*) having the highest increase in NPP than the rest in response to warming. The competitive advantage of shrubs has a physiological basis as observed by *Bret-harte*

et al [2001]. By examining growth of arctic shrubs in long term fertilization plots in the Arctic LTER, *Bret-harte et al* [2001] found that in response to increase nutrient availability, *Betula* reallocated growth efforts into growing more long shoots, thus boosting the production rate of branches and meristems, and the overall biomass. *Sturm et al* [2005] offered another hypothesis to explain the growth and expansion of shrubs across the arctic landscape. The hypothesis involved the interaction between snow and shrub: the snow-shrub hypothesis. Snow in the Arctic is actively transported by the frequent high wind. Shrubs are taller than graminoid vegetation, and therefore, preferentially trap blowing and drifting snow. This leads to deeper snow and higher soil temperatures in winter at sites with shrubs, which in turn result in higher than normal soil nitrogen (N) mineralization due to increased microbial activity. Since arctic vegetation are strongly N limited [*Shaver and Chapin., 1980, 1986; Shaver et al., 2001; Chapin et al., 1995*], the additional nutrients available could, in turn, lead to additional shrub growth and expansion and enhance C storage during the growing season.

(2) **Incorporation of deep soil carbon.** In this study, we focused on the fate of the soil carbon in the active layer and did not consider the fate of the deep soil carbon. Consideration of the fate of deep soil carbon can affect whether the ecosystem is a net sink or source of carbon [*Mack et al.,* 2004]. By including deep soil carbon in their carbon balance analysis of a fertilization experiment in the Arctic LTER, *Mack et al* [2004] showed that losses of carbon and nitrogen from the deep layers could offset the increase in carbon storage due to increase plant productivity. Further, thawing of permafrost may release significant amount of deep soil C [*Schuur et al.,* 2008]. An estimate of 1672 Pg of soil C is present in the northern circumpolar permafrost [*Schuur et*

al., 2008]. As the ground temperature continues to increase [*Osterkamp and Romanovsky*, 1999; *Stieglitz et al*., 2003], thawing of the permafrost will increase the amount of soil organic carbon available for microbial decomposition and subsequent release to the atmosphere. Further, thawing of the permafrost can cause land subsidence (thermoskarst), altering N availability and impact vegetation productivity and structure [*Schuur et al*., 2007]. *Schuur et al.* [2007] analyzed vegetation composition across sites with various degree of permafrost thawing. They found total plant nitrogen to be the highest in oldest thermokarst site, suggesting that thawing of the permafrost increases soil nitrogen availability.

(3) **Impact of increase in growing season length.** Another consequence of arctic warming is the increase in growing season length. Atmospheric CO_2 measurements [*Keeling et al.,* 1996] and remote sensing studies [*Myeni et al*, 1997] have revealed that the start of the growing season in the spring is shifting to earlier dates. The shift in growing season start date is attributed to earlier snowmelt. Analysis of snowmelt date in Barrow, Alaska has revealed that snowmelt date has advanced by ~10 days since 1941 [*Stone et al*., 2002]. The earlier spring snowmelt date can increase plant productivity [*Myeni et al.,* 1997; *Oberbauer et al*., 1998; *van Wijk et al*., 2003]. However, the start of the growing season is only part of the equation. Warming also increases ground temperatures and period of soil thaw, and thereby increasing soil microbial activities and rate of heterotrophic respiration. If soil microbial activities are able to continue well into autumn due to warmer soils, but photosynthetic activities of plants are limited by photoperiod, CO_2 efflux from heterotrophic respiration may not be offset by photosynthetic uptake by plants.

8.3 References

Bret-Harte, M. S., G. R. Shaver, J. P. Zoerner, J. F. Johnstone, J. L. Wagner, A. S. Chavez, R. F. Gunkelman, S. C. Lippert, and J. A. Laundre (2001), Developmental plasticity allows Betula nana to dominate tundra subjected to an altered environment, *Ecology*, *82*(1), 18-32.

Chapin, F. S., G. R. Shaver, A. E. Giblin, K. J. Nadelhoffer, and J. A. Laundre (1995), Responses of Arctic Tundra to Experimental and Observed Changes in Climate, *Ecology*, *76*(3), 694-711.

Euskirchen, E. S., A. D. McGuire, F. S. Chapin, S. Yi, and C. C. Thompson (2009), Changes in vegetation in northern Alaska under scenarios of climate change, 2003-2100: implications for climate feedbacks, *Ecol Appl*, *19*(4), 1022-1043.

Keeling, C. D., J. F. S. Chin and T. P. Whorf (1996), Increased activity of northern vegetation inferred from atmospheric CO2 measurements, Nature, 382(11), 146 – 149.

Mack, M. C., E. A. G. Schuur, M. S. Bret-Harte, G. R. Shaver, and F. S. Chapin (2004), Ecosystem carbon storage in arctic tundra reduced by long-term nutrient fertilization, *Nature*, *431*(7007), 440-443.

Myneni, R. B., C. D. Keeling, C. J. Tucker, G. Asrar, and R. R. Nemani (1997), Increased plant growth in the northern high latitudes from 1981 to 1991, *Nature*, *386*(6626), 698-702.

Natali, S. M., E. A. G. Schuur, and R. L. Rubin (2012), Increased plant productivity in Alaskan tundra as a result of experimental warming of soil and permafrost, *J Ecol*, *100*(2), 488-498.

Oberbauer, S., G. Starr, E. W. Popp (1998), Effects of extended growing season and soil warming on carbon dioxide and methane exchange of tussock tundra in Alaska. *Journal of Geophysical Research*, 103, 29075 – 29082.

Osterkamp, T. E., and V. E. Romanovsky (1999), Evidence for warming and thawing of discontinuous permafrost in Alaska, *Permafrost Periglac*, *10*(1), 17-37.

Perakis, S. S., and L. O. Hedin (2002), Nitrogen loss from unpolluted South American forests mainly via dissolved organic compounds, *Nature*, *415*(6870), 416-419.

Ping, C. L., G. J. Michaelson, M. T. Jorgenson, J. M. Kimble, H. Epstein, V. E. Romanovsky, D. A. Walker (2008), High stocks of soil organic carbon in the North American Arctic region, Nature Geoscience, 1(9), 615 – 619.

Qualls, R. G., B. L. Haines, W. T. Swank, and S. W. Tyler (2002), Retention of soluble organic nutrients by a forested ecosystem, *Biogeochemistry*, *61*(2), 135-171.

Rastetter, E. B., S. S. Perakis, G. R. Shaver, and G. I. Agren (2005), Terrestrial C sequestration at elevated-CO2 and temperature: The role of dissolved organic N loss, *Ecol Appl*, *15*(1), 71-86.

Shaver, G. R., and F. S. Chapin (1980), Response to Fertilization by Various Plant-Growth Forms in an Alaskan Tundra - Nutrient Accumulation and Growth, *Ecology*, *61*(3), 662-675.

Shaver, G. R., and F. S. Chapin (1986), Effect of Fertilizer on Production and Biomass of Tussock Tundra, Alaska, USA, *Arctic Alpine Res*, *18*(3), 261-268.

Schuur, E. A. G., et al. (2008), Vulnerability of permafrost carbon to climate change: Implications for the global carbon cycle, *Bioscience*, *58*(8), 701-714.

Schuur, E. A. G., K. G. Crummer, J. G. Vogel, and M. C. Mack (2007), Plant species composition and productivity following permafrost thaw and thermokarst in alaskan tundra, *Ecosystems*, *10*(2), 280-292.

Stieglitz, M., R. B. McKane, and C. A. Klausmeier (2006), A simple model for analyzing climatic effects on terrestrial carbon and nitrogen dynamics: An arctic case study, *Global Biogeochem Cy*, *20*(3).

Stone, R. S., E. G. Dutton, J. M. Harris, and D. Longenecker (2002), Earlier spring snowmelt in northern Alaska as an indicator of climate change, *J Geophys Res-Atmos*, *107*(D10).

Sturm, M., T. Douglas, C. Racine, and G. E. Liston (2005), Changing snow and shrub conditions affect albedo with global implications, *J Geophys Res-Biogeo*, *110*(G1).

Van Wijk, M. T., M. Williams, J. A. Laundre and G. R. Shaver (2003), Interannual variability of plant phenology in tussock tundra: modeling interactions of plant productivity, plant phenology, snowmelt and soil thaw, *Global Change Biology*, 9, 743 – 758.

9. APPENDIX: A SIMPLE METHOD TO EVOLVE DAILY GROUND TEMPERATURES FROM SURFACE AIR TEMPERATURES IN SNOW DOMINATED REGIONS

9.1 Introduction

In contrast to other land features, snow has a number of unique properties: it is a winter only feature; it has a substantially higher albedo than the surrounding vegetation, and has characteristically low thermal conductivity. Specifically, the surface albedo of snow ranges from 0.6 to 0.85, while that of vegetation ranges from 0.1 to 0.3, and the thermal conductivity of snow ranges from 0.1 to 0.5 Wm^{-1} K^{-1}, while that of soil ranges from 0.8 to 2.2 Wm^{-1} K^{-1}. In winter, therefore, snow strongly alters the surface energy budget [*Yeh et al*. 1983; *Namias* 1985; *Barnett et al*. 1989] and prevents effective heat exchange between the ground and the atmosphere. From an ecological standpoint, variations in timing and depth of snow cover impact soil processes such as winter net nitrogen mineralization [*Schimel et al*. 2004] and net ecosystem CO_2 efflux [*Welker et al*. 2000]. Evidence from long term snow manipulation experiments suggest that an increase in soil temperature due to an increase in snow depth (SD), as projected during this century, can lead to degradation of the permafrost [*Hinkel and Hurd* 2006].

Models of varying degrees of complexity have been developed to describe snow dynamics and the coupling of land, snow, and boundary layer processes. Some models realistically capture the exchange of energy, mass, and momentum across the atmosphere-snow-ground system, and explicitly include a suite of snow pack processes

such as the dynamics of gravitational settling, metamorphism, phase changes and heat transfer through the percolation of water [*Anderson* 1976; *Jordan* 1991; *Loth et al*. 1993; *Lynch-Stieglitz* 1994; *Stieglitz et al*. 2001; *Bartelt and Lehning* 2002; *Liston and Elder* 2006]. While these complex models can simulate ground temperatures with high fidelity [*Lynch-Stieglitz* 1994; *Koster et al*. 2000; *Stieglitz et al*. 1999, 2001], they are computationally expensive. Other models have been developed using simple empirical schemes [*Bartlett et al*. 2005; *Pollack et al*. 2005; *Stieglitz and Smerdon* 2007]. They employ frameworks that implicitly represent snow insulation impacts on subsurface temperatures by use of simple governing equations that depend on few parameters. For example, *Stieglitz and Smerdon* [2007] employed a one-dimensional diffusion equation coupled to the surface air temperature (SAT) through a time varying flux boundary condition at the land surface. The time varying flux boundary condition is a function of the SAT, ground surface temperature (GST) and a coupling function. The temporal character of the coupling function implicitly represents the cumulative thermal effects of the processes operating at the land-atmosphere interface. These processes include snow insulation, vegetative insulation, freeze-thaw processes, vapor transport in soils and evapotranspiration.

We develop a simple semi-empirical model to evolve daily ground temperatures from daily SAT and SD in snow-dominated areas. We generate the daily GST by propagating the daily SAT through the snow pack and attenuating the SAT signal amplitude. Subsequent subsurface heat transfer is then modeled using the analytical solution of the one-dimensional heat conduction equation. The thermal impacts of nonconductive heat transfer processes and seasonal freeze thaw are implicitly represented

through a time dependent apparent thermal diffusivity (ATD). The model is tested in four snow-dominated regions: Barrow, Council and Ivotuk, in Alaska, and Reynolds Creek Experimental Watershed (RCEW) in Idaho.

9.2 Methods

9.2.1 Model description

The analytical solution to a sinusoidal signal of mean temperature, $\overline{T}$, and amplitude A_o applied at the surface of a homogenous infinite half-space is [*Carslaw and Jaeger* 1959]:

$$T(z,t) = \overline{T} + A\sin(\omega t - \phi(z)) \tag{9.1}$$

where z is distance from the surface of the half space. ω is the radial frequency, which is 2π times the actual frequency of the signal. A is the signal attenuation of the form:

$$A = A_o \cdot e^{-k \cdot z} \tag{9.2}$$

and ϕ is the phase lag:

$$\phi = k \cdot z \tag{9.3}$$

k is the wave vector

$$k = \frac{1}{\lambda} = \sqrt{\left(\frac{\pi}{D \cdot \tau}\right)} \tag{9.4}$$

and λ, *D*, τ , are the damping depth for the snow/ground, defined as the characteristic depth at which the temperature signal is attenuated to *1/e* of the surface, the thermal diffusivity of the snow/ground, and the period of the forcing, respectively.

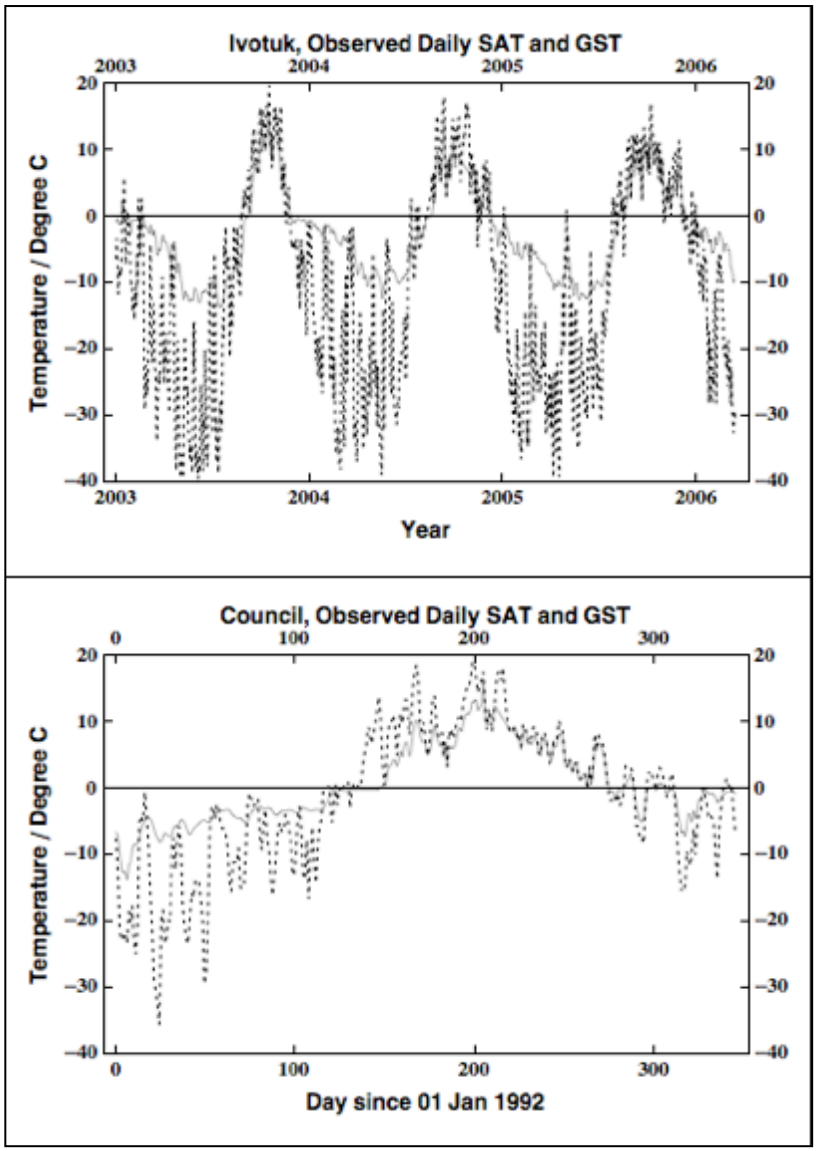

Figure 9.1. Observed daily SAT (dotted line) and GST (solid line) at Ivotuk and Council. At both sites, the observed SAT and GST are not phased lagged.

We modify equation 9.1 to evolve GST from SAT in the presence of snow cover. Based on observed daily SAT and GST data for Council, Ivotuk (Figure 9.1) and at Fargo, North Dakota [*Smerdon et al*. 2003], the SAT signal is not phase lagged with depth (*see Discussion*). equation 9.1 then reduces to:

$$GST(t) = SAT(t) \cdot e^{-\frac{SD(t)}{\lambda_{snow}}} \tag{9.5}$$

where λ_{snow} is the seasonal damping depth for snow, which is approximately 67cm [*Hillel* 1998] for a snow pack of density 300 kg m^{-3}. In our model, snow is an insulative material that only attenuates the daily SAT signals. The deeper the snow pack, the higher the attenuation of the daily SAT signals. During snow-free periods, $SD(t) = 0$, GST = SAT (*see Discussion*).

To generate subsurface ground temperatures from GST, equation 9.1 is again modified such that $\overline{T} = \overline{T}_g$, where $\overline{T}_g$ is the observed annual mean ground temperature, $A_0 = GST(t) - \overline{T}_g$, and $\omega = 2\pi/365$. At depth z, A_0 is attenuated by a factor of $e^{-\frac{z}{\lambda_{soil}(t)}}$ and phase shifted by the calibration parameter, $\phi_d(z)$. $\lambda_{soil}(t)$ is the damping depth for the soil such that:

$$\lambda_{soil}(t) = \sqrt{(2D_h(t)/\omega)} \tag{9.6}$$

where D_h is the time dependent ATD [*McGaw et al*. 1978]. The ATD represents the combined effects of conductive and non-conductive heat transport processes [*Chen and Kling* 1996; *Hinkel* 1997; *Hinkel et al*. 2001] resulting from freeze-thaw, soil water evaporation and movement, etc. Latent heat effects associated with seasonal freeze-thaw

increases the apparent volumetric heat capacity of the soil and decreases the ATD. D_h, therefore will vary over the course of a year. For example, a typical value of specific heat capacity for water is 4200 KJ m^{-3} K^{-1} [*Hillel* 1998], while that of ice is 1900 KJ m^{-3} K^{-1} [*Hillel* 1998]. As the soil thaws, the apparent heat capacity can become higher and reduce the ATD by at least an order of magnitude [*Ochsner and Baker* 2008]. To capture this seasonal variation of D_h, we choose a simple sinusoidal function (*see Discussion*):

$$D_h(t) = \overline{D}_h - B\sin(\omega t) \tag{9.7}$$

where $\overline{D}_h$ is the mean ATD and B is the amplitude of the sinusoid. Optimal values of $\overline{D}_h$ and B are determined through calibration. D_h is constrained to be below the thermal diffusivity of pure ice (11.6×10^{-7} m^2 s^{-1} or 0.1 m^2 day^{-1}) and above zero. This constraint is necessary since ATDs with values less or equal to zero will not yield physically meaningful solutions when used in the analytical solution (equation 9.6). ATD calculated using this methodology therefore represents the average bulk thermal diffusivity over the entire soil column. For high D_h, the damping depth is high, resulting in lower attenuation of the temperature signal at a given depth. For low D_h, the damping depth is low, resulting in higher attenuation of the temperature signal at the same depth.

9.2.2 Site and data description

The model behavior is evaluated using daily *SAT(t)* and *SD(t)* provided at four snow-dominated sites: Barrow, Alaska (71.3°N, 156.8°W); Ivotuk, Alaska (68°29′N, 155°44′W); Council, Alaska (64°53′N, 163°40′W) and RCEW, Idaho (43°05′N, 116°43′W). Barrow is located in northwestern Alaska on the coast of the Arctic Ocean. The climate is cold and dry with a mean annual air temperature of -12.2°C (1949-2003)

(*NOAA* 2002) and annual solid precipitation of 745 mm (water equivalent) (*NOAA* 2002). Barrow is snow covered for ~270 days a year [*Zhang et al*. 1996]. Ivotuk is located 350 km (220 miles) south of Barrow, at the foothills of the North Slope of the Brooks Range. The site experiences mean annual air temperature of -10.9°C and mean annual precipitation of 202 mm [*Riedel et al*. 2005]. Council is located in Central Seaward Peninsula and represents a transitional area between the boreal forest and tundra. Mean annual air temperature at Council ranges from -4.06°C to -4.62°C [*Chapin et al*. 2006]. The RCEW is located in the Owyhee Mountains in southwestern Idaho. Mean annual air temperature ranges from 4.7°C to 8.9°C [*Hanson et al*. 2001] while mean annual precipitation ranges from 230 mm to greater than 1100 mm [*Slaughter et al*. 2001]. Details of the datasets for each site can be found in Table 9.1.

Table 9.1. Information on datasets retrieved from each site. *SAT: Surface Air Temperatures, SD: Snow Depth, GT: Ground Temperature, SWE: Snow Water Equivalent.

Site	Data Downloaded and Used*	Data Duration	Source and Website
Barrow, AK	Daily SAT Daily SD Daily GT at 50cm	01/01/90 to 12/31/97	National Snow and Ice Data Center URL: http://www.nsidc.org/data/
Ivotuk, AK	Half-hourly SAT Half –hourly SD Half-hourly GT at 5, 10cm	09/17/03 to 12/31/06	Ameriflux database. URL:http://public.ornl.gov/ameriflux/
Council, AK	Hourly SAT Hourly SD Hourly GT at 5, 10, 15 and 20cm	01/01/92 to 12/11/92	Climate data for the Arctic Transitions in the Land-Atmosphere System (ATLAS) project. URL:http://www.uaf.edu/water/projects/atlas
Reynolds Creek, ID	Daily SAT Daily SWE Daily GT at 10, 20, 30, 40, 50, 60, 90 and 120cm	06/12/92 to 09/30/96	Northwest Watershed Research Center database. URL:http://www.ars.usda.gov/Main/site_main.htm?modecode=53-62-00-00

Data were inspected for missing values. Periods of less than one month with missing values were filled in through linear interpolation, while periods of missing data greater than one month were excluded from calculations. Daily SAT and SD time series records used in simulations for the four sites are shown in Figure 9.2. Model performance is evaluated using root mean square (RMS) errors, σ :

$$\sigma = \sqrt{\frac{\sum_{i=1}^{N} (T_o^i - T_s^i)^2}{N}} \tag{9.8}$$

where T_o^i is the observed temperature, T_s^i is the simulated temperature and N is the total number of data points.

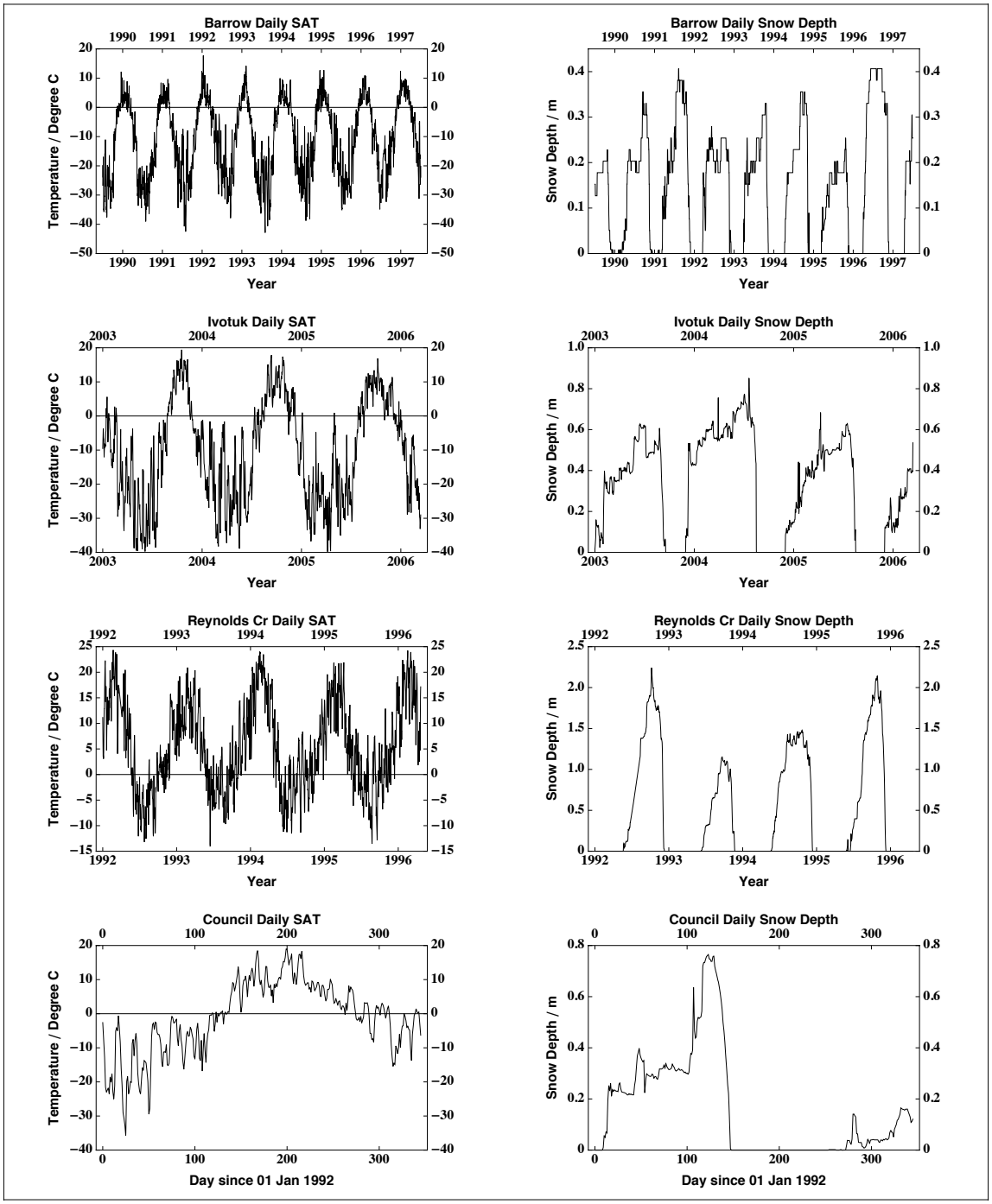

Figure 9.2. Observed daily SAT and SD at Barrow, Ivotuk, Council and RCEW.

9.3 Results

Figure 9.3 illustrates the best-fit ATDs for the four sites: for each site, ATDs peak towards the end of spring and decrease towards zero until fall. Values range from 0.0025 to 0.0775 m^2 day^{-1} in Barrow, 10^{-5} to $1.99x10^{-3}$ m^2 day^{-1} in Ivotuk, $3.5x10^{-4}$ to $1.05x10^{-3}$ m^2 day^{-1} in Council and 0.0015 to 0.0585 m^2 day^{-1} in RCEW (Figure 9.3).

Figure 9.4 illustrates observed and simulated ground temperature at 50cm from 01 Jan 1990 to 31 Dec 1997 in Barrow. At Barrow, observed ground temperature at 50cm range from -25 – 15°C. For the entire eight-year period, simulated ground temperature is in good agreement with the observed ground temperature. RMS error for Barrow is 3.87°C. Figure 9.5 illustrates the observed and simulated ground temperature at 5cm and 10cm from 17 Sept 2003 to 31 Dec 2006 in Ivotuk. Although the model captures much of the seasonal trend of the ground thermal regime for the entire period, it consistently underestimates the fall ground temperatures by ~2.0°C for all years. RMS error for Ivotuk are 3.49°C at 5cm, and 3.09°C at 10cm. Figure 9.6 illustrates the observed and simulated ground temperature at 5, 10, 15 and 25cm from 01 Jan 1992 to 11 Dec 1992 in Council. While the model captures the seasonal trend, it overestimates spring ground temperatures at all depths. RMS errors for Council range from 2.16 – 2.84°C. Figure 9.7 illustrates the observed and simulated ground temperature at 10, 20, 30, 40, 50, 60, 90 and 120cm from 12 Jun 1992 to 30 Sept 1996 for RCEW. At RCEW, simulated ground temperatures at all depths were remarkably similar to the observed ground temperatures. RMS errors for Reynolds Creek range from 2.39 – 3.49°C. RMS errors for all sites can be found in Table 9.2.

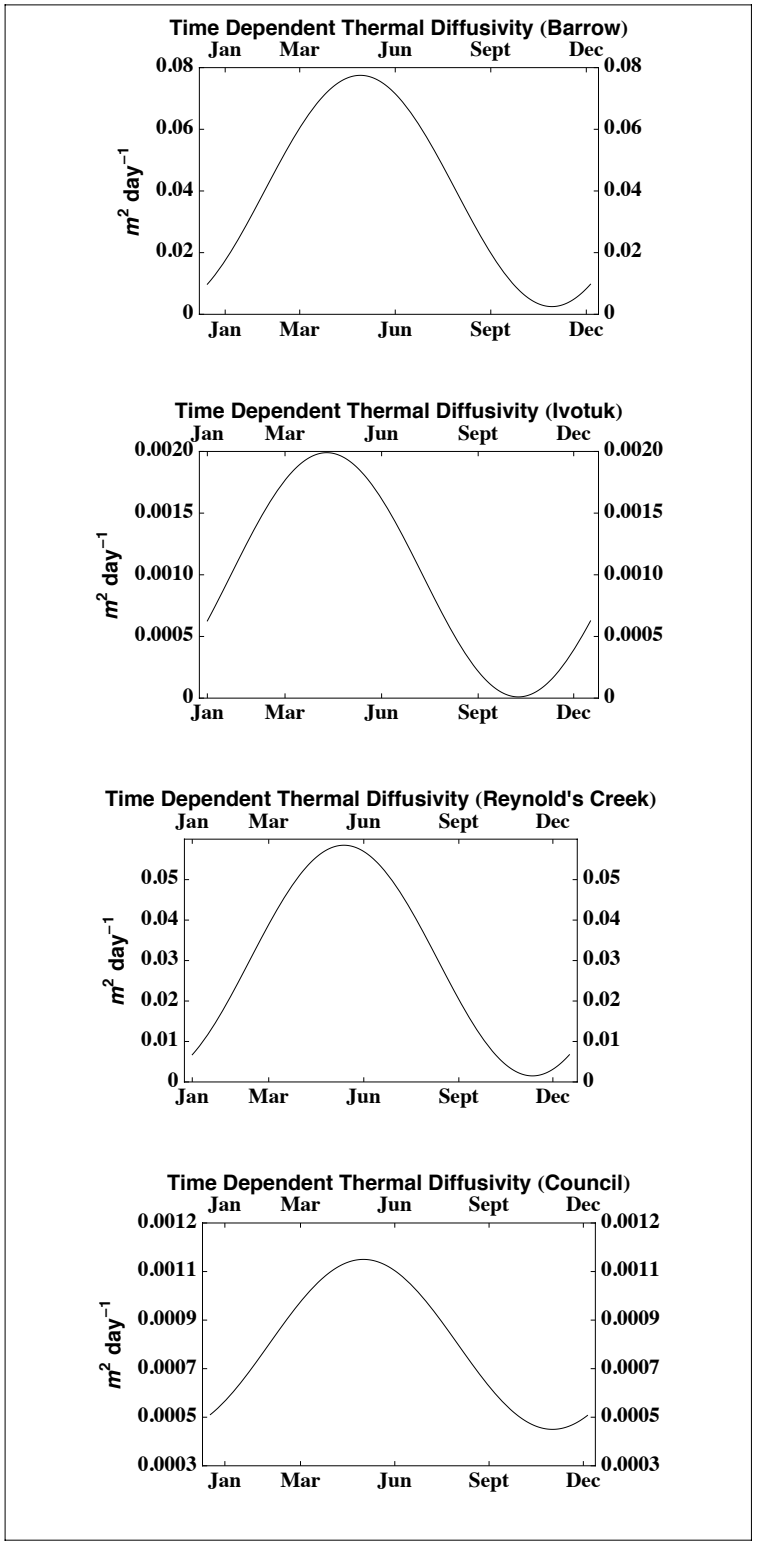

Figure 9.3. Simulated daily ATDs at Barrow, Ivotuk, Council and RCEW.

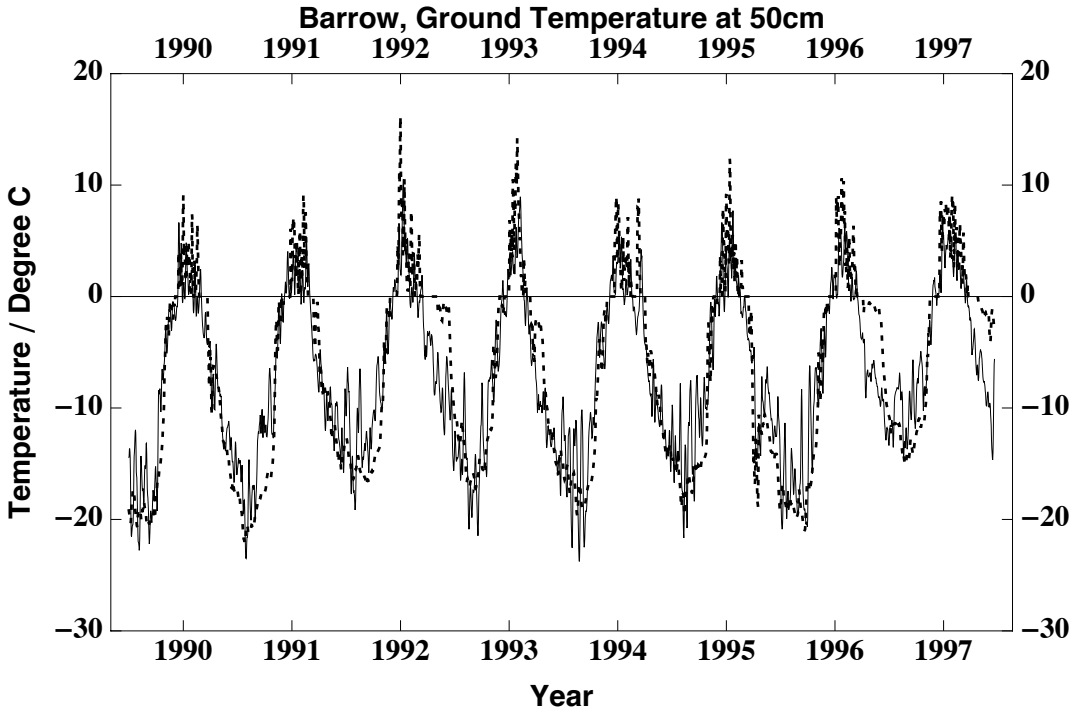

Figure 9.4. Observed daily (dotted line) and simulated daily (solid line) ground temperature at 50cm from 01 Jan 1990 to 31 Dec 1997 at Barrow.

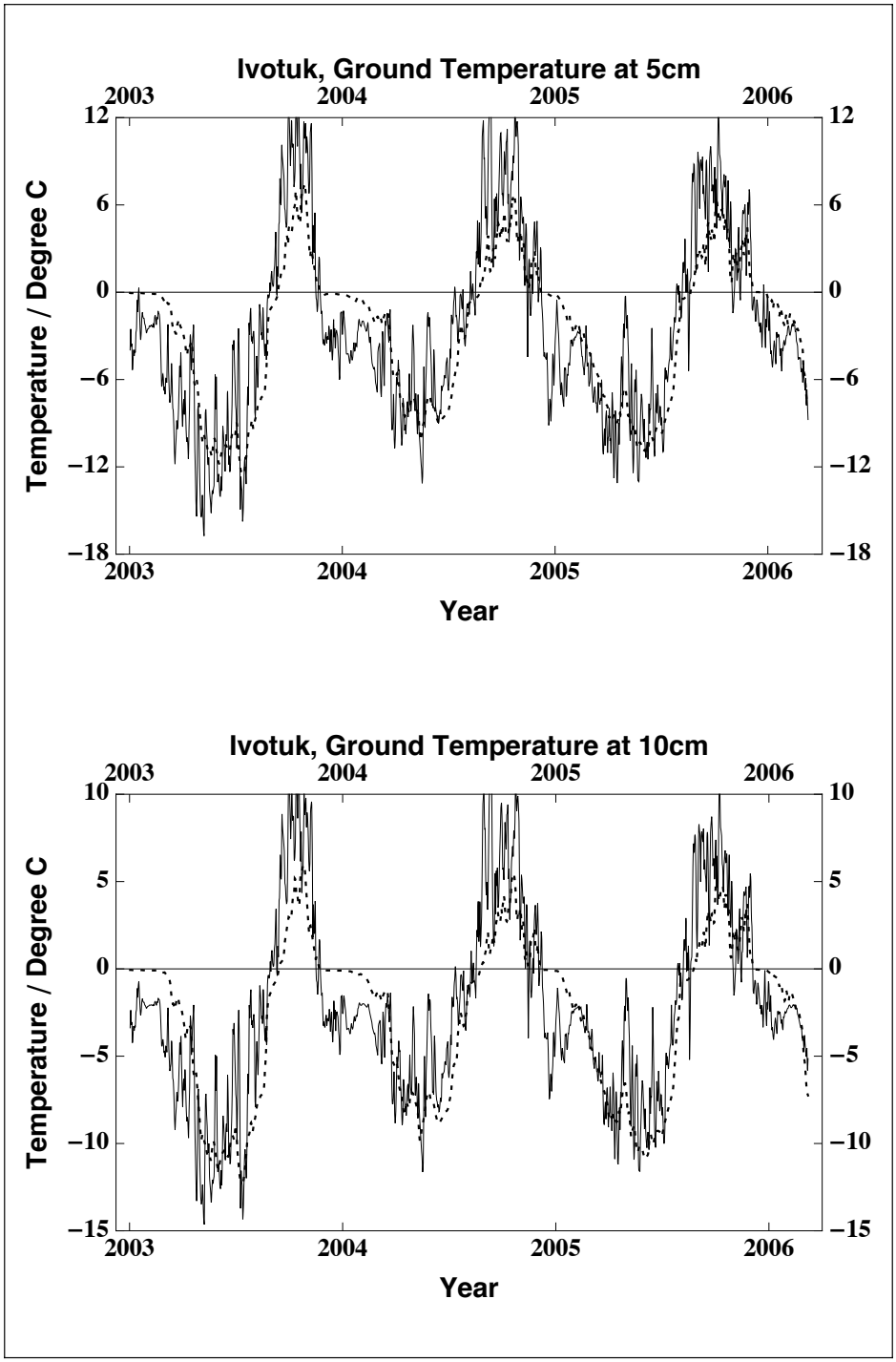

Figure 9.5. Observed daily (dotted line) and simulated daily (solid line) ground temperatures at 5cm and 10 cm from 17 Sept 20-03 to 31 Dec 2006 at Ivotuk.

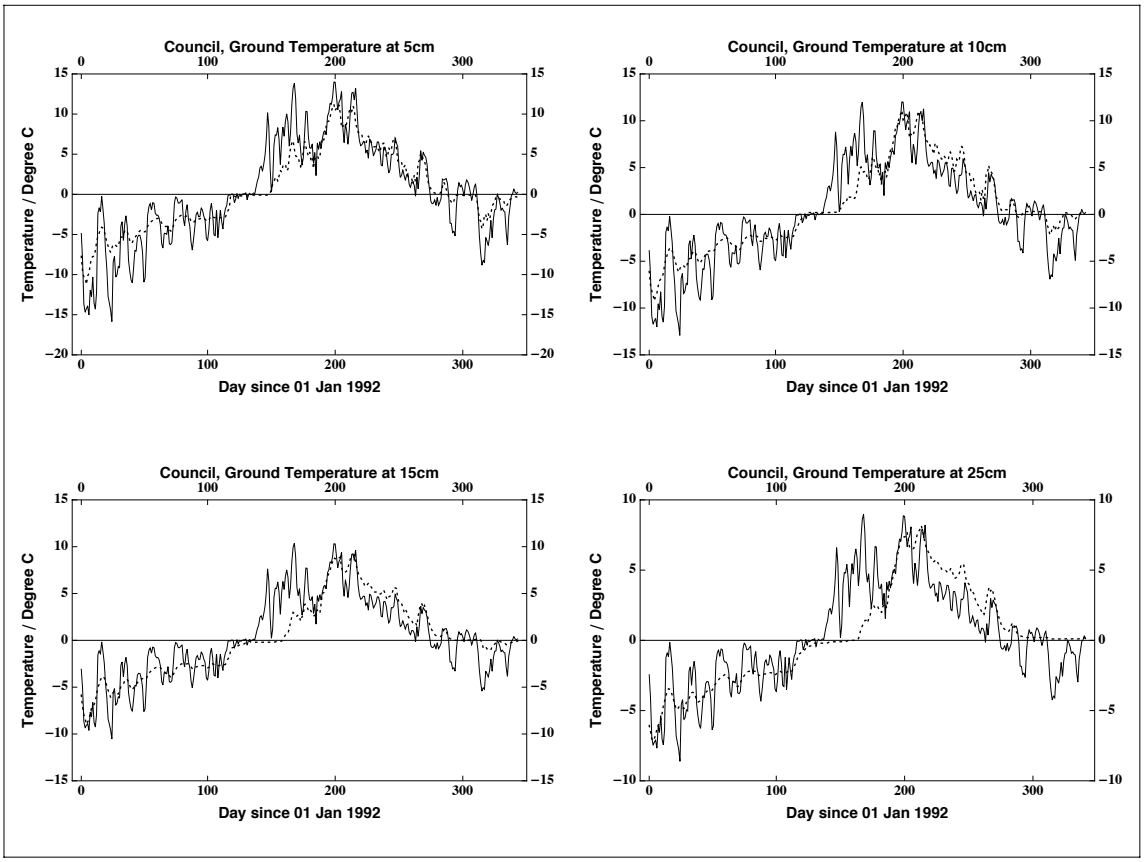

Figure 9.6. Observed daily (dotted line) and simulated daily (solid line) ground temperatures at 5, 10, 15 and 25cm from 01 Jan 1992 to 11 Dec 1992 at Council.

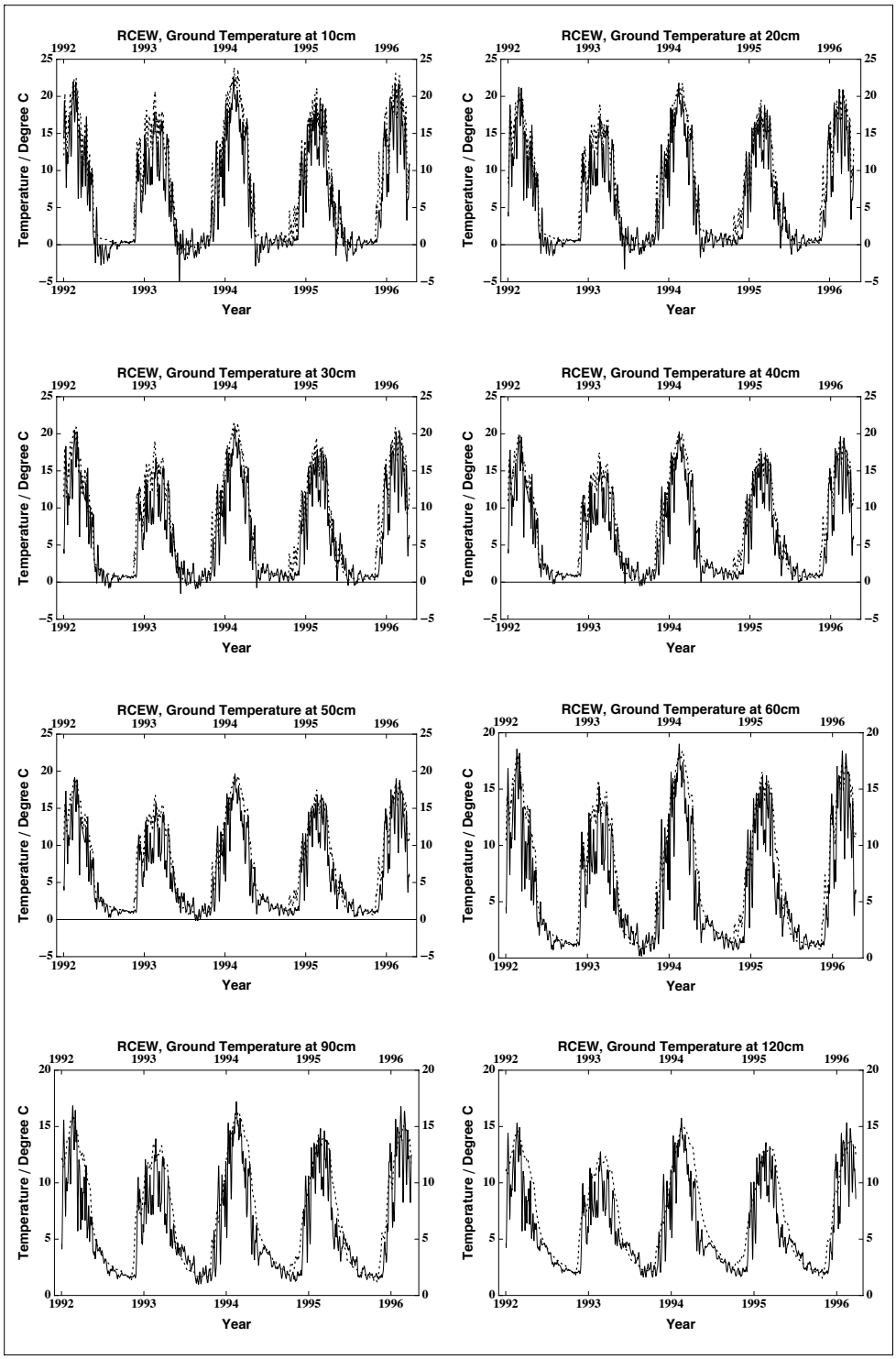

Figure 9.7. Observed daily (dotted line) and simulated daily (solid line) ground temperatures at 10, 20, 30, 40, 50, 60, 90 and 120 cm from 12 Jun 1992 to 30 Sept 1996 at RCEW.

Table 9.2. RMS errors for Barrow, Ivotuk, Council and Reynolds Creek Experimental Watershed.

	Depth, z / cm	**σ / °C**
Barrow		
	50	3.87
Ivotuk		
	5	3.49
	10	3.09
Council		
	5	2.84
	10	2.56
	15	2.40
	25	2.16
Reynolds Creek		
	10	3.02
	20	2.94
	30	3.49
	40	3.11
	50	2.97
	60	2.77
	90	2.58
	120	2.39

9.4 Discussion

Simulation results depict clear seasonal trend in ATDs. The simulated ATDs are the lowest in mid-fall and the beginning of winter (Figure 9.3). Ground temperatures during this period are falling and the soil water is freezing, which increases the apparent heat capacity of the soil and lowers the ATD to a minimum value. Ground temperatures continue to drop in winter and the freezing front propagates deeper into the soil. This in turn increases soil ice and the bulk ATD of soil column. As temperatures rise above 0°C in spring, the frozen soil begins to thaw. As the soil thaws, latent heat is absorbed, which increases the apparent heat capacity, and lowers the ATD of the soil from a maximum value.

To justify our sinusoidal ATDs (equation 9.7), we directly calculate ATDs for Ivotuk, RCEW and Council from observed ground temperature time series using a finite difference scheme [*McGraw et al*. 1978; *Outcalt and Hinkel* 1989; *Hinkel et al*. 1990; *Hinkel et al*. 2001]. We then compare them with our sinusoidal ATDs (Figure 9.8). Results show that our sinusoidal ATDs (equation 9.7) capture the main seasonal variations in Ivotuk and RCEW: lowest from the end of summer to mid winter and the highest towards the end of spring. At Council, there are no obvious trends in the calculated ATDs. The seasonal trends depicted by our sinusoids are also consistent with the results of earlier works that calculated thermal diffusivity from temporal ground temperature and meteorological data. For example, *Hinkel et al*. [2001] calculated thermal diffusivity from time series ground temperature records at Barrow and observed that the ATD decreases towards zero around September/October. Likewise, *Pollack et al*. [2005] quantified ten years of daily thermal diffusivity of the shallow subsurface empirically from daily meteorological records at Fargo, North Dakota. For the period of

their study, thermal diffusivities are lowest from the end of summer to mid winter and the highest towards the end of spring.

As expected, our sinusoidal ATDs (equation 9.7) do not capture the daily variability (Figure 9.8). Daily variability in soil ATDs are dependent on daily fluctuations in soil moisture and non-conductive processes such as evapotranspiration and vapor transport in soils. Moreover, our sinusoidal ATDs do not capture the negative values seen in the calculated ATDs (Figure 9.8). These negative calculated ATDs have been interpreted to reflect the dominance of the nonconductive heat transfer over conductive heat transfer in the soil column [*Hinkel et al*. 2001]. In our modeling framework, however, ATDs with values less or equal to zero do not yield physically meaningful solutions (equation 9.6), and therefore have been constrained to values greater than zero. Nevertheless, the validation strategies discussed above lend support to the notion that our sinusoidal ATDs capture the seasonal behavior of ATDs at our study sites.

Simulated mean ATDs differ by an order of magnitude across the sites (Figure 9.3). At Barrow and RCEW, simulated mean ATDs are 0.04 and 0.03 m^2 day^{-1} respectively, and are consistent with typical values of 0.0173 – 0.0432 m^2 day^{-1} [*Hillel* 1998; *Hinkel et al*. 2001]. At Ivotuk and Council, simulated mean ATDs are 10^{-3} and 7 x 10^{-4} m^2 day^{-1} respectively, and are an order of magnitude lower than typical values. However, at Ivotuk and Council, simulated ATD are of the same order of magnitude as the calculated ATDs (Figure 9.8). In order to ascribe why the differences in ATDs exist between the sites, a more complex model that includes for non-conductive heat transfer processes is needed.

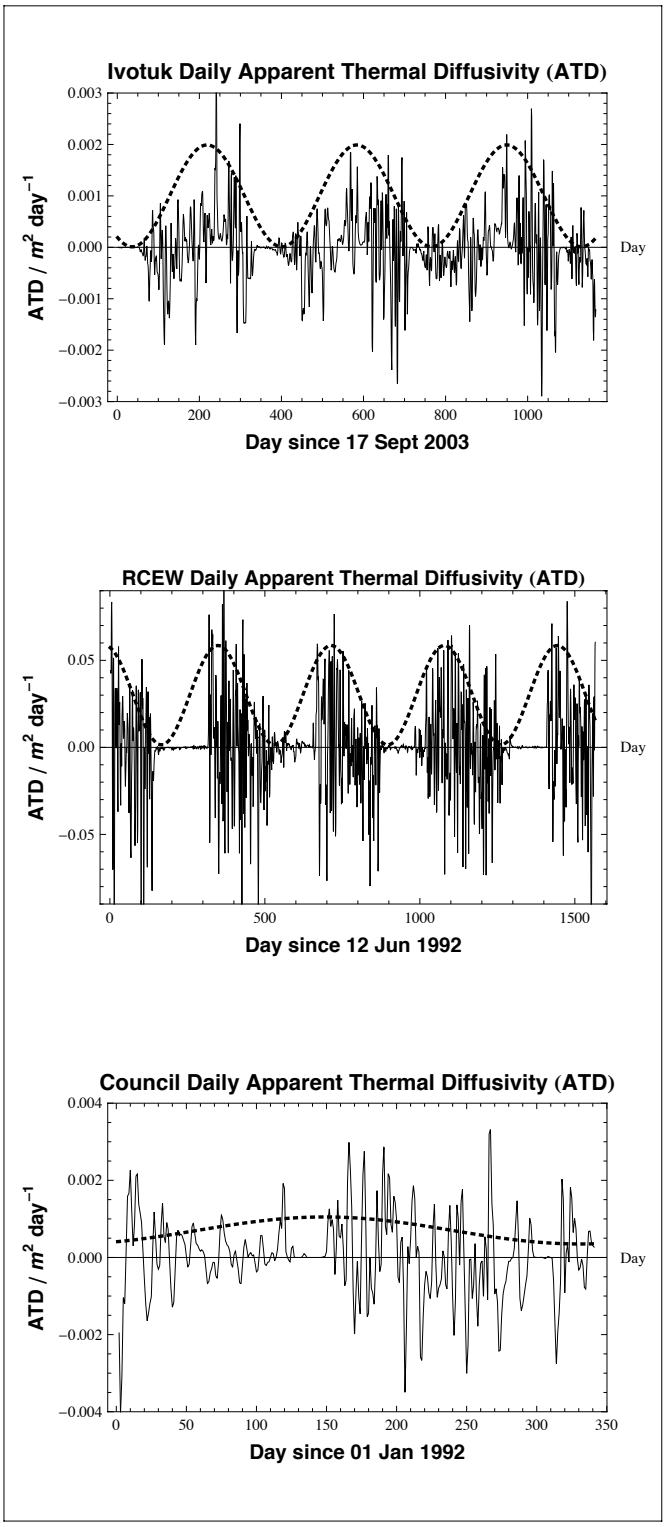

Figure 9.8. ATDs calculated directly from daily ground temperature time series (solid line) and sinusoidal ATDs (dotted line) for Ivotuk (top), RCEW (middle) and Council.

Although our model captures the seasonal evolution of ground temperatures, there are caveats to consider: (1) The depth dependence of the ATD has not been considered. Mineral soil fraction and soil moisture content vary with depth and affect the magnitude of the ATD. ATD typically decreases as volumetric soil moisture increases [*Hinkel et al.* 2001] but increases with mineral soil fraction. Future work is needed to incorporate a depth dependent ATD. (2) During periods of snow cover we assume a constant snow pack density of 300 kg m^{-3}, which translates into a constant λ_{snow} of 67cm for the snow pack. This assumption of a fixed snow density therefore results in early and late season biases, which contribute to notable differences between the simulated and observed ground temperatures during fall in Ivotuk and during spring in Council. Studies have shown that snow pack density varies geographically and seasonally [*Lynch-Stieglitz* 1994; *Sturm and Benson* 1997; i. 2001]: between 150 kg m^{-3} for fresh snow to 500-700 kg m^{-3} for the end-of-season snow pack [*Zhang* 2005]. (3) To maintain the simplicity of the model, we assume that ground-atmosphere decoupling due to vegetation is zero (SAT = GST) during snow-free periods. Analysis of the SATs and GSTs for a number of sites where snow cover is significant (http://public.ornl.gov.ameriflux/), has shown that the ground-atmosphere decoupling due to snow is significantly greater than the ground-atmosphere decoupling due to vegetation [*Stieglitz and Smerdon* 2007]. However, *Stieglitz and Smerdon* [2007] have also shown that ground-atmosphere decoupling due to vegetation can be significant in some sites. For example, at Campbell River, British Columbia, Canada, summer ground-atmosphere decoupling due to vegetation can attenuate the GST by as much as 25%. (4) We observe no phase lag between SAT and

GST in any of our datasets and model the GST as described by equation 5.5. This seems to contradict the common understanding of the propagation of a sinusoidal signal through any conductive material as described by *Carslaw and Jaeger* [1959]. For example, a hypothetical and permanent snow pack that is 1 m thick with λ_{snow} of 67 cm, will result in ~ 87 days of phase lag between SAT and GST. It seems that there are non-conductive processes such as vapor transport and water transport within the snow pack, that are responsible for significant reduction in phase lag between the SAT and GST. In order to isolate the thermal effects of these non-conductive processes, a more complex model is needed and is beyond the objectives of this work. (5) λ_{snow} and $\lambda_{soil}(t)$ are modeled as a function of a single radial frequency with an annual period. This assumption implies that all temperature fluctuations with higher frequencies will not be damped out by the snow and soil. This in turn results in higher variability in the simulated ground temperatures than the observed ground temperatures. Despite all the caveats, we have constructed a useful modeling framework that captures the first order controls of the ground-atmosphere heat transfer in snow-dominated regions. This simple scheme permits rapid prediction of daily ground temperatures over large areas using only daily SAT and SD.

9.5 Conclusion

A simple modeling framework is developed to evolve daily GST from SAT in snow-dominated areas and subsequently simulate ground temperatures using the analytical solution to the one-dimensional thermal diffusion equation. Complex latent heat effects of seasonal freeze thaw were incorporated into the framework through a time dependent ATD. Advantage of this modeling framework is that it permits rapid

prediction of ground temperatures using only SAT and SD data. Coupling of this simple ground temperature model with a spatially distributed snow model capable of generating SD, will provide a powerful tool for determining the magnitude of change in ground temperatures in high latitude regions undergoing changes in winter precipitation/snow at various spatial scales.

9.6 References

Anderson, E. A., 1976: A point energy balance model of a snow cover. *NOAA Tech. Rep. NWS 19, Office of Hydrology, National Weather Service*.

Barnett, T. P., L. Dumenil, U. Schlese, E. Roeckner, and M. Latif, 1989: The Effect of Eurasian Snow Cover on Regional and Global Climate Variations. *Journal of the Atmospheric Sciences*, **46,** 661-685.

Bartelt, P. and M. Lehning, 2002: A physical SNOWPACK model for the Swiss avalanche warning Part I: numerical model. *Cold Regions Science and Technology*, **35,** 123-145.

Bartlett, M. G., D. S. Chapman, and R. N. Harris, 2005: Snow effect on North American ground temperatures, 1950-2002. *Journal of Geophysical Research-Earth Surface*, **110,** -.

Bilello, M. A., 1984: Regional and seasonal variations in snow-cover density in the US.S.R, 84 - 22 pp.

Carslaw, H. S., Jaeger, J. C., 1959: *Conduction of Heat in Solids*. 2nd ed. Oxford University Press, 510 pp.

Chapin, F. S., M. W. Oswood, D. L. Verbyla, L. A. Viereck, and K. van Cleve, 2006: *Alaska's Changing Boreal Forest*. Oxford University Press, 368 pp.

Chen, D., Kling, J., 1996: Apparent thermal diffusivity in soil: Estimation from thermal records and suggestions for numerical modeling. *Physical Geography*, **17,** 419 - 430.

Hanson, C. L., D. Marks, and S. S. Van Vactor, 2001: Long-term climate database, Reynolds Creek Experimental Watershed, Idaho, United States. *Water Resources Research*, **37,** 2839-2841.

Hillel, D., 1998: *Environmental Soil Physics*, Academic Press, 771.

Hinkel, K. M., 1997: Estimating seasonal values of thermal diffusivity in thawed and frozen soils using temperature time series. *Cold Regions Science and Technology*, **26,** 1-15.

Hinkel, K. M. and J. K. Hurd, 2006: Permafrost destabilization and thermokarst following snow fence installation, Barrow, Alaska, USA. *Arctic Antarctic and Alpine Research*, **38,** 530-539.

Hinkel, K. M., S. I. Outcalt, and F. E. Nelson, 1990: Temperature variation and apparent thermal diffusivity in the refreezing active layer, Toolik Lake, Alaska. *Permafrost and Periglacial Processes*, **1,** 265-274.

Hinkel, K. M., F. Paetzold, F. E. Nelson, and J. G. Bockheim, 2001: Patterns of soil temperature and moisture in the active layer and upper permafrost at Barrow, Alaska: 1993-1999. *Global and Planetary Change*, **29,** 293-309.

Jordan, R., 1991: A one-dimensional temperature model for snow cover. Special Report, 49 pp.

Koster, R. D., M. J. Suarez, A. Ducharne, M. Stieglitz, and P. Kumar, 2000: A catchment-based approach to modeling land surface processes in a general circulation model 1. Model structure. *Journal of Geophysical Research-Atmospheres*, **105,** 24809-24822.

Lehning, M., P. Bartelt, B. Brown, C. Fierz, and P. Satyawali, 2002: A physical SNOWTACK model for the Swiss avalanche warning Part II: Snow microstructure. *Cold Regions Science and Technology*, **35,** 147-167.

Liston, G. E. and K. Elder, 2006: A distributed snow-evolution modeling system (SnowModel). *Journal of Hydrometeorology*, **7,** 1259-1276.

Loth, B., H. F. Graf, and J. M. Oberhuber, 1993: Snow Cover Model for Global Climate Simulations. *Journal of Geophysical Research-Atmospheres*, **98,** 10451-10464.

Lynch-Stieglitz, M., 1994: The development and validation of simple snow model for the GISS GCM. *Journal of Climate*, **7,** 1842-1855.

Marks, D., K. R. Cooley, D. C. Robertson, and A. Winstral, 2001: Long-term snow database, Reynolds Creek Experimental Watershed, Idaho, United States. *Water Resources Research*, **37,** 2835-2838.

McGaw, R. W., Outcalt, S.I., Ng, E., 1978: Thermal properties of wet tundra soils at Barrow, Alaska. *Third International Conference on Permafrost*, Edmonton, Alberta, National Research Council of Canada, Ottawa, 47 - 53.

Namias, J., 1985: Some Empirical-Evidence for the Influence of Snow Cover on Temperature and Precipitation. *Monthly Weather Review*, **113,** 1542-1553.

NOAA, 2002. http://www.wrcc.dri.edu/summary/climsmak.html

Ochsner, T. E. and J. M. Baker, 2008: In situ monitoring of soil thermal properties and heat flux during freezing and thawing. *Soil Science Society of America Journal*, **72,** 1025-1032.

Outcalt, S. I., Hinkel, K.M., 1989: Night frost modulation of near-surface soil-water ion concentration and thermal fields. *Physical Geography*, **10,** 336 - 346.

Pollack, H. N., J. E. Smerdon, and P. E. van Keken, 2005: Variable seasonal coupling between air and ground temperatures: A simple representation in terms of subsurface thermal diffusivity. *Geophysical Research Letters*, **32,** -.

Riedel, S. M., E. S. Epstein, and D. A. Walker, 2005: Biotic controls over spectral reflectance of arctic tundra. *International Journal of Remote Sensing*, **26,** 2391-2405.

Schimel, J. P., C. Bilbrough, and J. A. Welker, 2004: Increased snow depth affects microbial activity and nitrogen mineralization in two Arctic tundra communities. *Soil Biology & Biochemistry*, **36,** 217-227.

Slaughter, C. W., D. Marks, G. N. Flerchinger, S. S. Van Vactor, and M. Burgess, 2001: Thirty-five years of research data collection at the Reynolds Creek Experimental Watershed, Idaho, United States. *Water Resources Research*, **37,** 2819-2823.

Smerdon, J. E., Pollack, H.N., Enz, J.W., Lewis, M.J., 2003: Conduction-dominated heat transport of the annual temperature signal in soil. *Journal of Geophysical Research*, **108**.

Stieglitz, M., J. Hobbie, A. Giblin, and G. Kling, 1999: Hydrologic modeling of an arctic tundra watershed: Toward Pan-Arctic predictions. *Journal of Geophysical Research-Atmospheres*, **104,** 27507-27518.

Stieglitz, M., S. J. Dery, V. E. Romanovsky, and T. E. Osterkamp, 2003: The role of snow cover in the warming of arctic permafrost. *Geophysical Research Letters*, **30,** -.

Stieglitz, M., A. Ducharne, R. Koster, and M. Suarez, 2001: The impact of detailed snow physics on the simulation of snow cover and subsurface thermodynamics at continental scales. *Journal of Hydrometeorology*, **2,** 228-242.

Stieglitz, M. and J. E. Smerdon, 2007: Characterizing land-atmosphere coupling and the implications for subsurface thermodynamics. *Journal of Climate*, **20,** 21-37.

Sturm, M. and C. S. Benson, 1997: Vapor transport, grain growth and depth-hoar development in the subarctic snow. *Journal of Glaciology*, **43,** 42-59.

Welker, J., J. Fahnestock, and M. Jones, 2000: Annual CO2 flux from dry and moist arctic tundra: Field responses to increases in summer temperature and winter snow depth. *Climatic Change*, **44,** 139-150.

Yeh, T. C., R. T. Wetherald, and S. Manabe, 1983: A Model Study of the Short-Term Climatic and Hydrologic Effects of Sudden Snow-Cover Removal. *Monthly Weather Review*, **111,** 1013-1024.

Zhang, T., Osterkamp, T.E., 1995: Considerations in determining thermal diffusivity from temperature time series using finite difference methods. *Cold Regions Science and Technology*, **23,** 333 - 341.

Zhang, T., 2005: Influence of the seasonal snow cover on the ground thermal regime: an overview. *Reviews of Geophysics*, **43**.

Zhang, T., T. E. Osterkamp, and K. Stamnes, 1996: Influence of the depth hoar layer of the seasonal snow cover on the ground thermal regime. *Water Resources Research*, **32,** 2075-2086.

CURRICULUM VITAE

Yiwei Cheng

Education

Georgia Institute of Technology, Atlanta, Georgia, 2005 – 2013

Ph.D. in Civil and Environmental Engineering, GPA: 3.9 (May 2013 expected)
Areas of Concentration: Environmental Water Resource and Fluid Dynamics, Climate Change, Ecosystem Modeling and Management, High Performance Computing for Scientific Simulation
Minor: Geographic Information Systems

M.S. in Computer Science and Engineering, GPA: 3.9 2012
Areas of Concentration: High Performance Computing, Algorithm Optimization

M.S. in Civil and Environmental Engineering, GPA: 4.0 2009
Areas of Concentration: Environmental Water Resource and Fluid Dynamics, Climate Change, Ecosystem Modeling and Management

B.S. in Civil and Environmental Engineering, GPA: 3.8 (highest honor) 2007
Areas of Concentration: Environmental Engineering

Honors and Awards

- Keith Runcorn Award from European Geosciences Union 2011
- Everglades Foundation Fellowship 2010
- Georgia Institute of Technology International Student Scholarship, 2006 - 2007
- Faculty Honors and Dean's List for academic achievement from Fall 2005 to Spring 2007.

Skills

- Fluent in English, Mandarin and Hokkien (Chinese Dialect)
- Strong analytical and problem solving skills.
- Strong statistical analysis of data and technical writing.
- Proficient in the following computing language: NVIDIA CUDA, C++, Processing, Matlab, Mathematica, JAVA, javascript
- Proficient in software: JMP (by SAS, statistics), ESRI ArcGIS (Geographic Information System), ERDAS IMAGINE (Remote sensing), HEC-RAS (Hydraulics)

Research Experience

Ecohydrological Lab at Georgia Tech May 2006 — Present
Advisor – Dr Marc Stieglitz (CEE), Co-Advisor – Dr Greg Turk (Computer Graphics)

Thesis

Title: Impacts of Self-Organizing Mechanisms and Topography on Wetland Ecosystem Dynamics

- Understand how vegetation self-organizing mechanisms and topography operate together to impact C-N and hydrologic cycling in ecosystems, and applying the findings to explore how the incorporation of a mechanistic understanding of vegetation self-organization-topography interactions into models, affect predictions of landscape level vegetation patterning, and the implications for ecosystem carbon-nutrient cycles, under changing climate.
- Development and implementation of a spatially explicit eco-hydrological model in Graphics Processing Unit (GPU) framework (CUDA by NVIDIA) for computational speedup and application to real wetland ecosystems.
- Participated in drafting of proposal to funding agencies (NSF and NPS) that resulted in funding of ~$600,000 for the lab.

Other Projects

1. Arctic Tundra

- Conducted field experiments in Arctic Long Term Ecological Research Station (LTER) to develop a mechanistic understanding of how snow and shrubs independently and interactively affect physical and biological controls over decomposition and soil N dynamics in arctic tundra.
- Developed semi-empirical model to simulate first order processes operating at the land- atmosphere interface to understand the impact of snow on the ground thermal regime in arctic Alaska.

2. Florida Everglades

- Developed a spatially explicit eco-hydrological model in open-source language (Processing) to investigate the impacts of management and climate change on the C-N and hydrologic cycling of ridge and slough ecosystem in the Florida Everglades.

3. Pacific Northwest Old-growth Forest

- Participated in the development of a spatially explicit eco-hydrological model in open-source language (Processing) to investigate the impacts of clear-cutting and climate change on the C-N and hydrologic cycling of old growth coniferous (H J Andrews LTER).

International Arctic Research Center Summer School Aug 2006

- Workshop on arctic terrestrial and freshwater ecosystems with focus on ecosystem interactions with hydrology and climate.
- Attended lectures and demonstrations by Larry Hinzman, John Walsh, Vladimir Romanovsky, Syndonia Bret-Harte from UAF, and John Hobbie, Gus Shaver from Marine Biological Laboratory.

Environmental Microbiology Lab at Georgia Tech May 2005 – Dec 2006
Advisor – Dr Jim Spain

- Photobiological hydrogen production by cyanobacteria: Studied relationship between cyanobacteria and other organisms to develop tools for bioprospecting of cyanobacteria.
- Bioremediation: Isolation and analysis of bacteria capable of degrading natural occurring nitroaromatic compounds from the environment for bioremediation.

Teaching Experience

Teaching Assistant at Georgia Tech

Hydrology for Undergraduates (class size: ~50 students) Fall 2009, 2010
Physical Hydrology for Graduate (class size: 5 – 15 students) Spring 2010 - 2012

- Led and developed courses teaching students how to design eco-hydrological models in Processing.
- Conceived and organized class materials, prepared and delivered lectures, guided students through research projects.

Founder and President of X^3: Experience, Experiment and Excel 2011 - present

- Founded a non-profit educational organization, in collaboration with Dekalb Path Academy, Georgia.
- Led team in developing and guiding middle school students through creative scientific activities.

Instructor of Georgia Intern Fellowships for Teachers (GIFT) Summer 2010, 2011

- Led and developed courses teaching middle – high school teachers to design educational applications.

Conference Presentations

Cheng, Y., Stieglitz, M., Pan, F. *The Biological Response of a Small Catchment to Clear-Cutting*, American Geophysical Union Conference, San Francisco, USA, Dec 2006.

Cheng, Y., Stieglitz, M., Pan, F. *Simple Method to Evolve Daily Ground Temperatures From Surface Air Temperatures in Snow Dominated Regions*, American Geophysical Union Conference, San Francisco, USA, Dec 2008.

Cheng, Y., Stieglitz, M., Turk, G., Engel, V. *Parallel Vegetation Stripe Formation Through Hydrologic Interactions*, American Geophysical Union Conference, San Francisco, USA, Dec 2009.

Cheng, Y., Stieglitz, M., Turk, G., Engel, V. *Flow Field and Nutrient Dynamics Governing the Formation of Parallel Vegetation Patterns in the Florida Everglades*, American Geophysical Union Conference, San Francisco, USA, Dec 2009.

Cheng, Y., Stieglitz, M., Turk, G., Engel, V. *Parallel Vegetation Stripe Formation Through Hydrologic Interactions*, European Geophysical Union Conference, Vienna, Austria, May 2010.

Cheng, Y., Stieglitz, M. *Simulating Watershed Scale Hydrologic Characteristics From Fine Scale Processes*, Arctic LTER Meeting, Woods Hole, MA, USA, Feb 2010.

Stieglitz, M., Cheng, Y., Engel, V., Turk, G. *Scale Dependent Nutrient Feedback as a General Mechanism for Vegetation Patterning and Tree Island Formation in Wetland Ecosystems*. Greater Everglades Ecosystem Restoration, Naples, Florida, USA, July 2010.

Abdelnour, A., S. Patil, M. Stieglitz, R. McKane, F. Pan, and Y. Cheng. *Catchment hydro- biogeochemical response to climate change and future land-use*. American Geophysical Union Fall Meeting, San Francisco, USA, Dec 2010.

Cheng, Y., Stieglitz, M., Turk, G., Engel, V. *The Ubiquitous Nature of Nutrient Depletion and the Consequences for Ecosystem Structure*, European Geophysical Union Conference, Vienna, Austria, April 2011.

Cheng, Y., Stieglitz, M., Turk, G., Engel, V. *Demonstrating the Power of GPU Simulations for an Advection-Reaction-Diffusion Model*, European Geophysical Union Conference, Vienna, Austria, April 2011.

Stieglitz, M., Cheng, Y., Engel, V., Turk, G., Chen, J., Ross, J. *GPU Acceleration of an Advection-Diffusion-Reaction Model to Better Understand the Ubiquitous Nature of Nutrient Depletion and the Consequences for Ecosystem Structure*. Florida International University, Miami, Florida, USA, Sept 2011.

Cheng, Y., Stieglitz, M., Turk, G., Ross, J., Engel, V. *Exogenous and Endogenous Controls Impact Evolution and Resilience of Wetland Vegetation Patterns*. 9th INTECOL International Wetlands Conference, Orlando, Florida, USA, June 2012.

Publications

Book Chapter

Cherry, J., Déry, S., Cheng, Y., Stieglitz, M., Pan, F (*in press*). *Meteorology and Climate of Toolik Lake and the North Slope of Alaska: Past, Present and Future*. In: A Changing Arctic: Ecological Consequences for Tundra, Streams, and Lakes [J.E. Hobbie and G. W.

Kling (eds)]. Oxford University Press, New York, NY, USA.

Journal

Cheng, Y., Stieglitz, M., Pan, F. 2010. *Simple Method to Evolve Daily Ground Temperatures From Surface Air Temperatures in Snow Dominated Regions*. Journal of Hydrometeorology. **11**, 1395 – 1404.

Cheng, Y., Stieglitz, M., Turk, G., Engel, V. 2011. *Effects of Anisotropy on Pattern Formation in Wetland Ecosystems*. Geophysical Research Letter. Doi: 10.1029/2010GL046091.

Abdelnour, A., McKane, R., Stieglitz, M., Pan, F., Cheng, Y, 2013. *Effects of Harvest on Carbon and Nitrogen Dynamics in a Pacific Northwest Forest Catchment*. Water Resource Research, **49**, 1 - 22. Doi: 10.1029/2012WR020038.

Cheng, Y., Stieglitz, M., Turk, G., Engel, V. (*in USGS internal review*). *Influence of topography and self-organizing mechanisms over resource fluxes in ecosystems*.

Cheng, Y., Bret-Harte, M., Mack, M., Stieglitz, M., Demarco, J., Tape, K (*in prep*). *Effects of Overwinter Snow Manipulation of Arctic Tundra Across a Naturally Occurring Gradient of Shrub Density*.

Research Interests

- C-N and hydrologic cycling within ecosystems
- Responses of terrestrial ecosystems to climate change
- High performance computing for scientific simulation
- Nonlinear dynamics
- Advanced techniques for scientific visualization

Memberships

- Member of The Chi Epsilon and Tau Beta Phi.
- Member of American Geophysical Union
- Member of European Geosciences Union
- Member of Arctic Long Term Ecological Research Station

Professional Activities and Other Interests

- Reviewer of *Geophysical Research Letters* and *Journal of Theoretical Biology*.
- Convener in European Geosciences Union General Assembly 2011. Led and organize a session in the EGU Assembly 2011.
- Volunteer at the Atlanta Pet Rescue. Foster parents to dogs. Participated in fund raising event.
- Enjoys running, snowboarding and reading.